MASS FLOW SENSOR DEVELOPMENT FOR AN AIR SEEDING CART

A Thesis Submitted to

The College of Graduate Studies and Research

In Partial Fulfillment of the Requirements

For the Degree of Master of Science

In the Department of Chemical and Biological Engineering

University of Saskatchewan

Saskatoon, Saskatchewan

By

PANA BINSIRAWANICH

Fall, 2011

PERMISSION TO USE

In presenting this thesis in partial fulfilment of the requirements for a Postgraduate degree from the University of Saskatchewan, I agree that the Libraries of this University may make it freely available for inspection. I further agree that permission for copying of this thesis in any manner, in whole or in part, for scholarly purposes may be granted by the professor who supervised my thesis work or, in their absence, by the Head of the Department or the Dean of the College in which my thesis work was done. It is understood that any copying or publication or use of this thesis or parts thereof for financial gain shall not be allowed without my written permission. It is also understood that due recognition shall be given to me and to the University of Saskatchewan in any scholarly use which may be made of any material in my thesis.

Requests for permission to copy or to make other use of material in this thesis in whole or part should be addressed to:

Head of the Department of Chemical and Biological Engineering
University of Saskatchewan
Saskatoon, Saskatchewan
S7N 5A9

ABSTRACT

The air seeding cart is an important piece of farming equipment used in the seeding process. Three factors which are necessary to monitor during the seeding process are the seeding rate (material mass flow rate), air flow rate, and blockages. In current practice, there are systems that monitor and report air flow and blockages but not the actual seeding rate. Presently, the seeding rate is based on the metering calibration before the seeding process starts, which requires a lot of time and energy from the operator. If that goes wrong, it not only takes longer, but also costs more money and increases the already significant stress and fatigue which farmers and operators have during the seeding period. Therefore, the development of reliable, and easily calibrated, on-line sensors for flow monitoring would be beneficial. Further, such sensors would facilitate closed-loop control of the flow rate itself.

In order to develop a laboratory prototype for mass flow measurement, a model for mass flow estimation was established. This was accomplished by using pressure transducers to determine the pressure drop across an elevation in the primary air cart run (between the air seeding cart and the air hoe drill). An air seeding test station was designed and developed for the study.

Three different types of seeds and a granular fertilizer were chosen and tested. These tested materials were canola, wheat, chickpea and urea fertilizer (46-0-0). The general form of the model was developed using data from the canola tests. The input parameters for this mass flow estimation model were pressure drop and air flow information. The average percent error of the material mass flow rate's full range was under 10%, except for the highest rate which tested up to 20%. Overall, more than 75% of the estimations had percent errors being less than 5%. The form of the model was also applicable to other individual tested materials with the percent error of their full ranges up to 20%. However, their average of their median error was around 5% of their full ranges.

The general model was also applied to the combined data from all tested materials. The results were not as accurate as when the model was applied to the individual tested material. The median of the percent error (of material mass flow rate full range) varied from as low as 1% to as high as 30%, depending on the tested

materials. Nevertheless, it demonstrated that there were consistencies between the behaviour of the four tested materials.

ACKNOWLEDGEMENT

I would like to sincerely thank my parents, who allowed me to pursue my ambition of studying higher level engineering as opposed to business. I greatly appreciate my parents and my family's financial support that they have given me. I am grateful for their understanding and help.

I also would like to extend my thanks to Professor Scott Noble, my patient supervisor who has given me great advice and much of his time. He has done more for me than I could have ever imagined, and for that I am grateful. I have learned skills from him not exclusive to engineering as he goes above and beyond to help. I could not have finished my M.Sc. without his professional and insightful guidance. Thank you as well to Mr. Jim Henry, the Senior Project Engineer at the Innovation Competence Center, CNH Canada, for not only supplying the much needed equipment for my experiment, but for his financial support, too.

My extended thanks go to the advisory committee consisting of Dr. Venkatesh Meda, Dr. Huiqing Guo, and Dr. David Sumner for their valuable comments in helping me complete my thesis. Special thanks are in order for Dr. Sumner, who has helped me greatly in regards to fluid mechanics. His insight was greatly appreciated.

Thank you to the technical staff who assisted: Mr. Dave Deutscher from the Mechanical Engineering Department, and Mr. Mike Miller, and Mr. Louis Roth of the Chemical and Biological Engineering Department. Mr. Deutscher advised me on the airflow measurement discussions, as well as the pressure transducer calibrations. Mr. Miller and Mr. Roth provided me the much needed space in order for me to execute my experiment. I appreciate the kindness you have all shown me.

To my colleagues and friends, thank you very much for your helpful advice, discussions, and support especially Dr. Rujira Jitrwung, Mr. Varanon Urikul, Ms. Catherine Hui and Mr. Joel Gervais. And also special thanks to Mrs. Reisha Peters for assistance with thesis revisions.

Lastly, thank you to my darling girlfriend, Lisa. To my wonderful honey, thank you for being so supportive and taking care of me when I was busy working on my M.Sc. I appreciate all that you have done to help me through this difficult time.

DEDICATION

I dedicate my research to the farmers who provide the communities, the country, and the world with food and necessities. Without their hard work, the world would be without those. Therefore, I dedicate all that I have done in my research to them in hopes of helping aid improvements in their equipment, which in turn will hopefully reduce their workload and make their already busy and stressful lives simpler. Thank you to all of the farmers who enrich our lives.

TABLE OF CONTENTS

LIST OF TABLES

LIST OF FIGURES

NOMENCLATURE

Greek Symbols

Symbol	Quantity	Units
β	The diameter ratio, d_o/D	-
ε	The expansion factor of the air	-
κ	Isentropic coefficient = 1.4 for air	-
λ_L	Air resistance factor	-
λ_p	Material friction factor	-
μ	Absolute viscosity of air	$N \cdot s/m^2$
μ_0	Reference viscosity at reference temperature T_0 (18.27×10^{-6} Pa·s)	Pa·s
ρ	Air density	kg/m^3
ρ_p	Conveyed materials density	kg/m^3
Φ_m	Mass flow ratio (material/air mass flow rate)	-
ω_{rpm}	Roller speed	rpm

English Symbols

Symbol	Quantity	Units
A	Cross section area of the pipe	m^2
C	Discharge coefficient	-
D	Inside diameter of the conveying pipeline	m
d	Material mean diameter	m
d_o	Diameter of orifice	m
g	Acceleration due to gravity	m/s^2
ID	Inner diameter	m
K	Fitting loss coefficient for turbulent flow	-
L	Length of the conveying pipeline/hose	m
L_{eq}	The equivalent length	m
m_a	Mass flow rate of the air	kg/s
m_p	Mass flow rate of conveyed materials	kg/s
$m_{p,est}$	Estimated material mass flow rate	kg/s
$m_{p,set}$	Set material mass flow rate	kg/s
p_1	Upstream pressure	Pa
p_2	Downstream pressure	Pa
p_{atm}	Atmospheric pressure	Pa
Δp	Total system pressure drop	Pa
Δp_a	Pressure drop due to particle acceleration	Pa
Δp_b	Pressure drop in bends	Pa
Δp_c	Pressure drop accessories	Pa
Δp_g	Pressure drop due to vertical lift	Pa

Δp_L	Line pressure loss due to air only	Pa
Δp_o	Pressure difference across the orifice plate	Pa
Δp_p	Pressure drop due to material friction	Pa
Q	Volumetric flow rate of air	m^3/s
R	Bend radius of conveying pipeline	m
Re_D	Reynolds number calculated with respect to pipe diameter, D	-
T	Temperature	ºC
T_0	Reference temperature (291.15 ºK)	ºK
v	Average air velocity	m/s
v_c	Critical velocity	m/s
v_d	Drop velocity	m/s
v_g	Gas velocity	m/s
v_p	Material (particle) velocity	m/s
v_{set}	Set air velocity	m/s
Δz	Lift height	m

1. INTRODUCTION

The air seeding cart is an important main component of farming equipment which is used in the seeding process, particularly in large-scale production agriculture. This was pioneered in Germany in the 1950's and spread to Canada and Australia in the 1960's (Memory and Atkins 2005). The air seeding system is comprised of five main components: tanks (two, three, or more tanks depending on the model), meter boxes, an air supply, airlines, and the air hoe drill. The tanks are filled with the seeding materials (seed and/or fertilizer). The materials are metered from the tanks and are then blown through tubes to an air hoe drill. The air hoe drill subsequently distributes and delivers seeds and fertilizer(s) to the ground. As the air seeding cart is being towed, the rates with which materials are dispensed are varied according to the ground speed of the tractor and the desired seeding rate. A typical air seeding unit is shown in Figure 1-1.

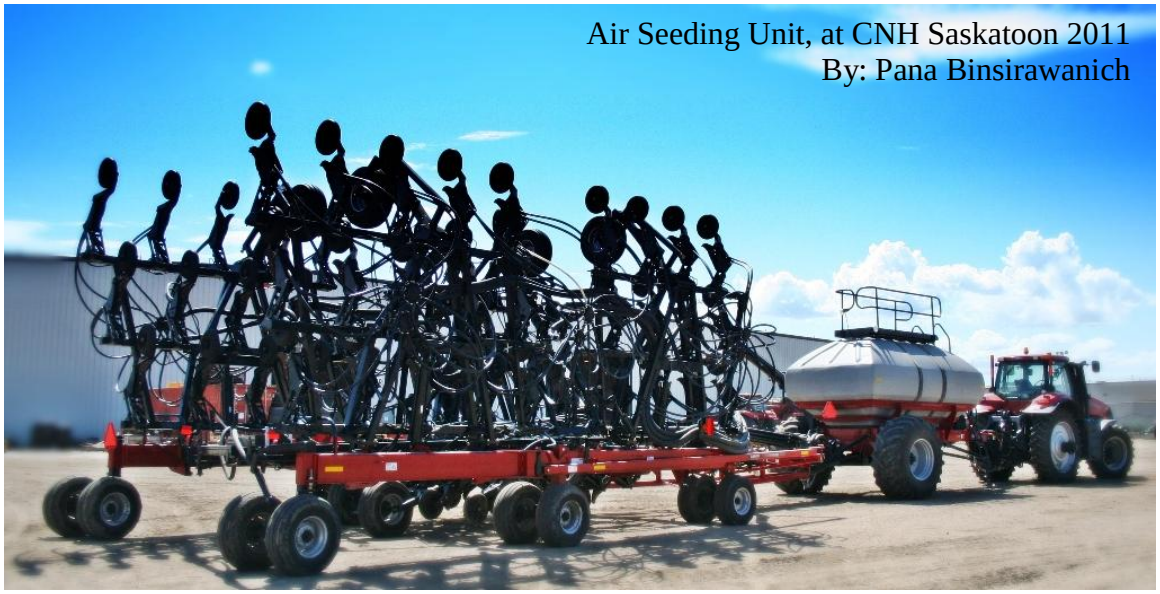

Figure 1-1: A typical air seeding unit which consists of an air hoe drill (left), in transport mode and air seeding cart (middle) being towed by a tractor (right).

Seeding is an important process in the cultivation of crops. In spring, the optimal seeding period is quite short, but the amount of farmland is large, especially in most prairie operations. If seeding cannot be completed in time it might lead to crop loss or lower crop values. Therefore, to save time during seeding, large and efficient air seeding systems are a solution. However, it is challenging for manufacturers to design and

develop these systems. It is not only important that the size of the system be expanded and the product delivery quality remains the same, but the improvement of operational energy consumption is also of great concern.

There are three factors which are necessary to monitor during the seeding process. They are seeding rate (material mass flow rate), air flow rate, and blockages. In current practice, there are systems which monitor and report moving air flow and blockages but not the seeding rate.

The seeding rate is currently based on the metering calibration before the seeding process starts. To perform this, operators have to detach the primary distribution manifold from the metering system. A large bag is placed under the air seeding cart and the seeding products are dispensed for a certain period of time. Subsequently, the dispensed materials are weighed and the seeding rates are calculated. Once the calibration process is completed, the primary distribution manifold is reattached to the metering system. Even though recent air seeding carts have a hydraulic system for detaching and attaching the primary distribution manifold, risks associated with performing this task still exist. Pictures of the primary distribution manifold when it is detached and attached on recent air seeding carts are shown in Figure 1-2.

Figure 1-2: The primary distribution manifold of a recent air seeding cart when it is detached (top) and attached (bottom) from the metering system.

The system used for monitoring air flow in current practice consists of sensing elements which detect the air flow. However, this only reports whether or not the air is moving in the conveying lines. It is not currently used to measure other information about air flow such as conveying air velocity (Henry 2009). In order to ensure that the air flow is sufficient to transport the seeding materials to the ground, "the seed fountain test" is conducted. The seed fountain test is conducted by removing the conveying tube from the farthest header on the air hoe drill (secondary distribution manifold) and holding it vertically. Then, the fan is operated at a relatively high air flow rate and the seeding materials are dispensed at the desired seeding rate into the air stream. Next, the fan speed is adjusted until the seeds are forced up into the air about 30 cm from the end of the conveying tube. The fan speed from this test is set and is the only speed used until the seeding process is completed. This air flow test not only consumes time, but also wastes seeding materials which costs farmers money. A picture of headers on the air hoe drill and the conveying hose which would be removed for the seed fountain test is shown in Figure 1-3.

Figure 1-3: Headers which are installed on an air hoe drill.

Product blockages have been a major problem for operators and farmers. Without any sensing systems, the blockages are difficult to detect in the air seeding process. Currently, the blockage sensing elements are installed on the hoses at the far ends of the

air hoe drill which have the lowest air flow in the system. If plugs occur during the seeding operation, the blockage alarm will go off. This has led to the current practice of increasing the air flow rate above what is required so as to prevent plugging. This practice significantly increases the energy consumed by the system.

The current air seeder calibration process (the seeding rate calibration, the seed fountain test, and the blockage prevention described previously) requires a lot of time and energy from the operator. If there is an incident in those processes, the length of time increases, as does money, stress, and fatigue for the farmers and operators who already have a lot to do during the seeding period. Therefore, the development of reliable, on-line sensors for flow monitoring could be helpful. A mass flow sensor could be part of a solution that would improve the detection of disturbances in the flow, and would assist in controlling the flow rates. If this innovation is successful, the current pre-seeding calibration process could be greatly reduced, simplified, and perhaps eliminated. This means that operators would not need to calibrate the metering system, conduct the seed fountain test, and set the fan speed higher than the system requires. As a result, this will save farmers time and money, and reduce stress and fatigue. It may also facilitate closed-loop control, which could potentially improve air-seeding performance and save energy.

In order to develop a mass flow sensor, the knowledge of pneumatic conveying systems, air seeding carts and their system, sensing techniques and approaches, and previous work were studied. These are described in Chapter 2. Chapter 3 describes the objectives of the study. Chapter 4 explains the experimental apparatus design, such as the experimental set up and the design of the air flow measurement apparatus. Chapter 5 explains the instrument calibration and validation of the instrument used for measurement in the test. The experimental design and test procedure are described in Chapter 6. Experimental results and analysis are shown and discussed in Chapter 7. Finally, the thesis research is summarized and concluded in Chapter 8.

2 LITERATURE REVIEW

To develop a mass flow sensor for an air seeding system, it is important to understand pneumatic conveying as it relates to the air seeding systems. This will assist in understanding how agricultural materials are conveyed and how they behave in the conveying line. Understanding present material flow rate estimation techniques used in industry will guide and help in developing a mass flow sensor for the air seeding cart. In this chapter the related knowledge and previous research of the pneumatic conveying theories, the air seeding cart and its systems, techniques for sensing mass flow rate, and pressure drop in pneumatic conveying systems are reviewed and summarized.

2.1 Pneumatic Conveying Systems

Pneumatic conveying is generally described as the transport of bulk material through a pipeline by either a negative or positive pressure air stream. It can also be described as the utilization of air movement to achieve work (Stoess 1983). In conveying systems, materials being conveyed can be any particulate or granular materials ranging from as small as micron-size to as large as particles 10 cm in diameter. The materials being conveyed can also be transported in high volumetric flow rates along lengthy fixed paths or pipelines. This material transport method is widely used in mills and factories (Mills et al. 2004).

Pneumatic conveying systems can be classified into three types: positive pressure, negative pressure and combination negative/positive pressure systems (Srivastava et al. 2007). Positive pressure systems are used to convey materials from one pick-up point to multiple destinations. The materials being conveyed are dropped from storage into feeders and are then dispensed into the moving air stream in pipelines. At the outlets, the materials are discharged to other storages while the moving gas, if it is clean, might be vented to the atmosphere directly. If the moving gas is dusty, however, it might be vented into dust collectors or dust filters. The pressure of the air stream in the positive pressure system can be high, medium, or low. The pressure (gauge) is considered to be high if the air pressure is between 310 kPa (45 psi) and 861 kPa (125 psi). If the air pressure is between 103 kPa (15 psi) and 310 kPa (45 psi), it is a medium system. If the air pressure

is less than 103 kPa (15 psi), it is a low pressure system (Shamlou 1988). The materials being conveyed, desired mode of transport, and distances are the primary factors that need to be considered to determine the desired pressure of the conveying systems.

Negative pressure conveying is used to transfer materials from single or multiple points of origin to one delivery destination. This is similar to how a vacuum cleaner operates. An example of this is would be the unloading of dry bulk materials from barges, ships, trains or trucks. The negative pressure system is also applied to convey materials from the discharge of mills or pulverizers to prevent dust from spreading (Stoess 1983).

Combination negative/positive pressure systems are used to convey materials from multi-pick up or originating points to multi-discharges or terminal points. They are also applied when negative pressure is applicable and suitable to pick up materials and positive pressure can deliver materials to destinations. After materials are discharged from the negative pressure conveying, they are usually delivered to the destinations by positive pressure which can be high, medium, or low depending on the transport distance and the materials being conveyed (Stoess 1983).

Pneumatic conveying systems are, for the most part, comprised of transport pipelines, an air mover, a material feeder, and a material/air separator (Stoess 1983, Mills et al. 2004). In order to choose appropriate parts for the systems, there are some factors that need to be considered. For the transport pipeline, the most important factors are diameter and material of the pipes. The smoothness of the pipe wall and radius of the bends are also important to minimize material damage and pressure drops within the pipes (Stoess 1983). Fans, blowers, and compressors are examples of air moving systems. The factors for choosing the air mover depend upon the system requirements which are air flow, pressure, and distance (Stoess 1983). When choosing the feeder, the conveyor system is the main factor to be considered. If the system is a negative pressure system, the feeder can be a rotary air-lock, a controlled feed hopper, or a self-regulating pickup nozzle. On the other hand, if the system is a positive pressure system, the material feeder can be a rotary air-lock, an airlock valve, or a discharge gate (Mills et al. 2004). Material/air separators, which are located at the discharge system, are used for separating materials from the air and/or are used for slowing the materials from falling to the

bottom. Cyclone-type separators are normally used. Screens or filters are also used but only for removing the dirt from the air before it enters into the air mover.

The properties of the conveyed material are major factors that are necessary to consider for pneumatic conveying systems. They directly influence the conveying capability as well as methods of material handling. The fundamental material characteristics to be considered are particle size, shape, surface area, density, moisture content, friability, erosiveness, cohesiveness, and combustibility (Mills et al. 2004). Materials which are large, have a less aerodynamic shape, or have high moisture content often require higher air stream velocities and pressure. If the materials are also friable, erosive, electrostatic, or combustible, the conveying systems have to be appropriately designed and constructed to handle those materials. These are the reasons that many researchers have studied pneumatic conveying systems focusing on specific materials. Understanding material properties also helps to decrease power consumption and improve efficiency (Mills et al. 2004).

The flow in the pneumatic conveying systems is classified into two phases: one is the dense phase and the other is the dilute phase. These two phases are presented in positive pressure conveying. In the dense phase, materials start forming clusters in the pipeline and have a solid/gas mass flow rate ratio of more than 15 (Srivastava et al. 2007, Shamlou 1988). This method is often used for high capacity or conveying cohesive materials. The main disadvantage of this method is the high pressure drop caused by the friction between the particles as well as between the particles and the conveying gas. In dilute phase, conveying is characterized by low material concentration. The flow is considered to be in dilute phase when a solid/air mass flow ratio is less than 15 (Srivastava et al. 2007, Shamlou 1988). This phase has a lower pressure drop for operating compared to the dense phase, but also has limited throughput.

Shamlou (1988) has described the flow behavior of the dilute phase in horizontal pipelines with varying solid-gas mass ratio. The “homogeneous flow zone” is the zone in which materials flow uniformly suspended. It happens at low-solid/air mass ratios. When the mass ratio is increased, the particles segregate toward the bottom of the pipelines and roll forward over each other. This is termed “saltation”. If the mass ratio is increased

continuously, the concentration of the saltation will also be increased along with an increase in pressure.

Klinzing (2001) and Barbosa and Seleghim (2003) studied and described the phenomenon of the gas-solid flow in horizontal pipelines by gradually varying the gas velocity from zero to the maximum speed while the material being dispensed as shown in the stage diagram (Figure 2-1). In Stage A, gas velocity (v_g) is not adequately high to raise and float the materials (saltation flow) until the velocity of gas is increased to critical velocity (v_c) which is called pickup flow. In Stage B, the material is fully dispersed in the gas stream ($v_g > v_c$). This is called "homogeneous gas-solid flow". If the gas velocity is decreased slowly from the maximum speed to Stage C, the different flow behaviors are presented. Examples of these include stratified flow, intermittent or pulsating flow, and dune flow. If the velocity of the gas decreases to the drop velocity (v_d), the materials will not be able to remain suspended in the gas stream. At this point, the materials will segregate and drop to the bottom of the pipelines. Some of the particles will bounce and roll over other particles or layers. If the velocity of gas is increased again from the drop velocity but less than the critical velocity ($v_d < v_g < v_c$), the materials introduced to the air stream after the drop velocity will be suspended in the gas stream. However, the materials which are on the pipeline bed from the previous stage still remain the same because the gas velocity is not sufficient to pick up the materials.

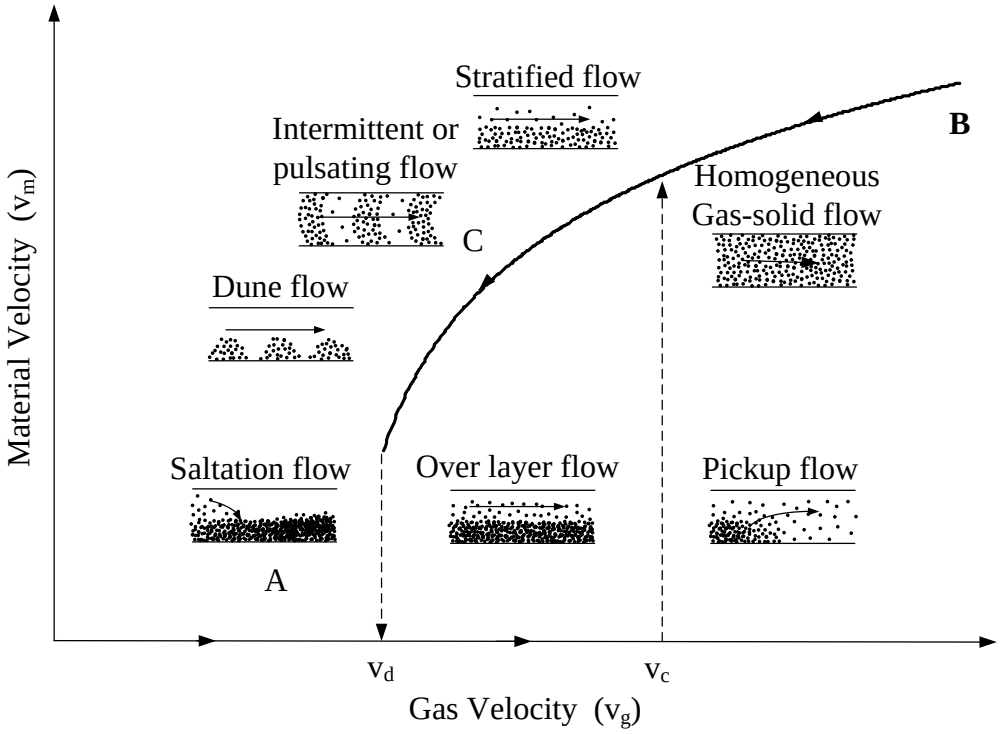

Figure 2-1: Flow regimes of gas-solid in horizontal flow when gas velocity is varied. (Adapted from Klinzing 2001 and Barbosa and Seleghim 2003)

Binsirawanich and Noble (2009) studied the flow behaviors of sample seeding materials in an air seeding cart simulator. It was found that the flows of sample materials (canola, wheat, chickpea, and granular fertilizer) over the recommended seeding ranges provided by an air seeding cart manufacturer were in the dilute phase with variation of mass flow ratio from 0.05 to 3. Figure 2-2 shows a picture of canola suspended in an air stream. The flow behavior of the other materials was also similar to Figure 2-2. The amount of material in the air stream varied between materials.

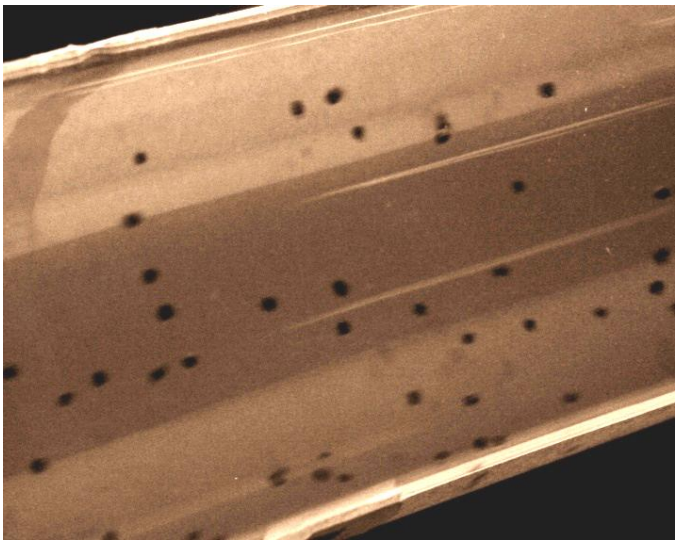

Figure 2-2: Flow behavior of canola at a material mass flow rate of 8.64 g/s and an air velocity of 13 m/s

2.2 Air Seeding Cart / Air Seeder

An air seeding cart or an air seeder is an application of pneumatic conveying and distribution. It carries fertilizer and seeds to a tilling implement called the air hoe drill. This is accomplished by transporting the fertilizer and seeds through the moving gas stream in the airlines or pipelines. However, the pneumatic system of the air seeding cart is slightly different from other general pneumatic conveying systems, with several features making it distinct from others. The first feature is the number of material inlets, which are single, double, or triple inlets with the massively parallel outlet. The ratio of the feeding point to outlets is approximately 1:15, with upwards of 18 feeding points in parallel. Second is a single source of moving air. Those feeding inlets with multiple stages of multi-outlets typically have only a single source of moving air for the whole system. Another feature which makes this air seeding system different from other pneumatic systems is its mobility and ability to change its position to adapt to its environment. The whole seeding system moves when it is operating on a rough and unlevel field surface. These make it very challenging to maintain balance in the system and entrainment of the materials to the destinations without any plugs or blockages. The pneumatic conveying and distribution system of the air seeding cart is simply illustrated by the schematic shown in Figure 2-3.

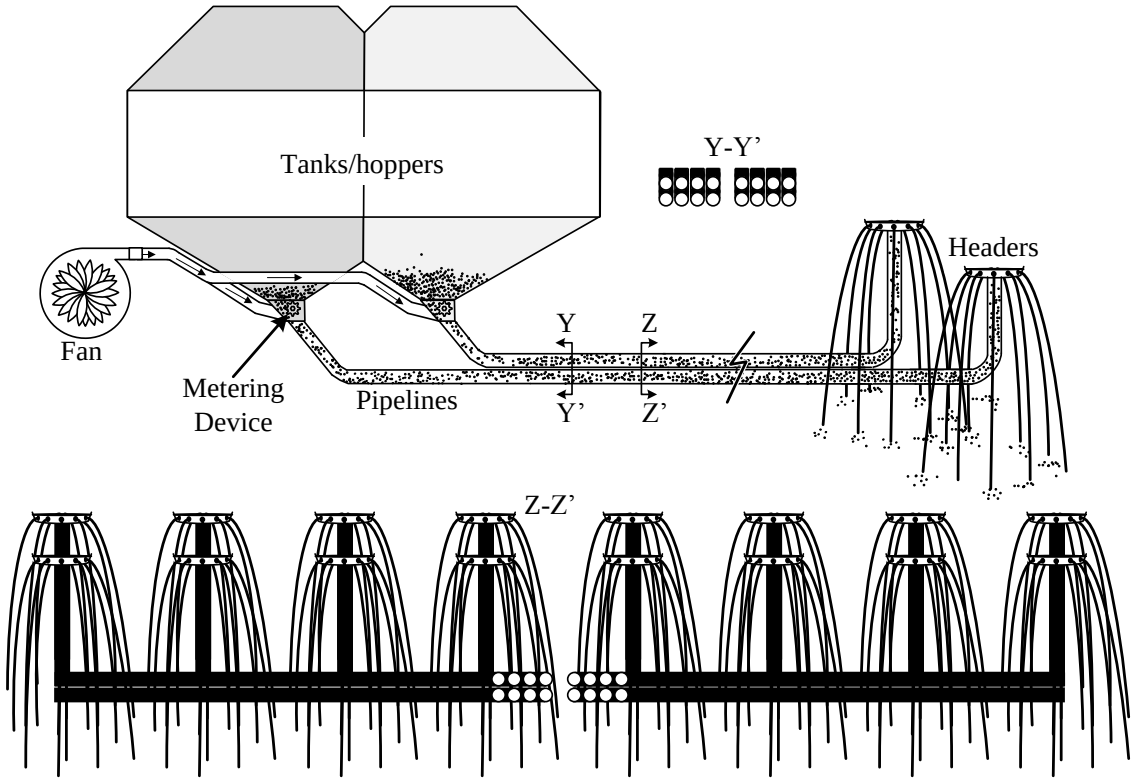

Figure 2-3: The schematic of the pneumatic distribution system for the air seeding cart. (Adapted from Flexi-coil Air Cart Operator's manual 1997).

An air seeding cart generally consists of material tanks/hoppers which are mounted on a frame. Metering devices are installed on the bottoms of the tanks/hoppers. Inside these metering devices, there is a series of fluted rollers which is used to dispense materials into the chambers where the materials are introduced into the air lines. One end of the primary distribution manifold has a centrifugal fan connected to it. This fan generates an air stream for the conveying and distribution systems. The air stream is then divided and directed when it passes through the primary distribution manifold which is comprised of multiple primary air lines. The other end of the primary manifold is attached to the air seeder pipelines which are connected to the series of the headers on the air hoe drill. The headers distribute the air stream and materials to multiple air lines for delivering materials to ground openers. At this point, the air stream is vented and materials are dropped to the field and covered with soil thus completing the seeding process. Pictures of machines and components used in the seeding process are shown in Figure 2-4.

Figure 2-4: Pictures of machines and components used in the seeding process.

2.3 Flow Sensing

Sensing technology for flow monitoring has been a major topic in pneumatic conveying. It is important in measuring the material flow rate, material quantity, and in observation of process efficiency. For the seeding process, the material (fertilizer and seed) flow rate and flow velocity are both important information for when an air seeding cart is being operated. At the present time the control system of air seeding carts is open-loop. The flow rate of materials is estimated based on a rough calibration, and is assumed to have a proper balanced flow in each line before the seeding starts. The development of a reliable

sensor for monitoring flow would allow the control system loop to be closed. As a result, the system would be able to inform operators/farmers about actual seeding information such as seeding rate, material and air flow rate, and/or potential blockages. To develop a sensor for this application, a non-invasive sensing approach is required. This means that the sensors must not interfere with the material flow, damage conveyed materials, cause plugging, or cause build-up of conveyed material in the line. The candidate technologies have been reviewed. Those candidate technologies which meet these application constraints are electrocapacitive, ultrasound, optical sensing, and pressure sensing. These reviews are summarized below.

Electrocapacitive detection is a method of detecting changes in the electric field between the flow medium and an alternating electrical field. In this application, the conveying materials must be dielectric (electrically insulating), and that the medium (air) and materials (conveyed materials) in it need to have different dielectric properties. The changes of the electric field are basically sensed by placing the dielectric sample between the parallel plates known as the capacitor. The dielectric properties of the materials can be determined by measuring changes in amplitude and phase shift between the transmitting and receiving plates by applying a known-frequency signal across the plates. The frequencies being applied to the system can range from radio frequencies (100 kHz) to the microwave spectrum (GHz) depending on the properties of the conveying materials and the design parameters. However, Sun et al. (2008) described that the devices which were used to detect changes in the electric field performed better when they were in dense flow conditions.

Ultrasound is a method of detecting perturbation in the reflection or absorption of sound waves at a frequency higher than 20 kHz. This is achieved by using information about the transit times of ultrasonic pulses. In order to detect the flow, a pair of ultrasonic transducers is mounted opposite to each other on the outside of the pipeline. One is used to transmit the ultrasonic waves, and the other is used to receive the transmitted ultrasonic waves. Velocimetry using ultrasounds is quite recognized with the availability of commercial models. However, the ultrasound technique has not been widely used in pneumatic conveying systems yet. Therefore, a study on the possibility of particle velocity measurement for the solid-gas phase using ultrasonic techniques is needed.

Optical methods typically detect interruptions of light beams. A pair of optical elements is needed: one is an optical transmitter and the other is an optical receiver. This technique is a non-invasive method with a fast response and low cost. Abdul Rahim (2008) reported that the optical method is an effective method in measuring the mass flow rate below 40% of the volumetric flow rates. However, the dust from conveyed materials, the installation of the elements, and the potential complexity of the optical system compared to the previous candidates makes this method less attractive.

Other than the electrocapacitive, ultrasound, and optical sensing, it was found that pressure sensing is another interesting candidate for estimating the material mass flow rate. It has several unique advantages compared to the previous candidate technologies. It does not require the construction of image profiles (tomography) as some of the techniques previously described do. It requires a less complicated sensing system, and it is cheaper than the other methods. Due to uncontrollable situations in the fields such as vibrations, weather, environmental changes, and sensing element installations, a pressure sensing element would be the better solution for developing a mass flow sensor for an air seeding cart. Pressure sensing elements are not only reliable and able to tolerate those situations, but they can be used over wider operating ranges. In addition, they are versatile and can be implemented with any of the conveying materials used in the air seeding cart.

There was a study on mass flow prediction in pneumatic conveying by Arakaki et al. (2009). The study involved a method to estimate the mass flow rate of solid in dilute phase by using pressure and air flow rate measurements as variables to calibrate a Partial Least Square (PLS) regression model. Eleven pressure transducers were installed along the conveying line (58-mm ID) at different locations. The total conveying length was approximately 26 m, which included the horizontal and vertical measurements. Dextrose monohydrate was used as a conveyed material in this test. Two data sets were collected. One was used for the calibration while the other one was used for the validation. The multivariate calibration was performed using Unscrambler v. 7.6 (CAMO software). The result showed that the model obtained from the tests had good potential for predicting the mass flow rate of dextrose monohydrate. Arakaki et al. (2009) summarized that this method had a high accuracy of prediction and could be used as a wide-range, non-

invasive, and inexpensive method. However, there were some disadvantages for using this method. These include the required calibration and calibrations needed to be done in-situ (Arakaki et al. 2009). From this study, it indicates and authenticates that pressure sensing methods can be used to estimate mass flow rate of particles in pneumatic conveying.

2.4 Pressure Drop

Designing a pneumatic conveying system generally necessitates the estimation of the conveying capacity, volume of air supply, power requirements, and pressure drop. In the conveying system, there are many causes of pressure drops. For instance, line pressure loss happens when air flows through the pipeline. Pressure drops occur due to friction between the solid materials and the pipeline wall, as well as interactions among the materials. Moreover, pressure can drop due to the changes in direction (such as by bends) or from accessory parts which can change depending on the design (Raheman and Jindal 1993 and Srivastava et al. 2007). Therefore, there would be a potential for adapting and applying this principle to estimate the mass flow rate of materials conveyed in the air seeding system.

Srivastava et al. (2007) described that the total system pressure drop is a sum of pressure loss due to air, pressure drop due to particle acceleration, material friction, vertical lift, bends and accessories. This is shown in Equation 2-1.

$$\Delta p = \Delta p_L + \Delta p_a + \Delta p_p + \Delta p_g + \Delta p_b + \Delta p_c \qquad 2\text{-}1$$

where Δp is total system pressure drop [Pa],

Δp_L is line pressure loss due to air only [Pa],

Δp_a is pressure drop due to particle acceleration [Pa],

Δp_p is pressure drop due to material friction [Pa],

Δp_g is pressure drop due to vertical lift [Pa],

Δp_b is pressure drop in bends [Pa], and

Δp_c is pressure drop accessories [Pa].

2.4.1 Line Pressure Loss

Line pressure loss is the pressure loss due to air flowing through the pipelines, with longer pipelines having a larger pressure drop than the shorter ones, all else being equal. This loss can be estimated by Equation 2-2 (Srivastava et al. 2007).

$$\Delta p_L = \lambda_L \times \frac{\rho}{2} \times v^2 \times \frac{L}{D}, \qquad 2\text{-}2$$

where λ_L is the air resistance factor,

ρ is the density of air [kg/m^3],

v is the average velocity of air [m/s],

L is the length of the conveying pipeline [m], and

D is the diameter of the conveying pipeline [m].

The air resistance factor can be estimated by the Koo equation (Klinzing et al. 2010) (Equation 2-3) as cited in Srivastava et al. (2007).

$$\frac{\lambda_L}{4} = 0.0014 + \frac{0.125}{Re^{0.32}}, \qquad 2\text{-}3$$

The Reynolds number can be calculated by Equation 2-4 (Klinzing et al. 2010 and Srivastava et al. 2007). However, Klinzing et al. (2010) and Srivastava et al. (2007) did not specify the valid range for the Reynolds number.

$$Re = \frac{\rho \times v \times D}{\mu}, \qquad 2\text{-}4$$

where μ is the absolute viscosity of air [kg/(m×s)].

2.4.2 Acceleration Pressure Drop

Acceleration pressure drop is the pressure drop due to the energy required to accelerate the materials being dispensed to the airstream. However, the final velocity of the materials will be less than that of the airstream. The material velocity (v_p) is sometimes called solid or particle velocity. This pressure drop is estimated by Equation 2-5 given by Srivastava et al. (2007).

$$\Delta p_a = \frac{m_p}{m_a} \times v \times \rho \times v_p, \quad 2\text{-}5$$

where m_p is the material mass flow rate [kg/s],

m_a is the air mass flow rate [kg/s], and

v_p is the velocity of materials (particle) [m/s].

The following equation reported by Klinzing et al. (2010) (which is a newer edition of Marcus et al. 1990) as cited in Srivastava et al. (2007) can be used to determine the velocity of materials. However, the range for validity and uncertainty in this equation were not specified.

$$\frac{v_p}{v} = 1 - 0.68 \times d^{0.92} \times \rho_p^{0.5} \times \rho^{-0.2} \times D^{0.54}, \quad 2\text{-}6$$

where d is the particle mean diameter [m] and

ρ_p is the density of conveyed materials [kg/m^3].

2.4.3 Pressure Drop Due to Conveyed Materials

Pressure drop due to the conveyed materials is due to the interaction between particles of conveyed material, and between conveyed materials and the pipe wall. This loss will also increase if the conveying distance is increased. Equations 2-7 given by Srivastava et al. (2007) is used to estimate this pressure drop.

$$\Delta p_p = \frac{m_p}{m_a} \times \lambda_p \times \frac{\rho}{2} \times v^2 \times \frac{L}{D}, \quad 2\text{-}7$$

where λ_p is the material friction factor.

Equation 2-8 given by Kenno and Saito (1969) as cited in Srivastava et al. (2007) can be used to calculate material friction factor.

$$\lambda_p = \frac{0.0285 \times \sqrt{g \times D}}{v_p}, \quad 2\text{-}8$$

where g is the acceleration due to gravity = 9.81 m/s^2.

2.4.4 Pressure Drop Due to Lift Height

Pressure drop due to lift height is the result of changes in the energy that occur when the particles are lifted to the desired height. It is estimated by Equation 2-9 (Srivastava et al. 2007).

$$\Delta p_g = \frac{m_p}{m_a} \times \frac{v \times \rho}{v_p} \times g \times \Delta z, \qquad 2\text{-}9$$

where Δz is the lift height [m].

2.4.5 Pressure Drop Due to Bends

There are many bends presented along the pipelines starting from the air seeding cart to the end of the tillage implement equipment. There are two particular locations where bends are present that can be used for this application. Between the air seeding cart and air hoe drill there are two bends that can be changed for the pipeline height. Another location is on the air hoe drill. This bend is present to allow a change in the direction. The pressure drop due to bends is the sum of the pressure drop due to the air and conveyed materials through the bends. Equation 2-10 given by Srivastava et al. (2007) is used to estimate the pressure drop due to the air.

$$\Delta p_{b,air} = L_{eq} \times \frac{\Delta p_L}{L}, \qquad 2\text{-}10$$

where L_{eq} is the equivalent length [m].

The equivalent length is calculated by Equation 2-11 (Srivastava et al. 2007).

$$L_{eq} = \frac{K \times D}{\lambda_L}, \qquad 2\text{-}11$$

where K is the fitting loss coefficient for turbulent flow which can be selected from Table 2-1 given by ASHRAE (Srivastava et al. 2007).

Table 2-1: Fitting loss coefficients for turbulent flow presented by ASHRAE (Srivastava et al. 2007)

Fitting	Geometry	K
Entrance	Sharp	0.5
	Well-rounded	0.05
Contraction	Sharp	0.38
90º elbow	Miter	1.3
	Short radius	0.9
	Long radius	0.6

The pressure loss due to the conveyed materials can be determined by Equation 2-12 (Srivastava et al. 2007).

$$\Delta p_{b,p} = 0.245 \times \rho \times v^2 \times \left(\frac{m_p}{\rho \times v \times D^2} \right)^{1.267} \times \left(\frac{R}{D} \right)^{-0.260}, \qquad 2\text{-}12$$

where $\Delta p_{b,p}$ is the pressure drop due to conveyed materials in bends [Pa] and

$\frac{R}{D}$ is the bend radius to pipe diameter ratio.

2.4.6 Pressure Drop in Accessories

Pressure drop in accessories depends on the design of the system. Some examples of accessories are blowers, inline filters, and cyclones. There is no simple equation provided to estimate this pressure drop. However, this loss of information is often provided by manufactures or available in literature (Srivastava et al. 2007).

2.4.7 Evaluation of Model by Srivastava

Binsirwanich et al. (2010) studied the particle velocity estimation model (Equation 2-6) which was described by Srivastava et al (2007) to evaluate its applicability for the air seeding system as shown in Figure 2-5.

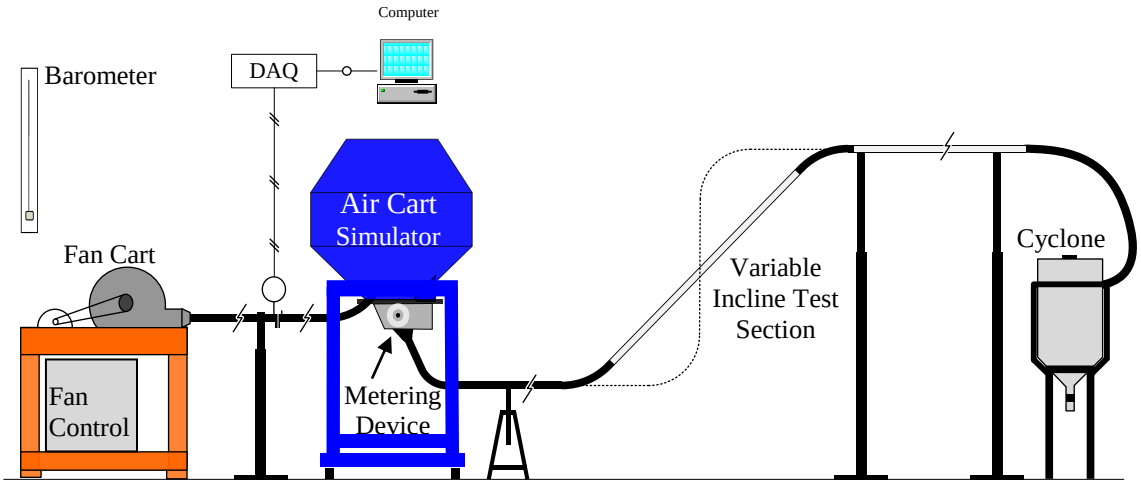

Figure 2-5: Experimental set up configuration for the material velocity test (Binsirwanich et al. 2010)

Binsirwanich et al. (2010) conducted the experiment for examining the velocity of conveying material in 45º and 90º inclined transition tubes. Table 2-2 shows the results of the material velocity tests. It was observed that canola had the lowest difference between the actual and estimated material velocity, but its errors were 59% and 67% for both 45º and 90º inclines. Wheat had an error a little different from fertilizer for 45º tests (62% and 65% respectively), but their vertical test errors were similar, at 71%. Chickpea had the largest error of about 80% for both tests. It was also noticed that larger materials or materials with higher densities had a bigger difference between the actual and estimated velocity.

Table 2-2: The test results from the velocity test for a 45º and 90º inclined transition (Binsirawanich et al., 2010)

Particle Type	Incline [°]	Material Density [kg/m^3]	Air Flow Rate [kg/s]	Material Flow Rate [kg/s]	Air Velocity [m/s]	Particle Velocity [m/s]		Error [%]
						Est.	Actual	
Canola	45	1150	0.051	0.026	16.0	15.9	6.5	59.3
	90	1150	0.050	0.026	15.5	15.3	5.0	67.3
Wheat	45	1300	0.058	0.011	18.2	17.6	6.6	62.4
	90	1300	0.057	0.011	17.9	17.3	5.0	71.2
Chickpea	45	1437	0.068	0.016	21.5	19.9	4.2	79.0
	90	1437	0.080	0.016	24.9	23.1	4.2	81.7
Fertilizer	45	1330	0.052	0.026	16.1	15.7	5.4	65.3
	90	1330	0.054	0.026	16.8	16.4	4.7	71.4

During the execution of this experiment, it was evident that the material velocity estimation equation (Equation 2-6) was inaccurate with respect to the system developed. Equation 2-6 was used to evaluate many of the equations used for obtaining the total pressure drop (Δp) in Equation 2-1. The equations used include the pressure drop due to particle acceleration Δp_a (Equation 2-5), the materials friction factor (Equation 2-8) which was used to calculate the pressure drop due to the materials Δp_p (Equation 2-7), and the pressure drop due to vertical lift, Δp_g (Equation 2-9). The results were then used to calculate the total system pressure drop, Δp (in Equation 2-1). If Equation 2-6 could not estimate or represent the actual particle velocity accurately, it could be implied that Equation 2-1 would not be able to estimate the pressure drop in the seeding system accurately. This means that the material velocity estimation model would not be applicable for developing a mass flow sensor on the air seeding system.

By tracing the original source of the material velocity model of Equation 2-6, it was found that, according to Klinzing et al. (2010), Hinkle (1953) developed an empirical correlation from the basic particle velocity data. The materials that Hinkle used in his test were polystyrene beads, tenite plastic pellets, alundum catalyst supports, and catalin spheres, which are artificial or synthesized materials (Hinkle, 1953). These materials were tested in pipes with inside diameters of 50.8 mm (2 in) and 76.2 mm (3 in) of straight glass piping that was 9.1m (30 feet) long (as a conveying line). Hinkle (1953) indicated that 99 % of the acceleration of the conveyed materials was reached in 30 to 65 diameters of the conveying pipe distance from the feeding location at the material mass flow rate of 0.03 to 0.30 kg/s (4 to 40 lb/min) in all cases. The above work has been broadly used for pneumatic transportation and for later research. In 1978, The Institute of Gas Technology modified Hinkle's work and obtained a model used for estimating the material velocity (Equation 2-6), which is a function of the system parameters only (IGT 1978, Klinzing et al. 2010).

Based on this information, there are several hypotheses as to why the model by Srivastava et al. (2007) was not accurately applicable to this study. The first reason is because the model originally developed was based on the non-agricultural materials, which have different properties from that of biomaterials (seed). The second reason is that the model was broadly developed for the pneumatic transportation used in the

industry. However, it might not be suitable to apply their works to the air seeding system which has different specifications and system configurations. Another reason for the difference is the distance available for particle acceleration and elevation change. In the study by Binsirawanich et al. (2010), the material velocity was measured in the middle of the elevation where the distance was less than 1.5 m. In contrast, Hinkle (1953) observed the material acceleration and velocity in the straight horizontal section. The properties of the tested materials and some test information from the studies of Hinkle (1953) and Binsirawanich et al. (2010) are summarized and shown in Table 2-3 and Table 2-4.

Table 2-3: The properties of the tested materials and test information from the study of Hinkle (1953)

Material	Polystyrene	Tenite	Catalin	Alundum
Density [kg/m^3]	1049	1129	1116	1810
Mean Diameter [mm]	0.2045	2.54	6.35	8.38
m_p max [kg/s]	0.129	0.367	0.113	0.302
m_p min [kg/s]	0.030	0.066	0.053	0.117
Conveying Air Velocity [m/s]	26-36	20-36	20-35.5	26.8-33.8
Shape	Spherical	Spherical	Perfect Sphere	Perfect Sphere
Diameter of the Conveying Line [mm]	50.8 mm ID (2 in) and 76.2 mm ID (3 in)			
Length [m]	9.1 (glass tube)			
Conveying Direction	Horizontal			

Table 2-4: The properties of the tested materials and test information from the study of Binsirawanich et al. (2010)

Material	Canola	Wheat	Chickpea	Fertilizer
Density [kg/m^3]	1150	1300	1437	1330
Mean Diameter [mm]	1.83	4.08	8.95	3
m_p [kg/s]	0.026	0.011	0.016	0.026
Conveying Air Velocity [m/s] at 45º	16.0	18.2	21.5	16.1
Conveying Air Velocity [m/s] at 90º	15.5	17.9	24.9	16.8
Shape	Spherical	Elongated	Round (dimpled)	Round (rough angular)
Diameter of the Conveying Line [mm]	63.5 ID (2.5 in)			
Length [m]	1.5 (acrylic tube)			
Conveying Direction	45º and 90º inclination			

Furthermore, from tracking sources of equations referred by Srivastava et al. (2007), it was found that there are many empirical models that can be used to estimate material velocity (v_p). Hinkle (1953) developed the original material model which was then developed again and improved by The Institute of Gas Technology and Yang (Klinzing et al. 2010). It was also found that Kenno and Saito (1969), who developed Equation 2-8, expressed the material velocity as the difference between the mean air velocity and free falling velocity of material, and was developed in the specific context of vertical conveying. Because of the multiple and inconsistent material velocity models in the various research reported, caution was exercised in using these models.

Even though the pressure drop model (Equation 2-1) by Srivastava et al. (2007) proved to be inadequate for the air seeding system implemented in this experiment, along with the uncertainty in the material velocity models used, the pressure sensing technique (pressure drop) is still the most appropriate approach for this study. The most interesting pressure drop location on the air seeding cart for mass flow sensor development is around the elevation, which is the change of pipeline level. At these points, the difference in pressure drop is higher and easier to detect for a short distance of a pipeline compared to the other pressure losses.

2.5 Summary

According to the information gathered in the literature review an air seeding cart is a positive pressure system. It has single, double, or more feeding inlets and multiple outlets with a single air moving source which supplies moving air to the whole system. The materials in an air seeding cart are transported in dilute phase or homogeneous flow zone. The air seeding system is comprised of a fan, a material tank, a metering system, conveying lines, and headers. Because this study was focusing on the primary run, the header was not required and a cyclone separator was used instead.

The pressure drop technique would be the most appropriate method for developing a mass flow sensor for an air seeding cart. Pressure sensing elements are reliable and able to tolerate the situations required for field use. They are low in price and can be used over wide operating ranges. Furthermore, they can be implemented with any of the conveying materials and the readings from the sensing elements will not be affected by changing those materials. Therefore, because of the advantages described previously, the pressure sensing approach was chosen to be studied and developed as a mass flow sensor for the air seeding systems.

In order to develop a mass flow sensor for an air seeding cart, a model for estimating the mass flow rate of the conveying materials is required. The pressure drop model by Srivastava et al (2007) would not to be applicable for the air seeding system; however, developing a mass flow sensor by using the pressure sensing approach would be still an alternate solution. As well, the ideas from Arakaki et al. (2009) would be used as a guidance for this study.

As a consequence, an empirical model for estimating the conveying material flow rate in the air seeding system would be specifically established and implemented in this study. This empirical model would be developed based on the pressure drop across the elevation on the air seeding cart and the correlation between the control parameters (which are the material mass flow rate, the air mass flow rate, and the air velocity).

3. OBJECTIVES

3.1 Main Objective

The main objective of this research was to develop and test a laboratory prototype for mass flow measurement of pneumatically conveyed products. This was to be accomplished by using the pressure sensing technique and applying this sensing approach across the elevation in the primary air cart run (between the air seeding cart and the air hoe drill). In order to achieve this goal, a mass flow model had to be developed and implemented from the relationship between material mass flow rate, air mass flow rate, and pressure drop across the elevation, $m_p = f(m_a, \Delta p)$.

The following specific goals were required in order to conduct the experiment.

3.2 Specific Goals

1) Develop the air seeding test station.
2) Develop an air flow measurement apparatus including pressure taps and flow conditioner.
3) Develop a data acquisition system including the user interface program and system control panel.
4) Test and evaluate the developed system.
5) Collect data for four materials (canola, wheat, chickpea, and granular fertilizer).
6) Develop and test an empirical model.

4. EXPERIMENTAL APPARATUS DESIGN

Pneumatic conveying for air seeding systems is a relatively new area of research in the department. Therefore, preliminary experiments and system development were necessary to define the scope of the project. An air flow measurement technique and method of measuring the pressure drop were designed and studied.

Three techniques for measuring the air flow were considered. These were hot-wire or hot-film anemometry, Pitot-static tube, and orifice plate. The orifice plate provided lower cost and greater robustness than the others. Moreover, the orifice plate gave flow rate directly and velocity profile measurements were not required. Hence, the orifice plate was chosen for measuring the air flow in the study.

There were two categories of pressure measurements. The first one was for the air flow measurement obtained from the pressure drop across the orifice plate. The other one was for observing the pressure drop along the conveying line. The air flow measurement required two pressure transducers used to measure the gauge pressure and pressure drop (difference in pressure) across the orifice plate. The ranges of the pressure transducers were estimated from preliminary testing using handheld digital manometers.

The pressure drop along the conveying line was originally going to be estimated based on the pressure drop model presented by Srivastava et al. (2007) shown in Equation 2-1. However, the study of Binsirawanich et al. (2010) indicated the pressure drop estimation model Equation 2-1 would not be accurately applicable in this circumstance. Therefore, handheld manometers were also used to verify the ranges of the pressure transducers. Five pressure transducers were used to observe the pressure differences and gauge pressures at different locations along the conveying line.

The following sections describe the details of the experiment set-up and the main equipment, such as the fan cart and air cart simulator, air flow measurement instrument design and their calculations, and line pressure measurement. The data acquisition system and the system control panel are also explained in this chapter.

4.1 Experimental Set-Up

Based on the experimental scope, the air flow measurement technique was chosen, preliminary estimates of pressure drops in this system were made, and the required equipment were selected and designed. The equipment used for the test is listed in Table 4-1 and the experiment set-up configuration is presented in Figure 4-1.

Table 4-1: List of equipment used in the experiment.

Main set up	1 Fan with Variable-Frequency Drive (VFD) 2 Air cart simulator 3 Flow conditioner 4 Cyclone 5 63.5 mm OD (2.5 in) pipes 6 63.5 mm ID (2.5 in) flexible tube 7 0.004762 m ID x 0.007938 m OD (3/16" ID x 5/16" OD) tubes
Air flow measurement	8 2 x 0-20 in H_2O pressure transducer (616-4, Dwyer Instruments) 9 1 x 0-40 in H_2O pressure transducer (616-5, Dwyer Instruments) 10 Orifice plate
Atmospheric pressure	11 Barometer (469 NOVA Economy Model, Princo Instrument)
Pressure measurement	12 1 x 0-1 in H_2O pressure transducer (616-00, Dwyer Instruments) 13 2 x 0-3 in H_2O pressure transducer (616-1, Dwyer Instruments) 14 3 x 0-6 in H_2O pressure transducer (616-2, Dwyer Instruments) 15 3 x 0-10 in H_2O pressure transducer (616-3, Dwyer Instruments)
Temperature measurement	16 3 x Type T thermocouples
Data acquisition system	17 Computer and LabVIEW8.6 18 Power supply and Multimeter 19 Control panel 20 NI 9203: 8-chanel, ±20mA, 16 bit Analog Current Input Module 21 NI 9265: 4-chanel, 0-20mA, 16 bit Analog Current Output Module 22 NI 9211: 4-chanel Thermocouple Input Module

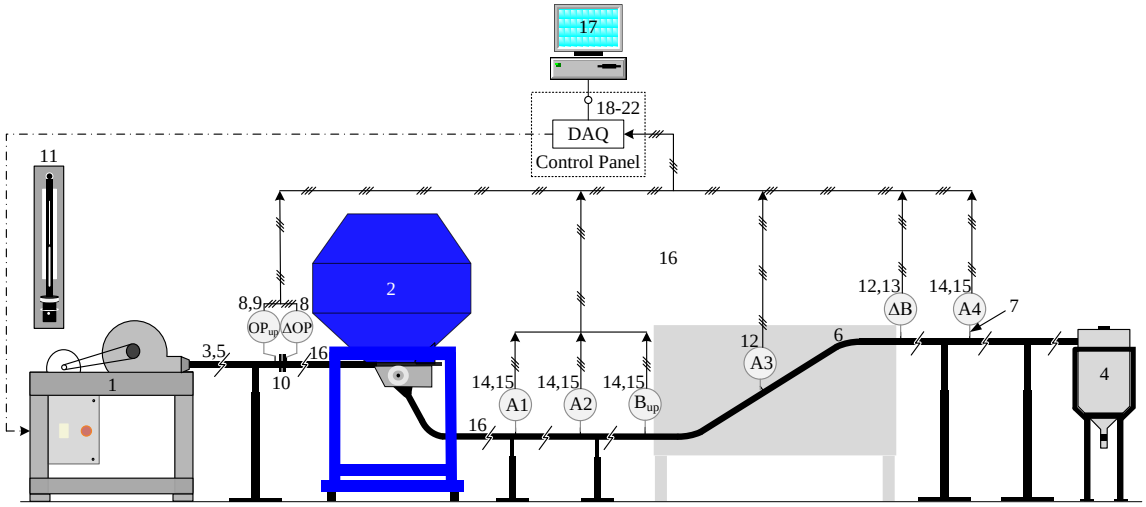

Figure 4-1: The experiment set up configuration. The numbers in figure indicate the parts which are listed in Table 4-1.

The experiment consisted of the fan (1) used to provide an airflow. It was driven by a 3.7-kW (5-hp) electric motor with a variable-frequency drive for speed control. The fan was connected to the air cart simulator (2) by a 59.5-mm inside-diameter (ID) pipe (5) which had an orifice plate (10) and a flow conditioner (3) installed for the airflow measurement.

At the top of the air cart simulator was a tank to hold the tested materials. A metering system was installed below this tank. This system was operated and controlled by stepper motor. At this point, the materials were dispensed from the tank into the airstream. Then they were conveyed along the 63.5-mm ID distribution flexible hose (6), which consisted of a hose with elevation and a cyclone (4) for separating the conveyed material from the airstream.

A barometer (11) was mounted on the wall and used to obtain an absolute reading of atmospheric pressure for converting gauge pressure readings to absolute pressure. Along the hose, pressure taps were installed for observing gauge pressure and pressure difference. There were three type T-thermocouples (16) installed on the system. The first one was used to observe the temperature at the orifice plate. The second one was used to observe the temperature in the downstream section of the air cart simulator. The third one was used to obtain the laboratory environmental temperature. The signals generated by

pressure and temperature were sent to the data acquisition (DAQ) system, which was connected to a computer (17).

4.1.1 Fan Cart and Drive System (Motor and VFD)

The fan unit was used to generate the air flow for the test and consisted of the FlexiCoil fan, a three-phase motor, and variable frequency drive (VFD). The fan was the same type as has been used on the FlexiCoil air seeding carts. The motor used in the experiment was a 3.7-kW (5-hp) 60 Hz, 230 V 3 ph electric motor with a maximum speed of 3,495 rpm at rated load. The model number was JVB184TTFW6001AA M and was manufactured by Marathorn Electric (Wausau, WI). The variable-frequency drive (Automation Direct 5.0 HP 230 V 3 ph, Model GS2-25P0) was used to drive the motor. The drive was set to operate the motor at a speed proportional to a 4 to 20 mA input signal. The fan system was able to operate by either auto or manual control mode and could generate the air flow rates as high as 38 m/s at the maximum control signal current (20 mA). Pictures of the fan cart and its component can be seen in Figure 4-2. The fan unit is displayed on the left of the figure with individual components displayed on the right.

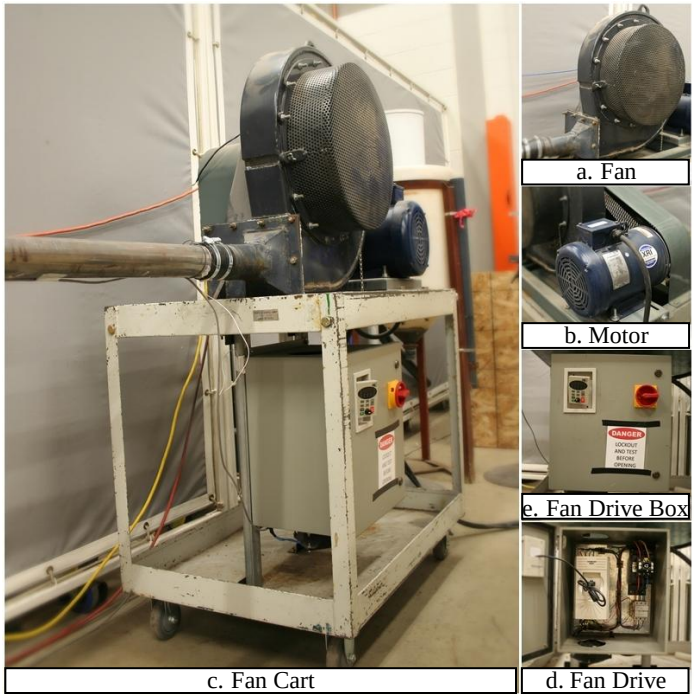

Figure 4-2: The fan unit and its components

4.1.2 Seed tank and metering system

The air seeding cart simulator was used to hold and dispense tested materials into the conveying airstream flown into the air seeding cart from the back of the material tank. The air seeding cart simulator consisted of the material tank placed on the frame and the metering system which was installed at the bottom of the tank. The product being conveyed was loaded into the tank and was dispensed to the conveying airstream at the bottom of the metering box. The metering system was controlled by a stepper motor (MDrive 42, Motor+Driver AC plus^2 by Schneider Electric, Marlborough, CT) equipped with a 10-to-1 reducing gearhead. The motor was operated by commands from the control program. The motor and gearhead unit were coupled to the meter roller shaft. The meter roller installed on the meter roller shaft was replaced according to the material being tested. In this study, three different types of production rollers were used, the extra fine (canola), fine (wheat), and extra coarse (chickpea and fertilizer) rollers. At the very low seeding rates for canola, the non-production quarter-extra fine roller was used. Pictures of the air seeding cart simulator and its components are shown in Figure 4-3. Pictures of the rollers are shown in Figure 4-4.

Figure 4-3: The air seeding cart simulator and its components.

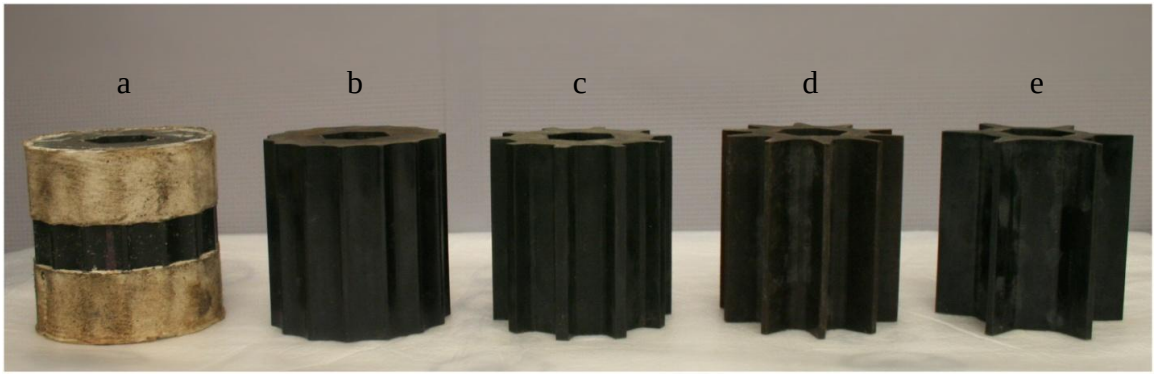

Figure 4-4: Different types of rollers; a. quarter extra fine roller, b. extra fine roller, c. fine roller, d. coarse roller, and e. extra coarse roller.

4.1.3 Bend

The elevation section consisted of two 45-degree bends each with a 0.45-m (18-in) radius. It was constructed from a 63.5-mm (2.5-inch) inside diameter flexible tube with the wall thickness of 5 mm mounted on a plywood board. There were pressure taps installed before, half way through, and after the elevation. A drawing of the elevation is shown in Figure 4-5.

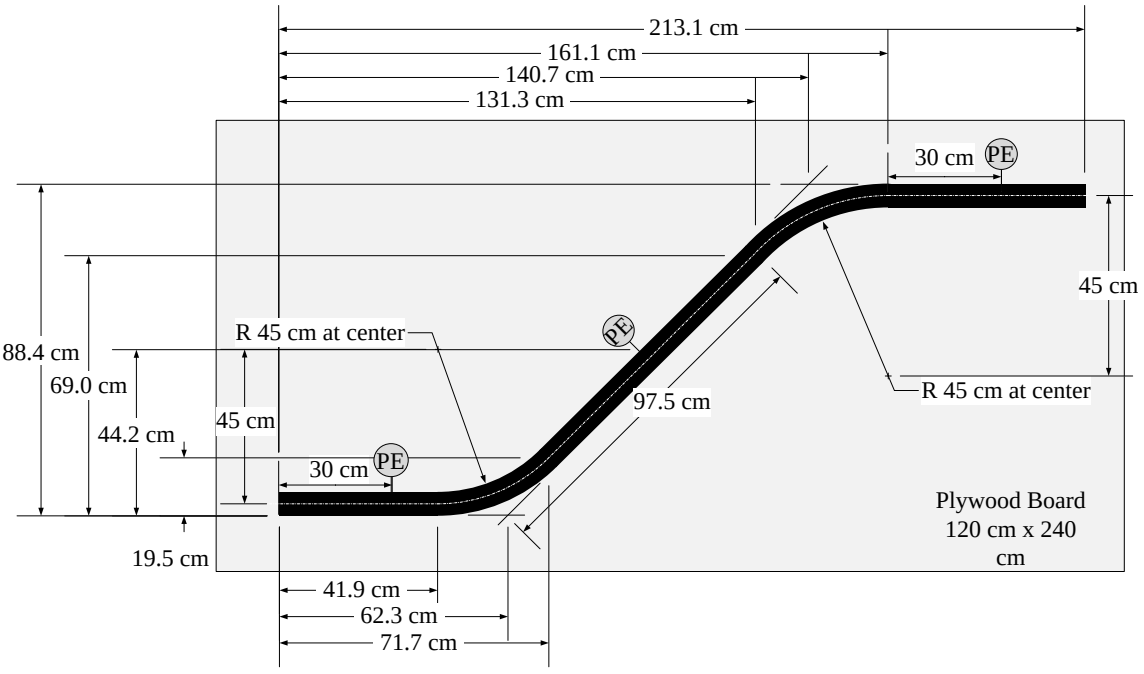

Figure 4-5: The specification of the elevation section which consisted of two 45-degree bends each with a 0.45 m (18 in) radius.

4.2 Air Flow Measurement Apparatus Design

Measurement of the air flow rate was important because it was one of the two control parameters used in the test and was also used for the test process control. The orifice plate was selected for measuring the air flow in this study. The orifice plate is a differential pressure type of flow meter (Gerhart and Gross, 1985). It obstructed the flow in the pipe and the different pressures across the obstruction were used to calculate the air flow rate. The main reasons for choosing the orifice plate were that it did not require the velocity profile measurements, it provided the air flow rate directly, and it was simply installed between pipe flanges. The orifice which was used in this study was designed and built by following International Standard ISO 5167-2:2003(E). Then the flow rate from the orifice plate was calculated by following International Standard ISO 5167-1:2003(E). The following section details the design for this particular apparatus and the mass flow calculations as applied in this study.

4.2.1 Orifice Plate Design

The orifice plate was used to measure the air flow in a 59.48-mm ID pipe, D. It was made of aluminum. The diameter of the orifice, d_o, was 45.0 mm. This had to be greater than 12.5 mm (ISO 5167-1 2003 (E)). According to those diameters, the diameter ratio, β (d_o/D), was 0.75 which had to be equal to or between 0.01 and 0.75 (ISO 5167-1 2003 (E)). The thickness of the orifice was 0.5 mm. This had to be equal to or between 0.298 mm and 1.190 mm (ISO 5167-1 2003 (E)). The thickness of the plate was 3.14 mm, which was more than the thickness of the orifice but less than the maximum thickness of 2.975 mm (ISO 5167-1 2003 (E)). The angle of bevels was $45^o \pm 15^o$. The drawing of the orifice plate and its dimensions are depicted in Figure 4-6.

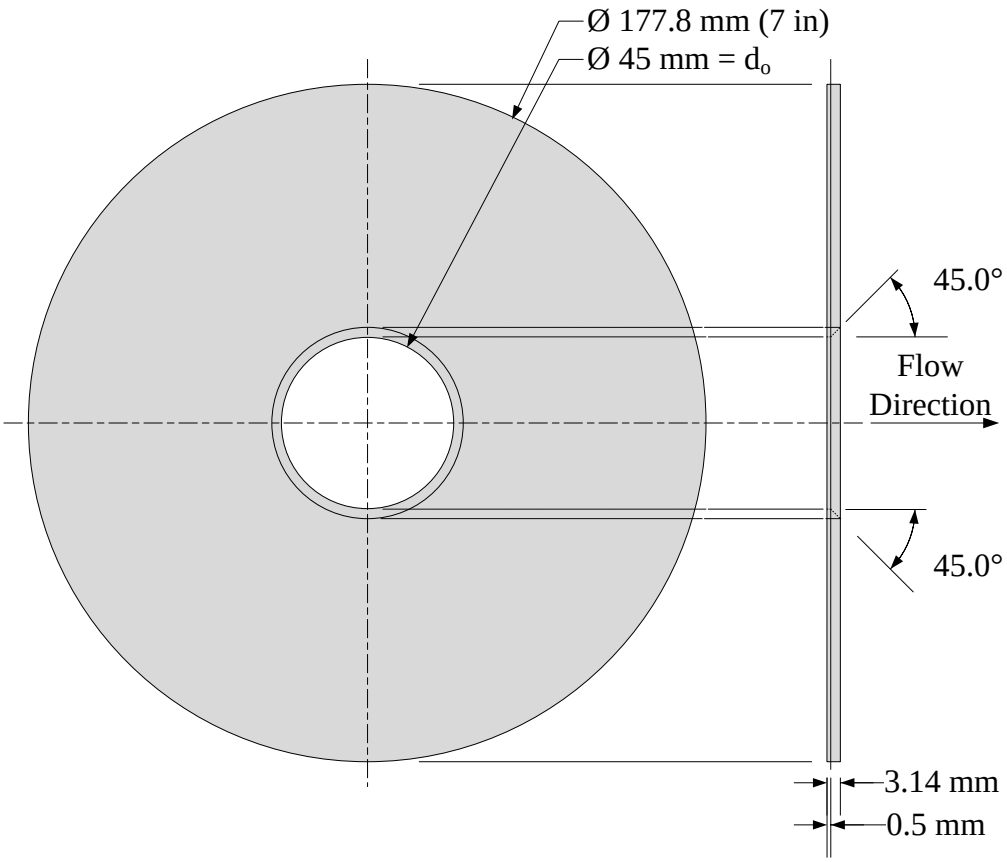

Figure 4-6: Orifice plate dimensions.

4.2.2 Flange Tap or D and D/2 Tap

In order to get the pressure across the orifice plate, pressure taps were required. Flange taps or D and D/2 types were chosen. The flange tap was also designed under the International Standard ISO 5167-2 2003 (E). The diameter of pressure taps and their length were 3.18 mm and 63.5 m, respectively. The distances from the center of the upstream pressure tap to the upstream face of the orifice plate and the distance from the center of the downstream pressure tapping to the upstream face of the orifice plate were 63.5 mm and 31.75 mm, respectively. The lengths of the upstream and downstream pipes were 1.143 m and 0.508 m, respectively. In the upstream pipe, there was a 19-tube bundle flow straightener that was installed about 60 cm before the orifice plate. This was used to reduce the swirl that could occur in the pipe. The flow straightener was made by gluing 19 bubble tea straws together (11.5-mm OD tubes). The wall thickness and the length of these tubes were 0.3 mm and 0.127 m (2D), respectively. These specifications were

designed under the suggestion of International Standard ISO 5167-2 2003 (E). The designs of D and D/2 pressure tapping with flow straightener are shown Figure 4-7 for the upstream and Figure 4-8 for the downstream.

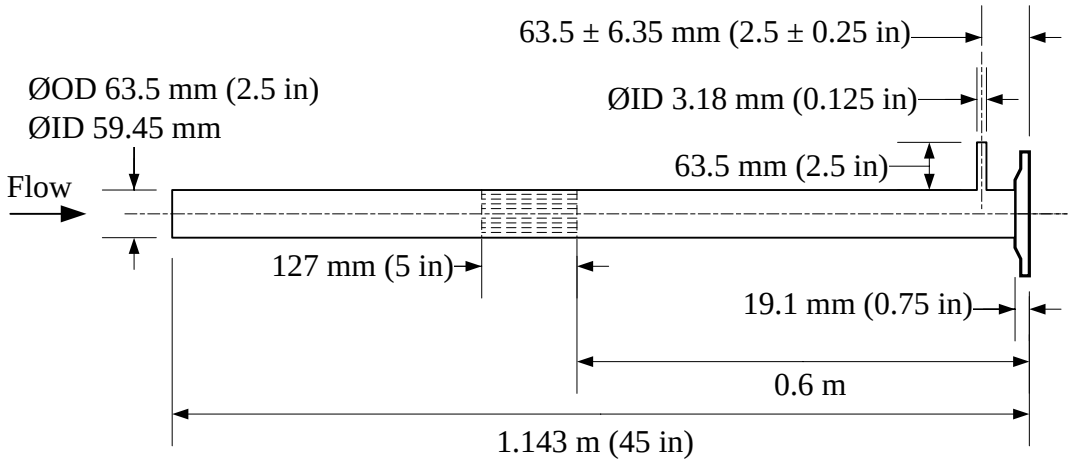

Figure 4-7: Upstream of D and D/2 pressure tapping design.

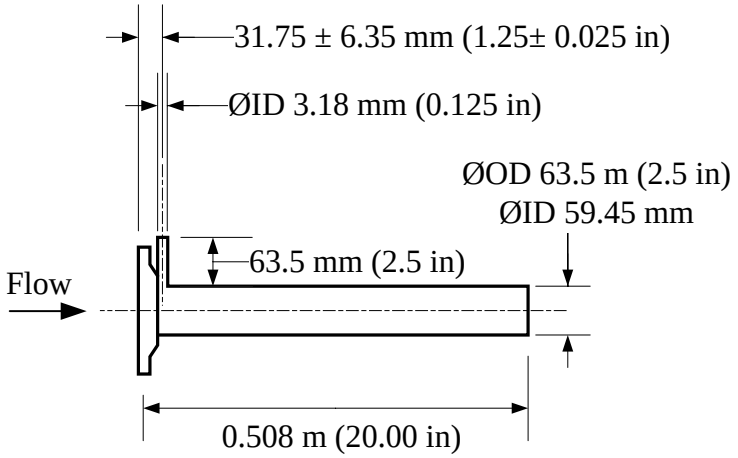

Figure 4-8: Downstream of D and D/2 pressure tapping design.

4.2.3 Air Flow Calculation

There were two pieces of air flow information required in the test. One was the air mass flow rate and the other one was the air velocity. The air mass flow rate was calculated by Equation 4-1 which was given by International Standard ISO 5167-1 2003 (E).

$$m_a = \frac{C}{\sqrt{1-\beta^4}} \times \varepsilon \times \frac{\pi}{4} \times d_o^2 \times \sqrt{2 \times \Delta p_o \times \rho}, \quad 4\text{-}1$$

where m_a is the mass flow rate of the air [kg/s],

C is the discharge coefficient of the orifice plate,

ε is the expansion factor of the air,

d_o is the diameter of the orifice in the plate [m],

Δp_o is the pressure difference across the orifice plate [Pa],

ρ is the air density [kg/m^3], and

β is the diameter ratio of the orifice to the pipe inside diameter.

If the air mass flow rate was known, then the air velocity could easily be calculated by Equation 4-2.

$$v = \frac{m_a}{A \times \rho} = \frac{m_a}{0.00278 \times \rho}, \quad 4\text{-}2$$

where v is the air velocity [m/s], and

A is the cross section of the pipe [m^2].

The discharge coefficient (C) is one of the parameters required for the air mass flow rate calculation. It is a function of Reynolds number (Re_D) which itself is dependent on the air mass flow rate. Hence, an iterative calculation for the mass flow rate was required instead of a direct calculation. The iterative calculation started by determining the expansion factor of the air (ε) which was a function of the diameter ratio (β) and the ratio of the downstream pressure (p_2) to the upstream pressure (p_1) from the orifice plate. The equation used for calculating ε is shown in Equation 4-3 (ISO 5167-1 2003 (E)).

$$\varepsilon = 1 - (0.351 + 0.256 \times \beta^4 + 0.93 \times \beta^8) \times \left[1 - \left(\frac{p_2}{p_1} \right)^{1/1.4} \right], \quad 4\text{-}3$$

Then, ε was used to calculate an invariant (A_n) by using Equation 4-4, which was the rearrangement of known variables from Equation 4-1 (ISO 5167-1 2003 (E)).

$$A_n = \frac{\varepsilon \times d^2 \times \sqrt{2 \times \Delta p \times p_1}}{\mu \times D \times \sqrt{1-\beta^4}}, \qquad 4\text{-}4$$

where μ is the absolute viscosity of air [N·s/m^2].

Then, the Reynolds number (Re_D) was determined by multiplying A_n by the initial guess of the discharge coefficient (C). For the first iteration, the initial guess of the discharge coefficient (C_1) was 0.5916. This initial guess was from the assumption that all the terms in the equation used for calculating the discharge coefficient (Equation 4-5) (ISO 5167-1 2003 (E)) were equal to zero ($\beta = 0$), except the first one. This assumption was not true. However, the value of C was corrected in later iterations.

Once the Reynolds number was obtained, it was used to re-calculate C again by Equation 4-5.

$$\begin{aligned} C = {} & 0.5961 + 0.0261 \times \beta^2 - 0.261 \times \beta^8 + 0.000521 \times \left(\frac{10^6 \times \beta}{Re_D} \right)^{0.7} \\ & + \beta^{3.5} \times \left(\frac{10^6}{Re_D} \right)^{0.3} \times \left(0.0188 + 0.0063 \times \left(\frac{19{,}000 \times \beta}{Re_D} \right)^{0.8} \right) \\ & + (0.043 + 0.080 \times e^{-10} - 0.123 \times e^{-7}) \times \left(\frac{\beta^4}{1-\beta^4} \right) \times \left(1 - 0.11 \times \left(\frac{19{,}000 \times \beta}{Re_D} \right)^{0.8} \right) \\ & - 0.031 \times \beta^{1.3} \times \left(\left(\frac{0.94}{1\text{-}\beta} \right) - 0.8 \times \left(\frac{0.94}{1\text{-}\beta} \right)^{1.1} \right) + 0.011 \times (0.75 - \beta) \times \left(2.8 - \frac{D}{25.4} \right). \end{aligned} \qquad 4\text{-}5$$

After the new C was determined, it was checked for convergence by comparing it with the discharge coefficient from previous iteration. If the difference between the new C (x^{th} iteration) and the previous C (x^{th}-1 iteration) was less than 1×10^{-n}, where n is the precision criterion and equal to seven in this study (chosen by the user), then the Re_D number and C from the x^{th} iteration was used for calculating the mass flow rate of the air (m_a). If the difference between them was more than 1×10^{-n}, C from x^{th} iteration was used to re-calculate Re_D to be used in the next iteration (x^{th} +1) and the process was repeated until convergence occurred. The details of the iterative calculation for the air mass flow rate are available in APPENDIX A.

From Equation 4-3 and Equation 4-5 which were used for calculating ε and C, it was noticed that changing the pressure ratio (p_2/p_1) changed ε and changing the Reynolds number changed C. According to the preliminary tests it was found that the change of ε over the pressure ratio range of 0.97 to 1 was less than 0.01 (0.9895 to 0.99834). when Reynolds number was changed from approximately 13,400 to 97,700, the corresponding changes in the values of the discharge coefficient, C, were from 0.669 to 0.648. Due to the small changes of ε and C over the test ranges for this experiment, they were assigned as fixed parameters which were equal to 0.995 and 0.65 for ε and C, respectively. Therefore, Equation 4-6 was used for calculating the mass flow rate.

$$m_a = \frac{0.65}{\sqrt{1-0.75^4}} \times 0.995 \times \frac{\pi}{4} \times 0.0445^2 \times \sqrt{2 \times \Delta p_o \times \rho}, \qquad 4\text{-}6$$

By setting ε and C as fixed parameters, the iterative calculation for the air mass flow rate was not necessary and was excluded from the fan control program. Consequently, the time that the control program took to processes the air mass flow rate calculation was reduced and the control system/program could monitor the system, report results, and response the command faster.

4.2.4 Atmospheric Pressure

The atmospheric pressure was used to calculate the air density which was also used in the mass flow calculation. The atmospheric pressure was read from the barometer in mmHg and then was inputted into the program. However, the reading obtained from the barometer needed correction for temperature (p_t) and gravity (p_g). The unit of measure also needed to be converted. Equation 4-7 was used to calculate the temperature-corrected barometer reading (Princo Instruments, INC. 1983). The equation was simplified for the calculation in the program. Equation 4-8 was used to calculate the gravity-corrected barometer reading (Princo Instruments, INC. 1983). The latitude used in the calculation was at 52°N. The last term of the equation was the interpolation of the gravity correction between 700 mmHg to 800 mmHg. After the barometer reading was corrected, it was used as the atmospheric pressure (p_{atm}). Lastly, Equation 4-9 was used to convert the units from mmHg to Pa.

$$p_T[\text{mmHg}] = p[\text{mmHg}] + p[\text{mmHg}] \times \left[\frac{(1 + 0.0000184 \times T[^\circ\text{C}])}{(1 + 0.0001818 \times T[^\circ\text{C}])} - 1 \right], \quad \text{4-7}$$

where p_T is the atmospheric pressure with the temperature correction [mmHg] and

T is the air temperature [ºC].

$$p_g[\text{mmHg}] = p_{atm}[\text{mmHg}] = p_t[\text{mmHg}] + \left(0.41 + (p_T[\text{mmHg}] - 700) \times \left(\frac{0.06}{100} \right) \right), \quad \text{4-8}$$

where p_g is the atmospheric pressure with the temperature and gravity correction [mmHg] and

p_{atm} is the atmospheric pressure with the temperature and gravity correction [mmHg].

$$p[\text{Pa}] = p_{atm}[\text{mmHg}] \times 133.32 \left[\frac{\text{Pa}}{\text{mmHg}} \right], \quad \text{4-9}$$

4.2.5 Air Density Calculation

Equation 4-10 was used to calculate the air density. This was simplified from the ideal gas law $p = \rho \times R \times T$, where R is specific gas constant for dry air which was 287.058 J/(kg×K), and T was the absolute temperature in Kelvin (Gerhart and Gross, 1985).

$$\rho \left[\frac{\text{kg}}{\text{m}^3} \right] = \frac{(p_{atm}[\text{Pa}] + p_1[\text{Pa}])}{287.058 \times (T[^\circ\text{C}] + 273.15)}, \quad \text{4-10}$$

where p_{atm} is the atmospheric pressure [Pa].

4.3 Line Pressure Measurement

A flexible tube was used for a conveying line in the experiment. The diameter and wall thickness of this flexible tube were 63.5 mm (2.5 inch) ID and 5 mm respectively. Elbow fittings having a bore size of 4.75 mm were adapted for use as static pressure taps, which were then used for obtaining line pressure. They were installed along the flexible

tube, sealed with silicone, and secured with pipe clamps. The diameter of each static pressure hole was 2 mm. They were counter bored to accept the fitting. To obtain the line pressure measurement, these static pressure taps were connected to pressure transducers by 4.76 mm × 7.94 mm OD tube (3/16" ID x 5/16"). These static pressure holes and static pressure taps were drilled and installed by following the suggestion of ANSI/AMCA 210-07 (2007). Figure 4-9 shows the details of the static pressure tap installation on the flexible tubes.

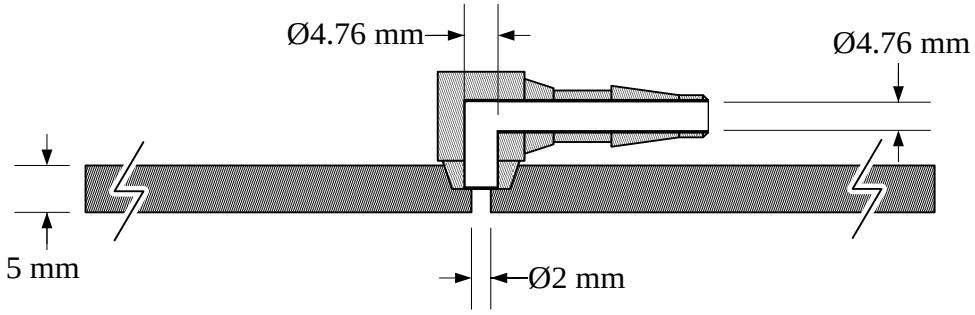

Figure 4-9: The details of static pressure taps and their installation which were on the flexible tube for observing the line pressure.

4.4 Data Acquisition System (DAQ)

In the experiment, two parameters were controlled and four parameters were monitored or measured. The control parameters were the air velocity and the material mass flow rate. The monitored or measured parameters were the atmospheric pressure, gauge pressure, difference in pressure along the conveying line, and the temperatures at the orifice plate and along the conveying line. The atmospheric pressure was read from the barometer mounted on the wall in the test area and was manually entered to the user interface. To retrieve the pressure information from the pressure transducers, the system required the analog current input module (NI9203: 8-Ch ±20 mA 16 bit Analog Input, National Instruments, Austin, Texas). For the temperature, the system required the thermocouple input model (NI 9211: 4-Ch ±80 mV 24-bit Thermocouple Input, National Instruments, Austin, Texas). The analog current output model (NI 9265: 4-Ch 20 mA 16-bit Analog Output, National Instruments, Austin, Texas) was used for the fan control current. The connections between sensing elements and modules are shown in

APPENDIX B. The stepper motor was controlled via RS-485 serial communication and used in-house LabVIEW drivers.

The DAQ was used for sampling pressure and temperature signals and controlling the fan control current and stepper motor. Control software was developed in LabVIEW software and used for controlling the DAQ. The following explanations are the details of the DAQ used in the test.

4.4.1 LabVIEW Programming

The user interface was developed using LabVIEW software (National Instruments, Austin, TX). In the program, there were three independent loops that ran in parallel. The first one was the pressure monitoring loop, the second was the fan control loop, and the last one was the stepper motor control loop. Before testing, the program required the operator to enter the atmospheric pressure. The atmospheric pressure had to be manually entered because the barometer did not have a DAQ function available. Once the program was started, the pressure monitoring loop ran rapidly. Then, the pressure readings and calculated air velocity were shown on the screen. The pressure monitoring loop was set as the first priority to run and was initiated every 500 ms. When the fan button was activated and the air velocity set point was entered, the system sent the fan control current to the fan drive based on the set air velocity. The priority of this loop was the second. It was set to initiate every second. This loop monitored the air velocity by obtaining the pressure and temperature readings and recalculating the air velocity. If the actual air velocity did not meet the set air velocity, the system adjusted the fan control current. When the fan button was deactivated the fan control current was set to zero and the loop was ignored. The stepper motor control loop was similar to the fan control loop. This control loop was the third priority to run and also initiated at every second. Figure 4-10 shows the flow chart of LabVIEW program developed for the test.

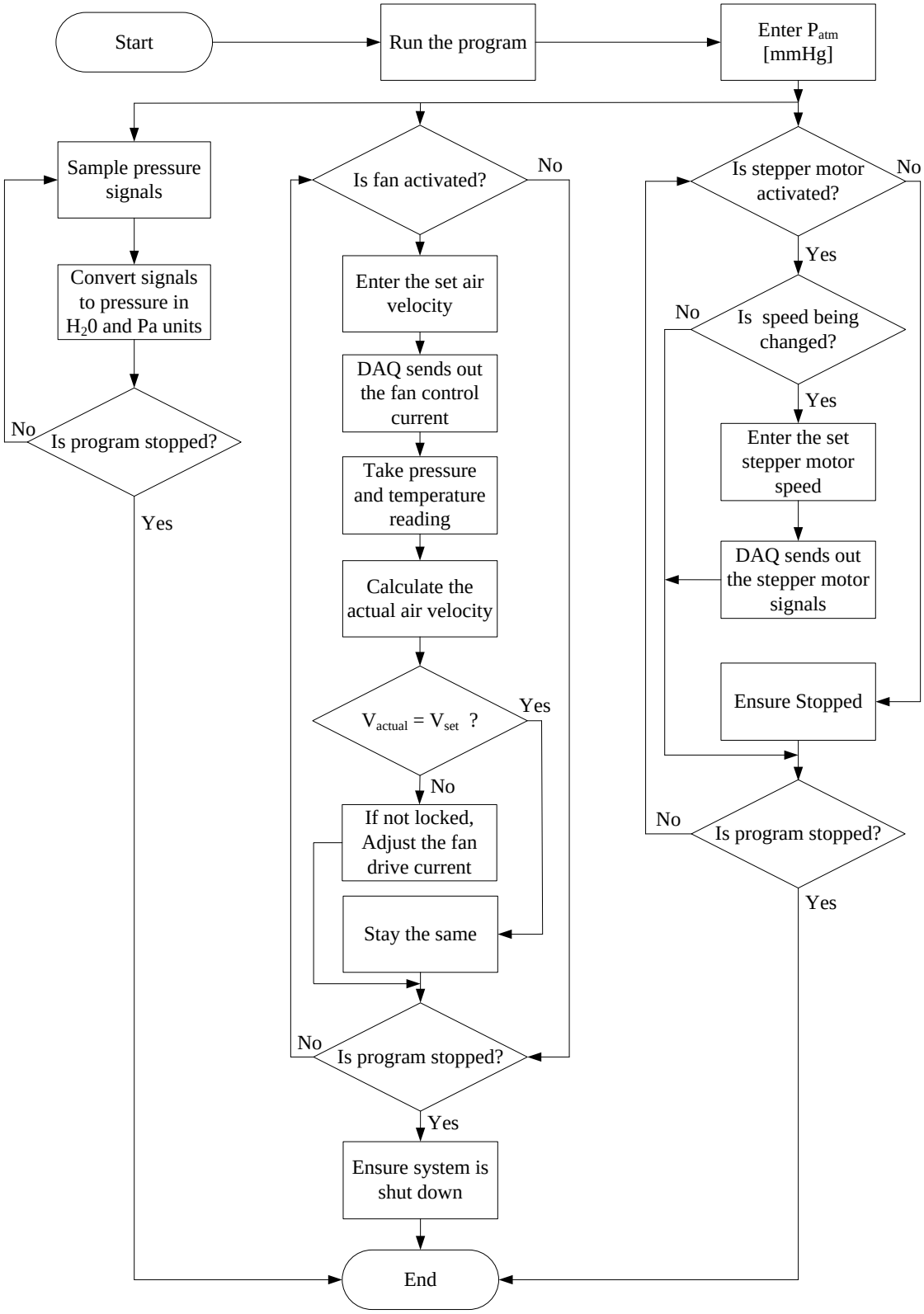

Figure 4-10: The flow chart of the LabVIEW program developed for the test.

4.4.2 Front Panel (User Interface)

Figure 4-11 shows the front panel of LabVIEW program used in the experiment. The screen was divided into seven sections: fan control, stepper motor control, pressure indicator, air information, material information, pressure and air velocity plot, and experimental diagram.

The fan control section was on the top left of the display. The main components of this section were the Run button (green), the Stop button (red), the Hold Drive Current buttons, and the Target Airspeed input block. The other important components were gain and current adjustment. The Hold Drive Current button was used to lock the air velocity after the set air velocity was achieved and stable. This reduced the fluctuation in the fan control signal due to the control scheme. When the drive current was set to hold but the air velocity was slightly different from the set air velocity, the drive current was manually adjusted by entering the change in current in the current adjustment block in units of one tenth milliamps (decimilliamps).

The stepper motor section mainly consisted of the run button (green), the stop button (red), and the motor speed entering block. These were used to turn the stepper motor on and off and to set the stepper motor speed. If there were any changes in this section, the program sent commands to the stepper motor through the serial communication cable. There were also other blocks such as Run Current, Hold Current, Acceleration and Deceleration. These values were set as default. This section was presented in the middle-left of the interface.

The pressure meter section was located at the bottom left of the screen. This section was used to display the pressure reads of each pressure transducer in mmHg and Pa. If the red lights on the meters were on, they indicated that those pressure transducers were operating at or over their operating ranges.

The top right section was for the air information and testing material information sections. In the air information section, there was the barometer reading block which required operators to enter the barometer reading in mmHg. This reading did not need any correction or conversion because these correction calculations were performed by the program. The calculated result was shown in the P_{atm} block. The air density, the total pressure drop across the elevation, and temperature readings were also displayed in this

section. There were three temperature readings that were monitored. The first one indicated the air temperature at the orifice plate. The second one indicated the air temperature downstream of the air cart simulator. The last one reported the laboratory environment temperature which was used for comparison with the other two temperature readings.

The last two sections were used for displaying the plots of the pressure readings and the actual air velocity and the pressure transducer location. For the pressure transducer location section, there was an experimental set up diagram which indicated the static pressure taps. The bottom of the diagram had blocks for entering the full ranges values of each pressure transducer in the system. If any pressure transducers were changed, the full range numbers were also changed so that the correct current-to-pressure conversions were applied.

Two file path controls were located near the top of the window. One was for the raw data file which recorded every test detail on the screen. This was on the left of the screen. The other one was for the data file which was on the right of the screen. Lastly, there was a green button in the middle of the screen beside the fan control section. If the button was pressed, all the information on the screen was recorded into those two file paths. The details of operating the front panel are explained in APPENDIX C.

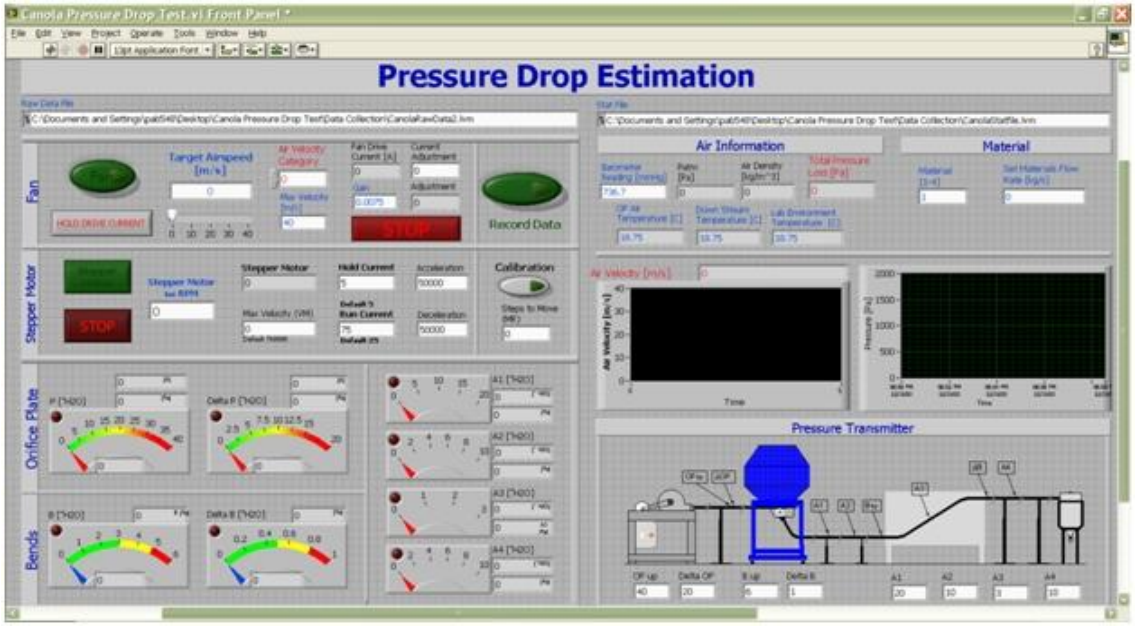

Figure 4-11: The front panel of LabVIEW program (user interface)

4.4.3 Calculations in LabVIEW Programs

Most values such as pressure readings, temperature, and actual air velocity shown on the front panel were converted or calculated by the program from the raw data. The following shows the details of the calculations in the program other than the calculations of the air flow in the previous section (4.2.3).

4.4.4 Pressure Signal Conversion

The DAQ system received current signals (4-20 mA) from the pressure transducers and converted those signals to the pressure readings in inches of water (in H_2O). Those were calculated by multiplying the received signal by 1000 mA/A and then subtracting 4 mA. After that, the results were divided by 16 and multiplied by the full scale range of the pressure transducers. This is shown in Equation 4-11.

$$p\left[\text{in } H_2O\right] = \frac{\text{current}\left[A\right] \times 1000\left[\frac{mA}{A}\right] - 4\left[mA\right]}{16\left[mA\right]} \times \text{Full Scale}\left[\text{in } H_2O\right]. \qquad 4\text{-}11$$

Then the pressure readings in inches of water from Equation 4-11 were multiplied by 249.1 Pa/″H_2O (Gerhart 1985) to convert them to Pascal unit. This conversion is shown in Equation 4-12.

$$p\left[Pa\right] = p\left[\text{in } H_2O\right] \times 249.1\left[\frac{Pa}{\text{in } H_2O}\right]. \qquad 4\text{-}12$$

4.4.5 Fan Calibration Equation

When the fan was operating, the program sent a 4-20mA control signal to the fan drive. If the fan was started from zero, the first fan control current sent out was estimated from the calculation based on the fan calibration equation which is shown in Equation 4-13. After the first loop of fan control was completed, the air velocity was regulated or adjusted according to the gain. At the beginning, the value of gain was set at around 0.007. Then it was decreased to around 0.003 when the air velocity was close to the set value. This helped the system to reach the set target faster.

$$\text{Fan Control Signal [mA]} = \text{Target Air Velocity}\left[\frac{\text{m}}{\text{s}}\right] \times 0.0003\left[\frac{\text{mA}}{\frac{\text{m}}{\text{s}}}\right] + 0.0044\,[\text{mA}] \quad \text{4-13}$$

4.5 Pneumatic Conveying System Control Panel

All electronic instruments and equipment were connected together at the control panel. The connection of modules and sensor elements and the overall control panel design schematic are shown in APPENDIX B. Pictures of the control panel which was developed for the pneumatic conveying system are shown in Figure 4-12 and Figure 4-13.

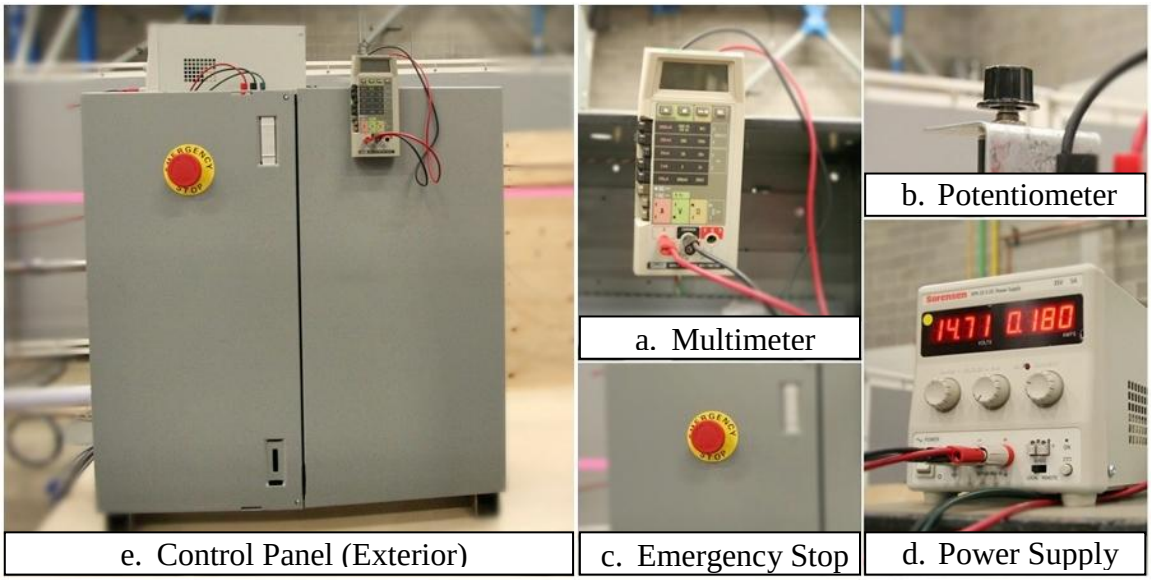

Figure 4-12: The exterior of the control panel

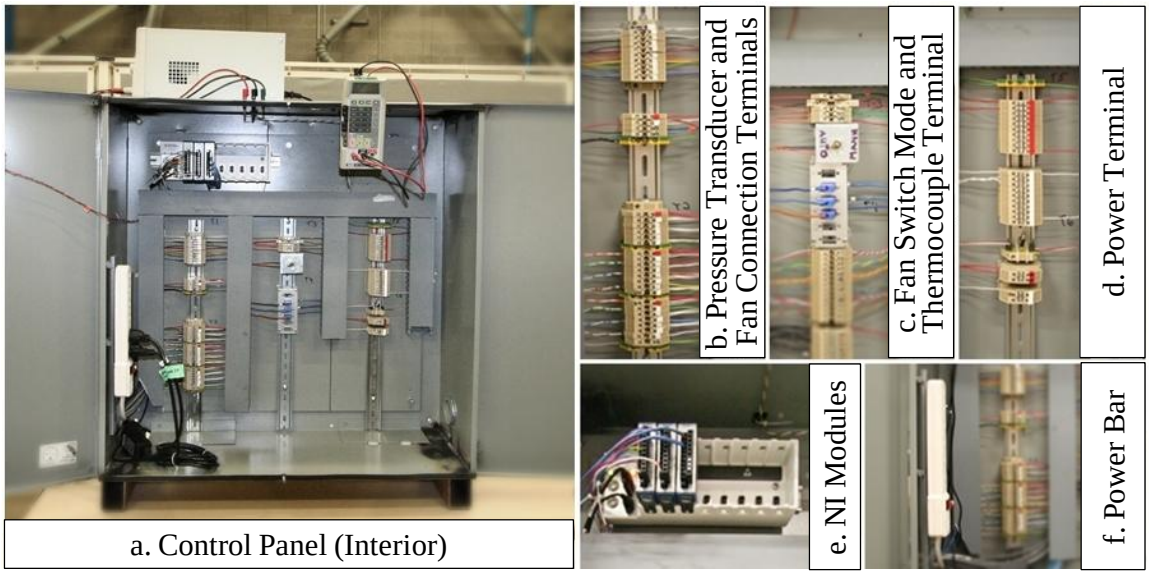

Figure 4-13: The interior of the control panel

5. INSTRUMENT CALIBRATION AND VALIDATION

In order to achieve accurate and reliable results, the measurement instruments were calibrated and validated. The metering system (roller) on the air cart simulator, pressure transducers, and thermocouples required calibrations. The orifice plate system required validation which was performed using a Pitot-static tube. The following are details of the calibrations and results.

5.1 Roller Calibration

The material mass flow rate was one of the main input (control) parameters in the study. This was controlled by rotating the roller in the metering system at a set speed (roller speed). In order to know the quantity of material dispensed from the tank at each roller speed (material mass flow rate), the rollers were calibrated for the material to be tested. There were two sets of calibrations. One was for all tested materials (first test) which were used in data collection set 1. Three different types of rollers were used for this calibration. The extra fine and fine rollers were used for testing canola and wheat, respectively. The extra coarse roller was used for the testing both chickpea and granular fertilizer. The roller calibration details and roller speed calculations/conversions can be seen in APPENDIX D and APPENDIX E, respectively.

The ranges of roller speed for the calibration were 4-24 rpm, 10-100 rpm, 25-65 rpm, and 2-75 rpm for canola, wheat, chickpea, and fertilizer, respectively. Those ranges were divided into five categories. The details of the ranges and intervals for the calibration can be seen in Table 5-1 and their calibration results are shown in Figure 5-1 and Table 5-2. From the calibration results, it was found that when the roller speed was low (about 50-60 rpm), the relationship between the material mass flow rate and the roller speed was linear. However, when the roller speed was high (above 50-60 rpm), the material mass flow rate started increasing disproportionately (non-linear). This was assumed to be a result of the materials not having enough time to fill the roller grooves while it was rotating and the roller pushing the materials away when it was operated at the high speed. This was the reason why the calibration data were fitted by the power equations with the exception of canola.

The test ranges used in this study were based on the actual seeding rate information recommended by the air seeding cart manufacturer combined with the information provided by several provincial agricultural Ministries gathered by Gervais (2011).

Table 5-1: The details of the roller calibration for tested material, data collection set 1.

Roller Type	Material Type	Roller Speed [rpm]	Roller Type	Material Type	Roller Speed [rpm]
Extra fine	Canola	4	Fine	Wheat	10
		9			33
		14			55
		19			78
		24			100
Extra coarse	Chickpea	25	Extra coarse	Granular Fertilizer	2
		35			20
		45			38
		55			56
		65			75

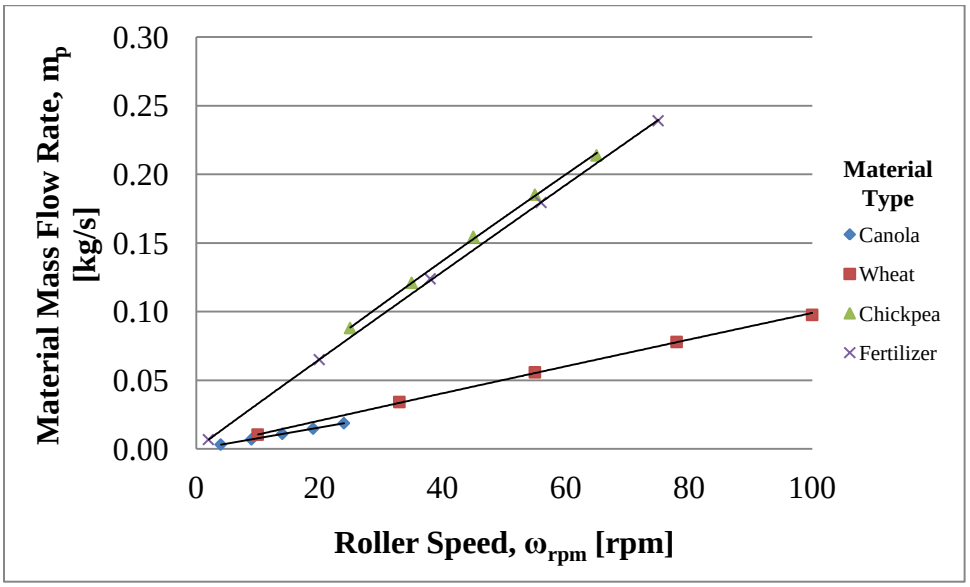

Figure 5-1: The calibration results for the data collection set 1.

Table 5-2: The calibration equations for the data collection set 1.

Material Type	**Calibration Equations**	**R^2**
Canola	$m_p = 0.0008\omega_{rpm}$ - 9E-06	0.9999
Wheat	$m_p = 0.0011\omega_{rpm}^{0.9752}$	0.9998
Chickpea	$m_p = 0.0044\omega_{rpm}^{0.9334}$	0.9996
Fertilizer	$m_p = 0.0034\omega_{rpm}^{0.9842}$	1

The second calibration was only for canola and was used for data set 2. The test range of the second data collection was larger than the range for data collection set 1, having roller speeds from (relatively) 1 rpm to 39 rpm. The extra fine roller was also used for this calibration but only at roller speeds higher than 4 rpm. For roller speeds less than 4 rpm, the quarter extra fine roller was used instead to decrease the discontinuity in dispensing which occurred when the roller operated at the low speeds. This roller was modified from the regular extra fine roller by filling the roller grooves with latex caulking which was wrapped by cloth tape. The details of the set roller speed and the results of the roller calibration for the second test are shown in Table 5-3 and Figure 5-2. Figure 5-2 shows the linear relationship between the material mass flow rate of canola and the roller speed. However, it was noticed that the results from the first calibration were a little bit different (less than 1 g/s) from the second calibration. The most likely reason for this difference is human error when the stepper motor was activated and deactivated. This human error was presented because pressing the button to start and stop the stepper motor was performed manually and thus the time for each calibration run could not be exactly the same. Other minor reasons that might have affected the difference in the calibration were the amount of seed in the tank and the set air velocity. The different amount of seed in the tank and the different set air velocity affected the amount of pressure which was exerted to press the materials down to the metering box. These influences were reduced by maintaining the same level of the seed in the tank and using the same set air velocity. As a result of this, all levels of the roller speed used in the second data collection were calibrated again.

Table 5-3: The details of the roller calibration for canola, data collection set 2.

Roller Type	Roller Speed [rpm]	Roller Type	Roller Speed [rpm]
Quarter extra fine	4	Full extra fine	9
	8		14
	12		19
	16		24
	-		29
	-		34
	-		39

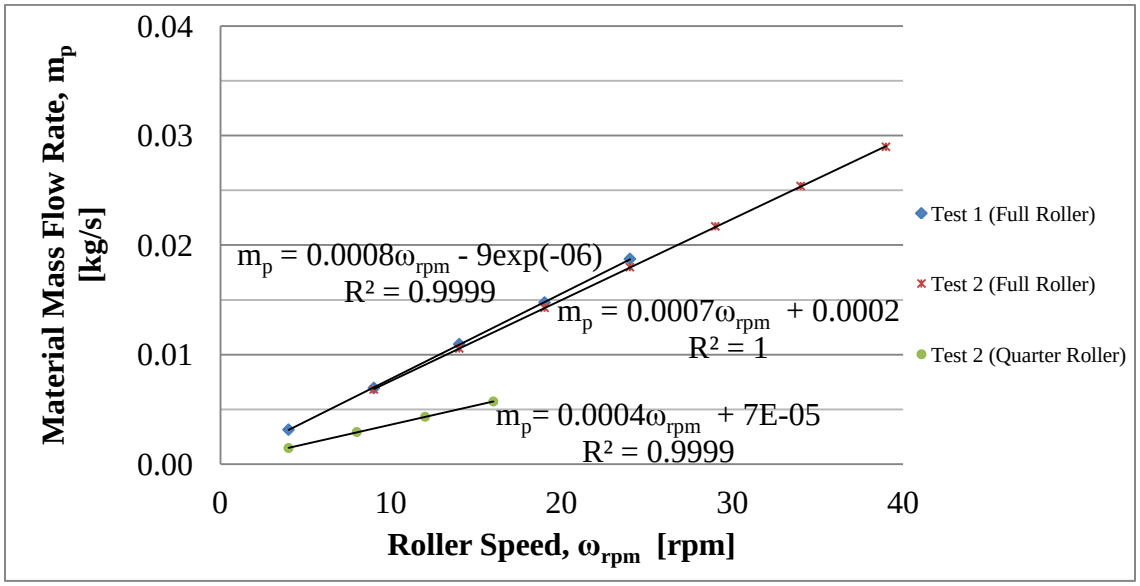

Figure 5-2: The calibration results for data collection set 2.

5.2 Thermocouple Calibration

The thermocouples used in the test were type-T thermocouples. Even though the LabVIEW program had a built-in function, the calibration to reset the ice point (0 ºC) was still required. To calibrate the thermocouples, each of their junctions was dipped into an ice bath which had water and ice mixed well together (slush) and this temperature was recorded as the reference temperature by pressing the calibration button as shown in Figure 5-3. This was easily accomplished because the LabVIEW program had a built in

function provided for this. The uncertainty of this thermocouple type was about 0.4 ºC (NIST, 2011).

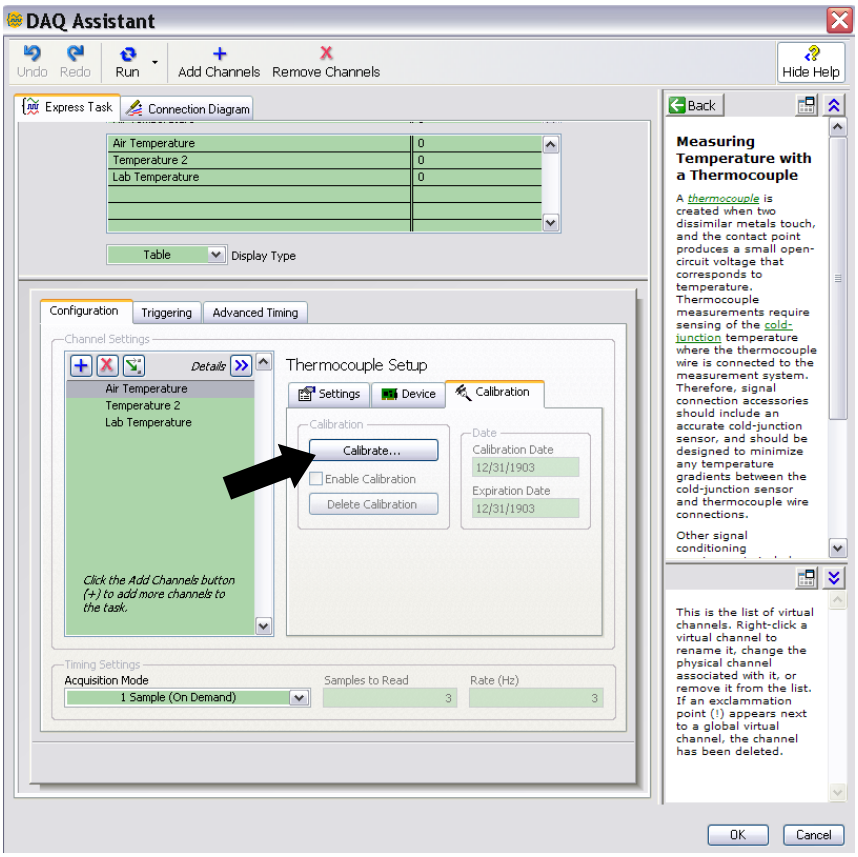

Figure 5-3: The DAQ Assistant Express VI for the thermocouple.

5.3 Pressure Transducer Calibration

The calibration for the pressure transducer could be done in two ways. The first was by determining the calibration equations for each pressure transducer. The second was by adjusting the span and zero on the pressure transducers. All the pressure transducers used in the study were calibrated by using the second method. As a result, when the pressure transducers were changed, the operator did not have to change the calibration equations in the LabVIEW program. The full operating range numbers on the front panel needed to be changed. Figure 5-4 shows the pressure transducer calibration schematic. This was performed in the Wind Tunnel Laboratory at the Department of Mechanical Engineering, using the pressure regulators, a Druck precision pressure indicator, and a +/- 20 in of water Manometer. The pressure which was used for

calibration was generated by the pressure regulators. The Druck precision pressure indicator was used for the precision pressure adjustment. The Meriam manometer +/- 20 inch of water was used as a reference pressure for calibrating the pressure transducers.

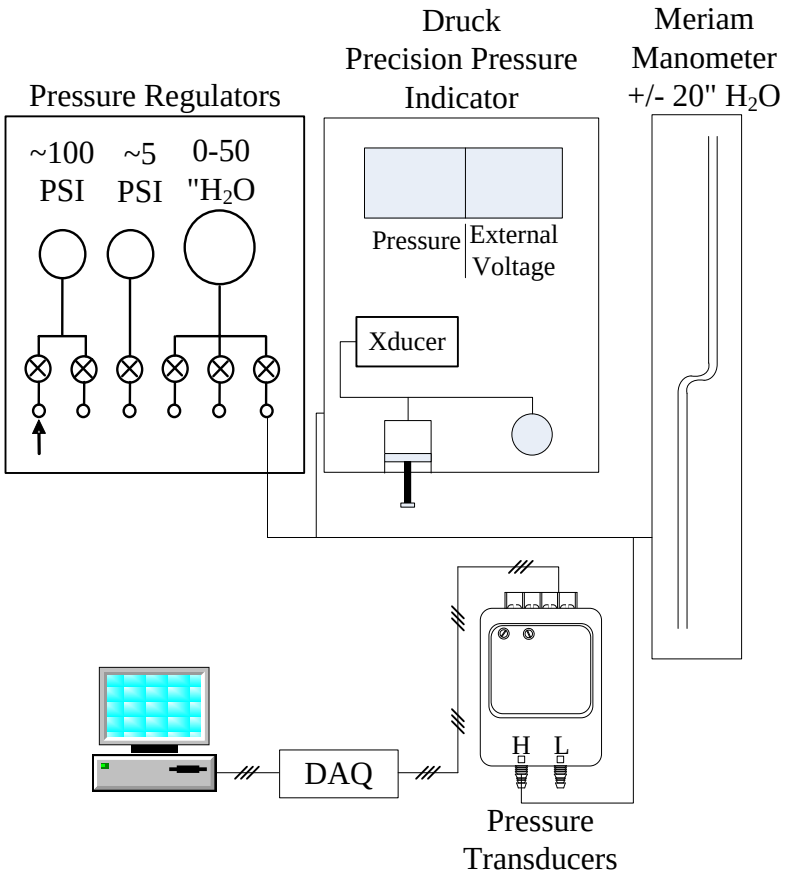

Figure 5-4: The pressure transducers calibration schematic

5.4 Air Flow Validation

Air velocity was another main control parameter. It was necessary to ensure that the measurement from the orifice plate was accurate and reliable. A Pitot-static tube was selected for verifying the measurement received from the orifice plate. This was achieved by using the traverse method suggested by ASHRAE (2005). The air flow test set up and the traverse diagram are shown in Figure 5-5 and Figure 5-6.

To obtain the air flow information for the validation, the program was set to read and average information from the pressure transducers for 10k samples at 1 kHz. This meant that each data point was the average for the pressure information over 10 seconds.

The data were recorded for a minute when the air velocity reading from the orifice plate was stable for at least 30 seconds. Table 5-4 shows the validation result of the orifice plate which was verified by using the Pitot-Static probe. The result shows that the measurement from using the orifice plate was similar to the measurement from the Pitot-Static probe, 21.25 m/s and 21.27 m/s, respectively. According to these results, it was concluded that the orifice plate used for measuring the air flow in the experiment operated properly. The raw data for the air flow validation can be seen in APPENDIX F.

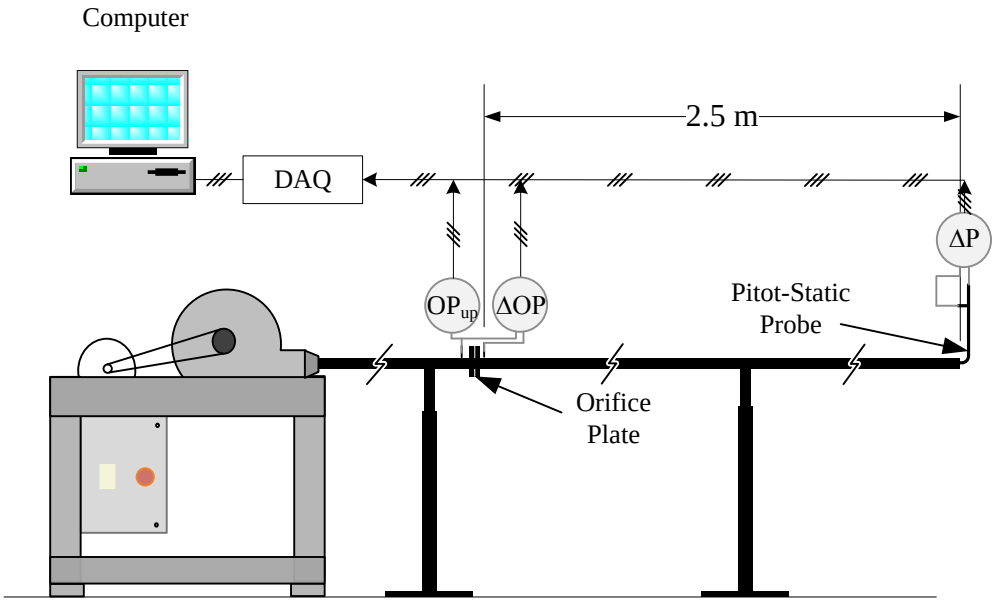

Figure 5-5: The schematic of the air flow validation set up

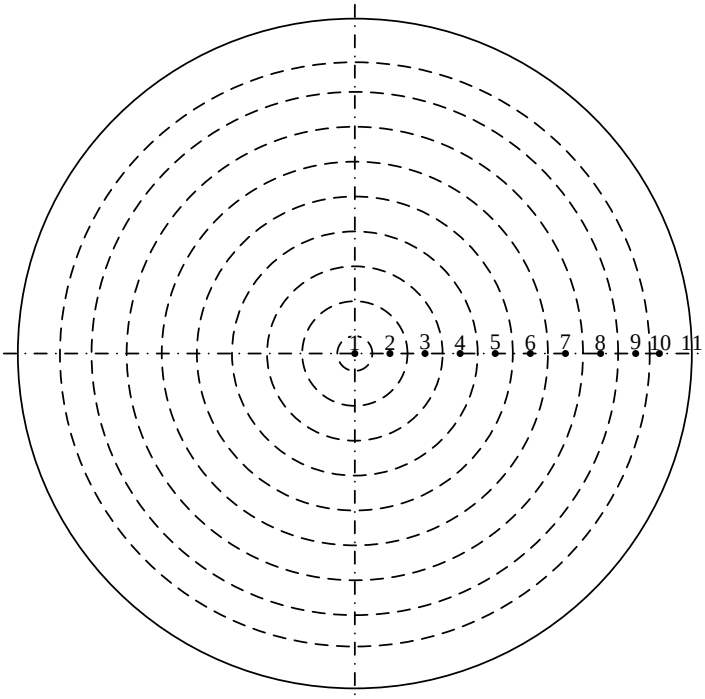

Figure 5-6: The traverse diagram for the orifice plate validation

Table 5-4: The comparison between the measurement results from the orifice plate and the Pitot-static tube

Order	Data				Calculation (Pitot-Static Tube)			
	r [mm]	p_{total} [Pa]	$v_{Orifice}$ [m/s]	v_{Pitot} [m/s]	$r_{interpolated}$ [mm]	dr [mm]	$v_{interpolated}$ (v_{in}) [m/s]	$Q=2\times\pi\times v_{in}\times r\times dr$ [m^3/s]
1	0	360	21.3	25.1	0.750	1.50	25.1	0.000190
2	3	358	21.3	25.1	3	3	25.1	0.00142
3	6	352	21.3	24.8	6	3	24.8	0.00281
4	9	340	21.3	24.4	9	3	24.4	0.00414
5	12	326	21.3	23.9	12	3	23.9	0.00541
6	15	306	21.2	23.2	15	3	23.2	0.00655
7	18	287	21.2	22.4	18	3	22.4	0.00761
8	21	267	21.2	21.6	21	3	21.6	0.00856
9	24	246	21.2	20.8	23.7	2.47	20.9	0.00766
10	25.9	231	21.2	20.1	27.4	4.79	18	0.0148
11	29.7	0	0	0	Sum of Q			0.0591
					Area [m^2]			0.00278
					V_{avg} [m/s] Pitot-Static (Q/A)			21.3
					V_{avg} [m/s] Orifice			21.2

6. EXPERIMENTAL DESIGN

Two phases of the experiment were undertaken. All the required testing materials (canola, wheat, chickpea, and granular fertilizer) were tested in the first set. Once these data were analyzed and development of the model was attempted, it was found that the data should have been collected in a different way to better facilitate model development. If the data were collected by categorized air velocity instead of the material mass flow rate, a model could be established which would give better results. Moreover, it was also found that the fan capacity was limited, most likely due to the losses in the orifice plate and losses in the reducer coupling between the fan and the pipe. As a result, only the test of canola could be completed across a full range of air velocities and product rates.

For these reasons, the second data collection was required and canola was the only material tested. After the model was successfully developed, the model was applied to the first data set to test its applicability. The following are details of the experimental design for those two tests.

6.1 Data Collection

In order to collect data, control parameters had to be established. There were two control parameters in this research. One was material mass flow rate and the other was air velocity. The details of the data collections are described below.

6.1.1 Data Collection Set 1

The ranges of the material mass flow rates for the tested materials were estimated based on a tractor's ground speed, width of the tilling implement (air hoe drill) per run, field seeding rates, and the calibration equations for each tested material. The details of these calculations are shown in APPENDIX E.

The minimum conveying air velocities of each material were determined by dispensing materials to the air stream at the different air speeds and ensuring there was no material building up at the bottom of the hose. After the minimum conveying air velocities were found, they were multiplied by 1.5 to obtain the maximum conveying air velocities. It was multiplied by 1.5 to observe the pressure loss between the minimum

conveying air flow up to 150% of the minimum conveying air flow. Then, the ranges of the air velocity were divided into five equal intervals (five categories) for each product. The design control parameters of data collection set 1 are shown in Table 6-1.

Table 6-1: The test condition of the control parameters for data collection set 1.

Material	Roller Type	Roller Speed [rpm]	Mass Flow Rate Category	Mass Flow Rate [kg/s]	Air Velocity [m/s]				
					1	2	3	4	5
Canola	Extra fine	4	1	0.003	9	10.5	12	13.5	15
		9	2	0.007	10	11.5	13	14.5	16
		14	3	0.011	10	11.5	13	14.5	16
		19	4	0.015	10	11.5	13	14.5	16
		24	5	0.019	11	12.5	14	15.5	17
Wheat	Fine	10	1	0.010	15	17	19	21	23
		33	2	0.034	19	22	25	28	31
		55	3	0.056	21	24	27	30	33
		78	4	0.078	23	26	29	32	35
		100	5	0.098	25	28	31	34	37
Large Kabuli Chickpea	Extra Coarse	25	1	0.088	25	28	31	34	37
		35	2	0.121	27	30	33	36	39
		45	3	0.154	29	32	35	38	41
		55	4	0.185	31	34	37	40	43
		65	5	0.214	32	34	36	38	40
Granular Fertilizer	Extra Coarse	2	1	0.007	15	17	19	21	23
		20	2	0.065	20	22.5	25	27.5	30
		38	3	0.124	25	28	31	34	37
		56	4	0.179	28	31	34	37	40
		75	5	0.239	31	33	35	37	39

Data were collected in triplicate for data set 1. Each collection had their control parameters varied in different orders. The first data collection was started from the lowest material mass flow rate and lowest air velocity. After that the air velocity was increased. When the air velocity reached the fifth category (highest air velocity), the material mass flow rate was increased to the next category. This was continued until both the test material mass flow rate and the air velocity were in their highest category. The diagram of the test direction of the first collection can be seen in Figure 6-1a. For the second

collection, the test was started in the opposite direction of the first one with the highest material mass flow rate and highest air velocity. Following this, the air velocity was decreased. The material mass flow rate was lowered when the air velocity met the lowest category. The second collection finished at the lowest material mass flow rate and the lowest air velocity. Figure 6-1b shows the test direction of the second data collection. The last collection was started from the highest mass flow rate of the materials with the lowest air velocity. Then, the mass flow rate of the material was decreased. When the material mass flow rate reached the lowest rate, the air velocity was increased. Then, the material mass flow rate was also increased. The air velocity was increased again when the material mass flow rate reached the last category. This was continued and finished at the highest air velocity and the lowest material mass flow rate. The test direction diagram of the third collection can be seen in Figure 6-1c.

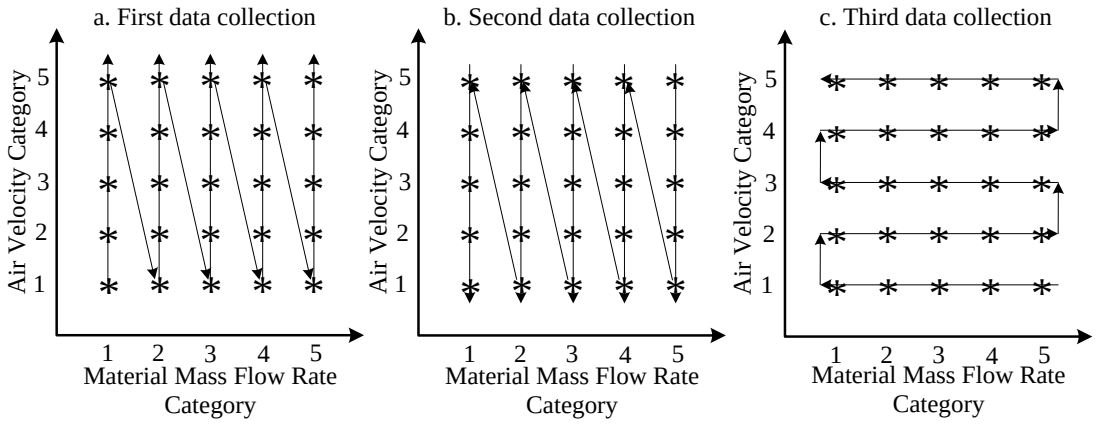

Figure 6-1: The directions of the first (a), second (b), and third (c) data collections

To collect the first data set, the program was set to read and average information from the pressure transducers for 250 samples at 1 kHz. This meant that each data point was the average of the pressure information over a quarter of a second. At each tested condition, the data were recorded for 30 seconds. Two averaged data points were collected every one second.

6.1.2 Data Collection Set 2

Data collection set 2 focused only on canola. The range of the control parameters was expanded from the previous data collection. The minimum material mass flow rate of the canola was decreased from 0.0031 kg/s to 0.0015 kg/s. This was less than half of the previous test. The maximum material mass flow rate was increased to almost twice as much as the previous test, from 0.0187 kg/s to 0.0290 kg/s. The material mass flow rate was divided into eleven categories. The air velocity range was changed from 9-17 m/s to 9-33 m/s. This was divided into 9 categories. The direction for collecting the data for all three data collections in this set is shown in Figure 6-2. The first condition was at the lowest air velocity and the lowest material mass flow rate. Then the material mass flow rate was increased until the highest category. After that, the air velocity was increased to the next category. These were performed until the highest air velocity and the highest material mass flow rate categories were completed. The details of the control parameters for data collection set 2 are illustrated in Table 6-2. These data were also collected in triplicate. Two full collections were obtained for the training set at all conditions listed in Table 6-2 except at the mass flow rate category 8-11 and at the air velocity category 1 in which case the air velocity was not sufficient for conveying those amounts of material. A third partial collection was performed for the validation data set and only the shaded conditions were tested.

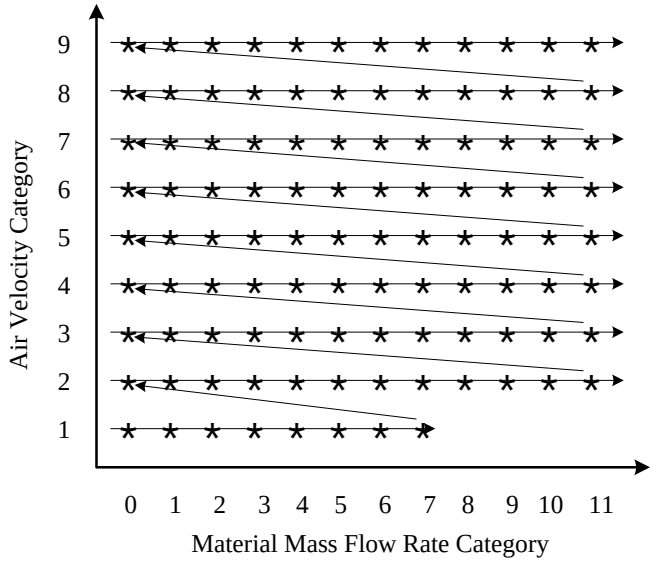

Figure 6-2: The directions of data collection set 2

Table 6-2: The test condition of the control parameters for data collection set 2. For the training set, all conditions were tested. For the validation set, only data of the shaded conditions were collected.

Roller Type	Mass Flow Rate Category	Roller Speed [rpm]	Mass Flow Rate [kg/s]	Air Velocity [m/s]								
				1	2	3	4	5	6	7	8	9
Quarter extra fine	0	0	0	10	11.5	13	14.5	16	19	23	28	33
	1	4	0.002	10	11.5	13	14.5	16	19	23	28	33
	2	8	0.003	10	11.5	13	14.5	16	19	23	28	33
	3	12	0.004	10	11.5	13	14.5	16	19	23	28	33
	4	16	0.006	10	11.5	13	14.5	16	19	23	28	33
Full extra fine	5	9	0.007	10	11.5	13	14.5	16	19	23	28	33
	6	14	0.011	10	11.5	13	14.5	16	19	23	28	33
	7	19	0.014	10	11.5	13	14.5	16	19	23	28	33
	8	24	0.018	-	11.5	13	14.5	16	19	23	28	33
	9	29	0.022	-	11.5	13	14.5	16	19	23	28	33
	10	34	0.025	-	11.5	13	14.5	16	19	23	28	33
	11	39	0.029	-	11.5	13	14.5	16	19	23	28	33

For the second data collection set, the information from the pressure transmitters were sampled at 500 Hz with 1000 samples read. This meant that each data point was the average of the pressure information gathered for two seconds. At each tested condition, data were collected for two minutes. The data were collected longer if the air velocity was fluctuating. According to this set up, the raw data should have contained less noise and at least 60 raw data points for each tested condition. After the raw data were collected, the data were then scanned and filtered again by using the air velocity as the reference. If the actual air velocities were 2% more or less than their set air velocities, then those data points were not used for the initial model development.

6.2 Test Procedure

Even though the tested materials and conditions were different, the procedure of testing and collecting the data remained the same. Before the tests were performed, the system was checked for loose hose connections and disconnected wires on the pressure transducers. The pressure transducer log book was updated and the tested conditions were recorded. This was helpful when errors were found and more information was needed to

track them down. After the testing materials were loaded into the tank and the system and LabVIEW program were ready, the atmospheric pressure (from the barometer) and the test information (such as control parameter categories and tested information) were entered to the program. The next step was to turn on the fan. The fan velocity was varied due to the test conditions. Before introducing the tested materials to the conveying line, the pressure information due solely to air was recorded. Then, the tested materials were introduced to the system. The dispensing rate was also varied based on the designed test conditions. Once the air velocity was steady after the material was dispensed to the conveying line, the pressure information along the system was record. The data were recorded for 30 seconds for data collection set 1, and for two minutes for data collection set 2. Then the control parameters were changed to the next test condition according to the test trajectories. This was continued until the test was finished. The details of operating the different parts of pneumatic conveying system, such as the fan and front panel operations are explained in APPENDIX C.

7. EXPERIMENTAL RESULTS AND ANALYSIS

7.1 Experimental Result

The three parameters for the study were material mass flow rate, air velocity, and pressure drop across the elevation in the conveying line. The first two parameters were the control parameters and the third was the observed parameter. In this study, it was assumed that the tested materials were dispensed continuously to the system at the constant rate to which it was set. The test results from the first and second collection are shown in the sections below. The summarized data can be seen in APPENDIX G.

7.1.1 Data Set 1

Data set 1 was collected and recorded in triplicate at the rate of two data points per second for 30 seconds. There were 25 test categories. Those categories were tested with the air only and with the tested material conditions. After the data were collected, the data from all three collections for each tested material were combined to observe their variability and distribution.

The total numbers of data points collected for canola, wheat, chickpea, and fertilizer were about 9,600, 8,800, 5,370, and 7,500, respectively. Based on the experimental design, each tested material was supposed to have approximately 9,000 data points. Some test categories could not be accomplished due to air flow limitations at the high material mass flow rate and air velocity test conditions of chickpea and fertilizer. As a result of this, fewer points could be collected.

After the data were combined, their statistical summaries were plotted in a box-and-whisker plot. According to the large spread of the overall pressure drop information and test conditions, only sample data from each tested material were used to illustrate the variability and the distribution of the pressure loss. The pressure information was originally collected in Pa, but then was changed to kPa to facilitate data analysis and the model development. On the diagrams, the pressure loss is presented on the y-axis. The typical material mass flow rates and set air velocities are presented as categorical variables on the x-axis at the top and the bottom of the diagrams, respectively. Two typical material mass flow rates and three set air velocities from those two material mass

flow rates were chosen and presented in diagrams. The pressure losses due to the air only for all velocities chosen from those two material mass flow rates were also presented together in 0 kg/s category. The box-and-whisker plots for those tested materials are illustrated below.

Figure 7-1 shows the box-and-whisker plot for canola. It was noticed that the distribution of the pressure loss for canola at each test condition appear normally distributed. This was seen from their medians which were at the middle of the boxes. The diagram also shows the variability of pressure losses which were relatively small, especially at the low set air velocity and low material mass flow rate. It increased slightly as the material mass flow rate and set air velocity increased. Canola was only the test that had small variations of the pressure loss compared to the rest of the tested materials. This was because canola size and the mass ratio (material/air flow rate) were smaller than the other materials.

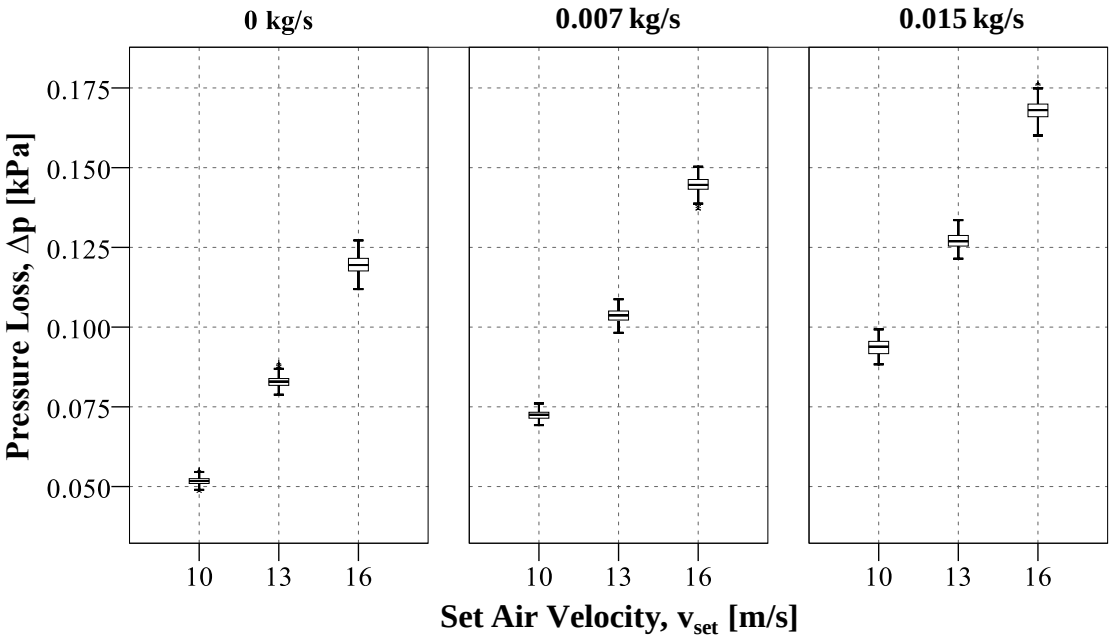

Figure 7-1: The box-and-whisker plot of typical data for canola, data set 1

Figure 7-2, Figure 7-3, and Figure 7-4 show the box-and-whisker plots for typical data from wheat, chickpea, and fertilizer, respectively. From the diagrams, it was seen that the distribution of the pressure loss for those three materials were not as normally distributed as canola. The variation of the pressure loss also varied as the material mass

flow rate and the set air velocity were changed. The variation and the distribution of the data were very small when there was no material (0 kg/s) except for chickpea. The reason for the effects on the data distribution and variation was the fluctuation in the air velocity which occurred when the airstream was interrupted. There were three main factors which would cause the unsteady air velocity. The first one was that sometimes dramatic changes in the air temperature happened when the laboratory's main door (Hardy Lab) was opened (cold winter days). Second was the geometry of the tested materials. The small and round materials seemed to have less influence to the air flow fluctuation than the elongated or the bigger materials. The final reason that possibly had an effect on the air flow stability was the discontinuity of dispensing tested materials. This would be noticed easier with the extra coarse roller. Different materials would have different reasons that would cause the air velocity to be unsteady. For example, the change in the pressure loss variation of wheat may be from its geometry. This was because wheat turned or rotated when it was introduced to the air flow and when the transport direction changed.

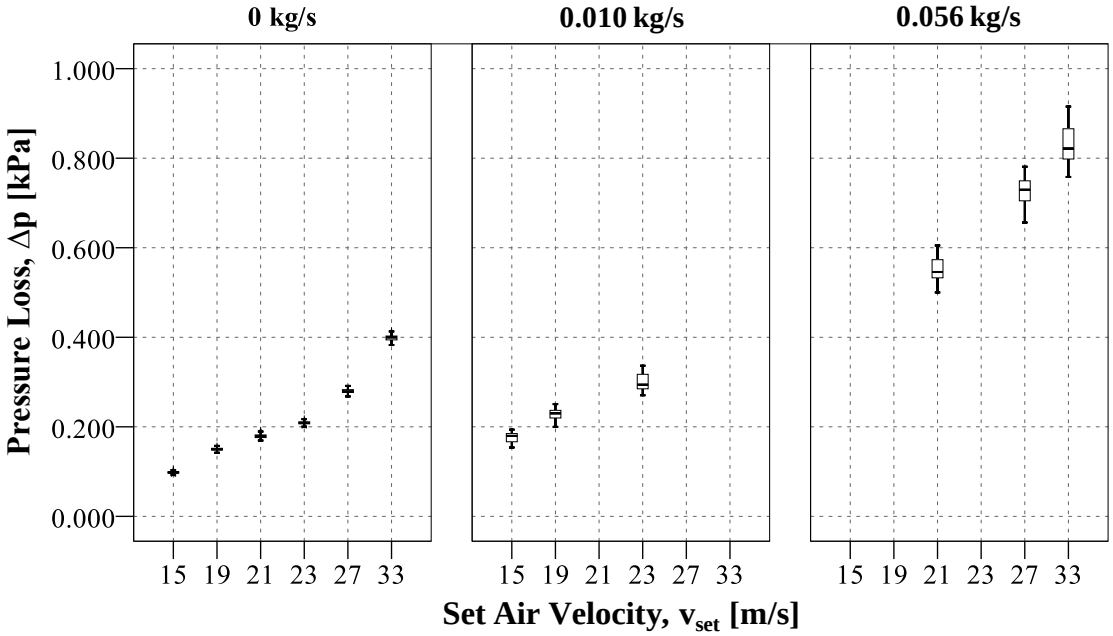

Figure 7-2: The box-and-whisker plot of typical data for wheat, data set 1

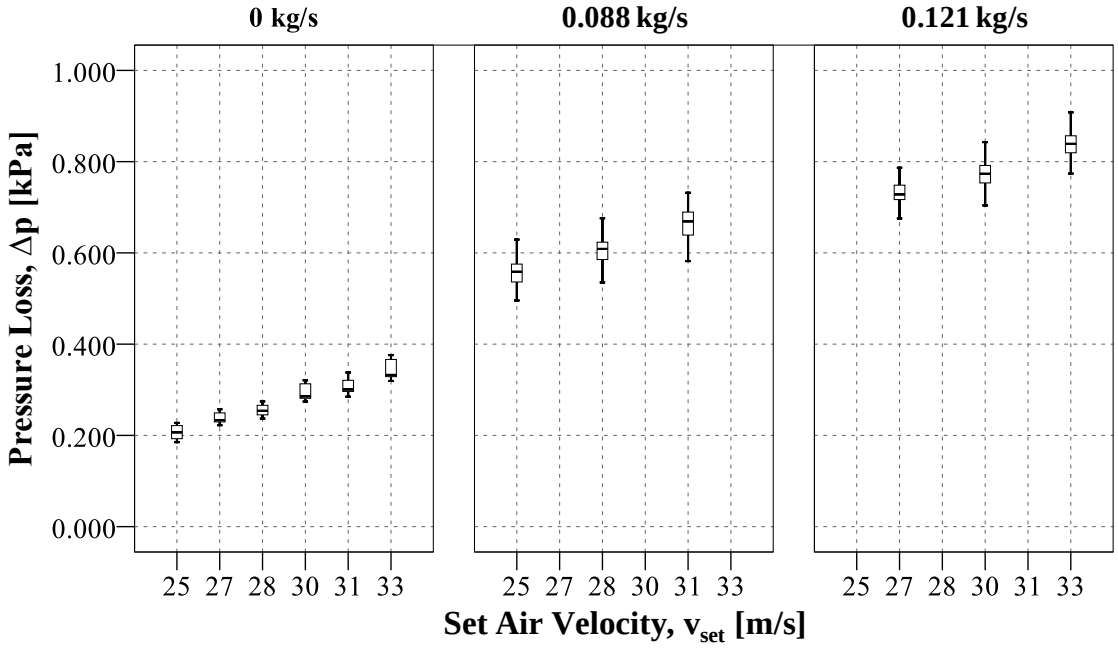

Figure 7-3: The box-and-whisker plot of typical data for chickpea, data set 1

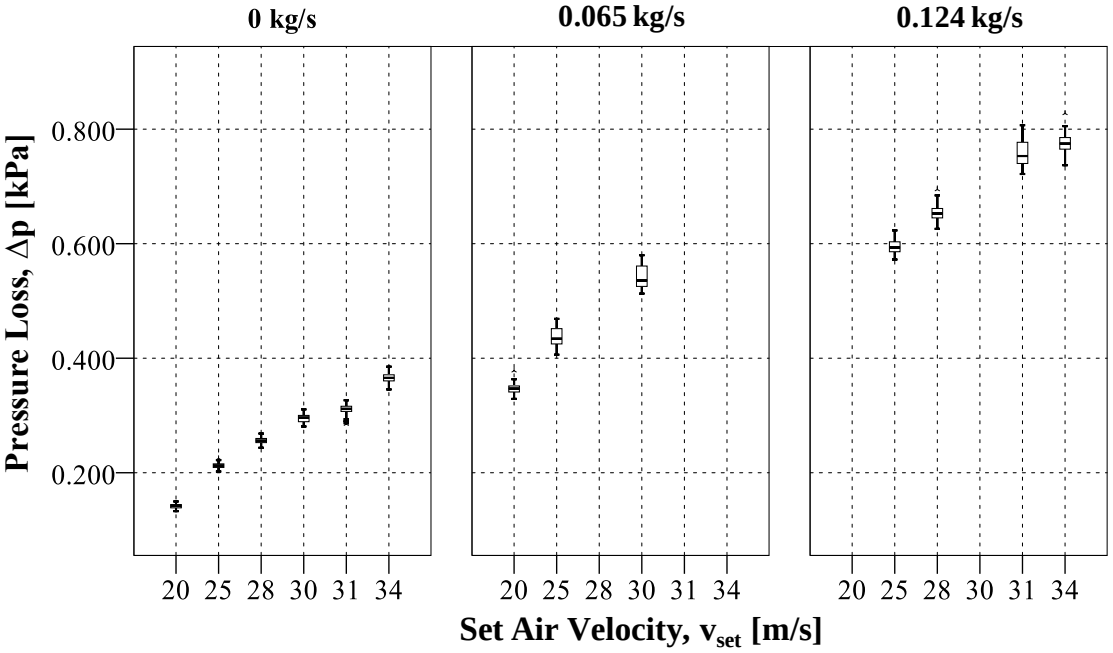

Figure 7-4: The box-and-whisker plot of typical data for fertilizer, data set 1

7.1.2 Data Set 2

The data collection of set 2 was focused only on canola with the expansion of the control parameters from the data collection of set 1. The data in set 2 were collected in three sets. Then they were combined and processed the same way as the data in set 1. The total number of data points for the data set 2 was around 14,800 points. The typical result data are presented in the box-and-whisker plot, Figure 7-5.

The diagram shows the variation and distribution of the pressure loss across the elevation for canola from the second data collection. It was clearly seen that the variation of the pressure loss at different test conditions was comparatively small. This was because the variation of the air velocity was purposely controlled in the ranges of ±2% of the set air velocities. Even though the air velocity was controlled, the distribution of the pressure loss for some test conditions was not normally distributed. However, the distribution of the data did not affect the quality of the mass flow estimation model development as the variation of the data did.

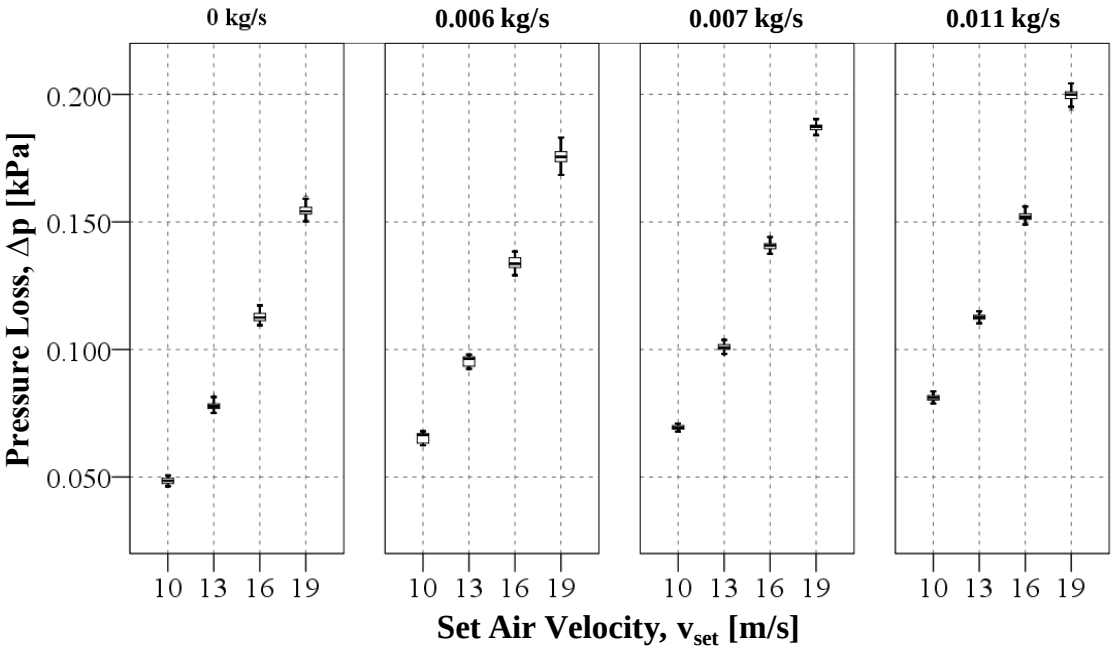

Figure 7-5: The box-and-whisker plot of typical data for canola, data set 2

After both data set 1 and set 2 were examined for their variability and distribution, the data were analyzed and used for the material mass flow rate estimation model in the following section.

7.2 Data Analysis and the Preliminary of Model Development

From the experimental results, it was observed that the pressure drop increased when the material mass flow rate increased. The pressure drop also increased when the set air velocity increased. These observations followed the general expectations when the experiment was designed.

Later, the data set 1 from all four tested materials (canola, wheat, chickpea and fertilizer) was combined together. The data were then rearranged in the relationship between pressure drop and mass flow ratio, which was the ratio of the material mass flow rate to the air mass flow rate (shown in Figure 7-6).

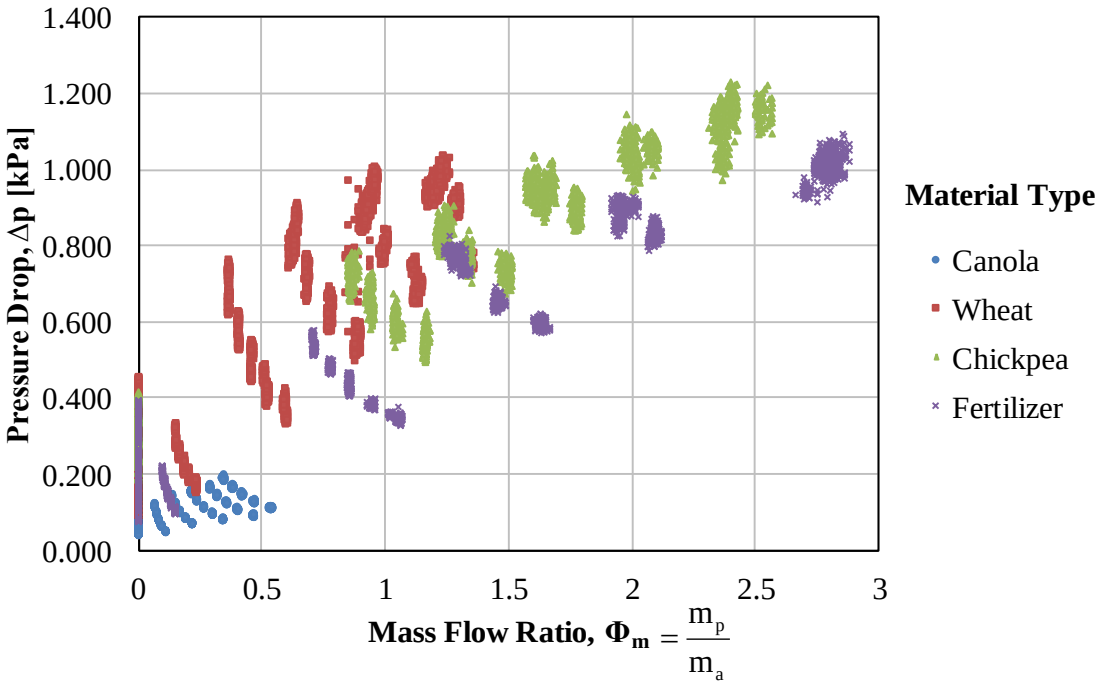

Figure 7-6 The relationship between pressure drop and mass flow ratio (the ratio of the material mass flow rate to the air mass flow rate) for canola, wheat, chickpea, and fertilizer combined together from data set 1

From the graph (Figure 7-6), it was seen that the data were clustered or grouped together. These clusters or groups of data arose due to their test conditions between the

material mass flow rate and the air velocity. It was also seen that those clusters or groups of data appeared to form their series of data according to their set material mass flow rate. These phenomena were easier to notice from the canola's results which are presented with the blue dots. The data that are presented on the pressure loss axis (y-axis) indicated the pressure losses occurred from the air velocity only (at material mass flow rate of 0 kg/s). This seemed like they were proportionally varied according to the conveying air velocities. Furthermore, there were some clusters of data which had a bigger spread and did not trend to form their series. This was because the system could not perform those test conditions (air velocity could not be attained).

Canola was the only material which had an attainable full range of air velocities. It was selected to be the focus case for developing the model. The test results from canola were the only ones re-plotted and shown in Figure 7-7. The fit equations from Figure 7-7 were put together and shown in Table 7-1.

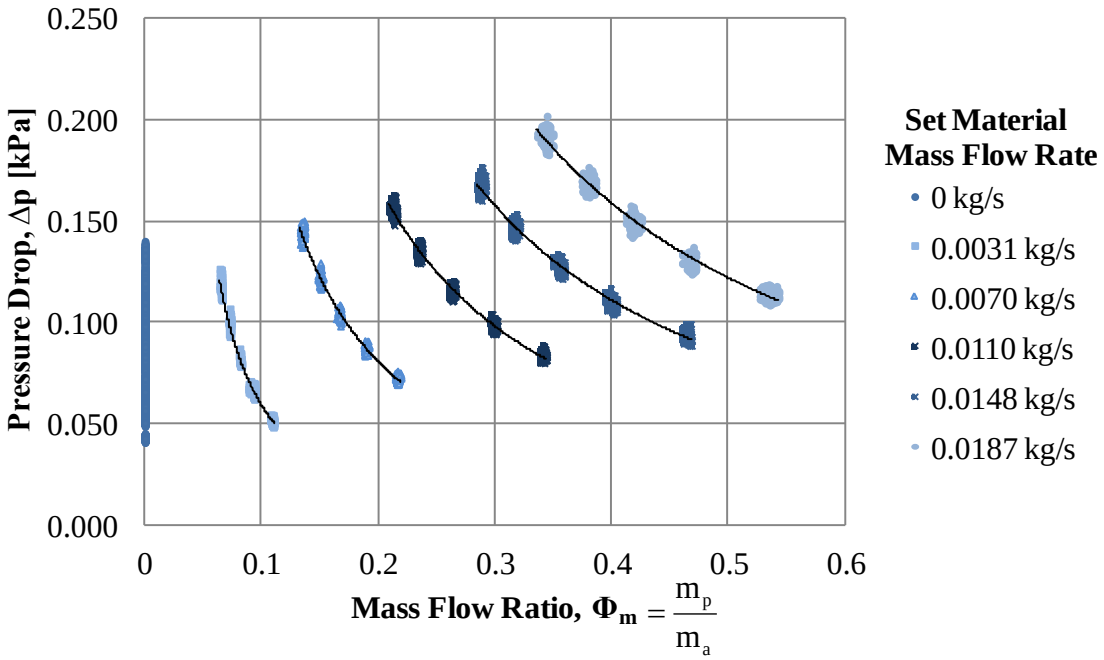

Figure 7-7: The relationship between pressure drop and mass flow ratio for canola, data set 1

Table 7-1: The fit equations from Figure 7-7

Set Material Mass Flow Rate, $m_{p,set}$ [kg/s]	Fit Equations	R^2
0.003	$\Delta p = 0.0015 \cdot \Phi_m^{-1.610}$	0.9931
0.007	$\Delta p = 0.0077 \cdot \Phi_m^{-1.461}$	0.9918
0.011	$\Delta p = 0.0198 \cdot \Phi_m^{-1.330}$	0.9908
0.015	$\Delta p = 0.0361 \cdot \Phi_m^{-1.225}$	0.9877
0.187	$\Delta p = 0.0538 \cdot \Phi_m^{-1.182}$	0.9856

Figure 7-7 shows the relationship between the pressure drop and mass flow ratio for canola only in a material mass flow rate series. It was found that a power model ($y = a \cdot x^b$) could represent these data when sub-grouped by the material mass flow rate with R^2 values greater than 98.5%. However, if the data were presented by material mass flow rate, the model would not be able to predict when there was no material in the air stream. After attempting this method, it was discovered that the data should be rearranged in series by air velocities rather than material mass flow rate. Nonetheless, this did not succeed because the data set collected was based on the series of the material mass flow rate. Grouping the existing data by air velocity provided only four test conditions, which was insufficient. This was the motivation for collecting data set 2. In order to see the entire range of flow behavior and develop a broadly applicable model, the ranges of the material mass flow rate and air velocity were expanded, and the number of test conditions increased by about four times.

7.3 Model Development

Data set 2, which was collected from canola, was only used for developing a material mass flow rate estimation model. Two full data collections (all test conditions) were used for training the model. A third, partial collection was used for validating the model which was developed.

To develop a model, there were three variables that interrelated. Those variables were material mass flow rate, air mass flow rate and pressure loss. When the data were collected, the pressure loss across the elevation was the observed or dependent variable.

In contrast, to estimate the material mass flow rate, this variable had to become the dependent or observed variable. The pressure drop, air mass flow rate, and/or air velocity would then be the input variables for the model.

7.3.1 The Variable Arrangement

The relationship between the three main variables (material mass flow rate, air mass flow rate, and pressure drop) was visualized by arranging the data in terms of mass flow ratio (material mass flow rate: air mass flow rate) and pressure drop. The data were then plotted and grouped by air velocity. After the data were plotted, the best fit models for each air velocity group (using the trend line option in Excel) were then examined. It was found that a linear model ($y = a \cdot x + b$) could fit to all 9 groups of data with respective coefficients of determination greater than 97%. These can be seen from Figure 7-8.

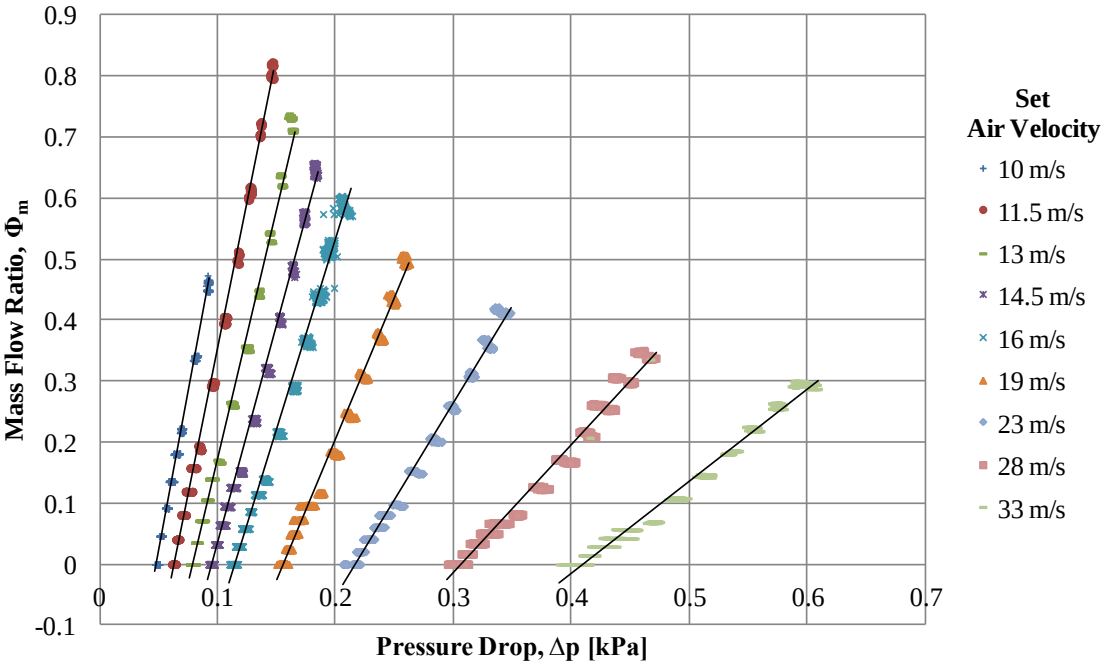

Figure 7-8: The relationship between mass flow ratio and pressure drop with their linear trends, where x is pressure drop and y is mass flow ratio

7.3.2 Coefficient Model Development

The next step was to determine the relationships of the linear model coefficients and air velocity. The coefficients from Figure 7-8 were put together and shown in Table 7-2.

Table 7-2: The fit equations from Figure 7-8

Set Air Velocity [m/s]	Fit Equations	R^2
10	$\Phi_m = 10.346 \cdot \Delta p - 0.4983$	0.9914
11.5	$\Phi_m = 9.556 \cdot \Delta p - 0.6047$	0.9962
13	$\Phi_m = 8.227 \cdot \Delta p - 0.6502$	0.9930
14.5	$\Phi_m = 7.188 \cdot \Delta p - 0.6893$	0.9934
16	$\Phi_m = 6.211 \cdot \Delta p - 0.7132$	0.9903
19	$\Phi_m = 4.614 \cdot \Delta p - 0.7184$	0.9883
23	$\Phi_m = 3.170 \cdot \Delta p - 0.6857$	0.9877
28	$\Phi_m = 2.100 \cdot \Delta p - 0.6448$	0.9811
33	$\Phi_m = 1.512 \cdot \Delta p - 0.6195$	0.9752

The relationship between the coefficient ‘a’ and their set air velocities is illustrated in Figure 7-9. It was found that the most suitable model form that could fit this relationship was an exponential model, giving an R^2 value of 99.64%.

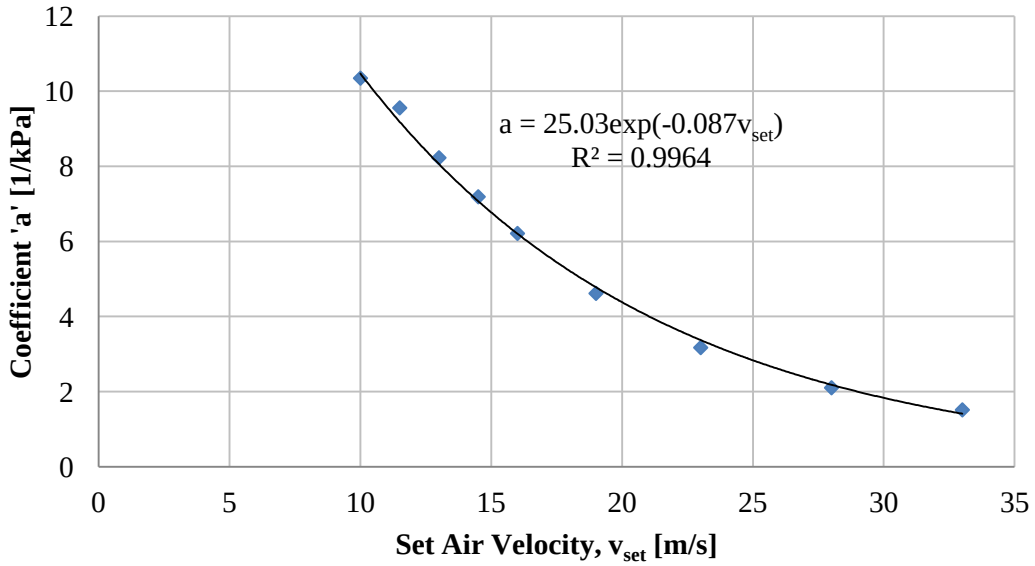

Figure 7-9: The relationship between coefficient ‘a’ and the set air velocity with the fit trend

The relationship between coefficient ‘b’ and the set air velocities is illustrated in Figure 7-10. The two most suitable models which would represent the coefficient ‘b’ were examined. The first one was the third-order polynomial model with R^2 value of 98.04%. This was plotted in green dots. The other model was the inverse exponential of ‘b’ with a third-order polynomial which presented in blue dots. The R^2 value from this model was 98.66%. It seems to be that the value of R^2 from the second model was not significantly different from the first one as the complexity of the model increased. From the examinations and comparisons between those two models in further steps, it was found that the second model (the inverse exponential with the third-order polynomial) presented statistically better results than the first model. Therefore, the inverse exponential of ‘b’ with a third-order polynomial was represented in the coefficient ‘b’.

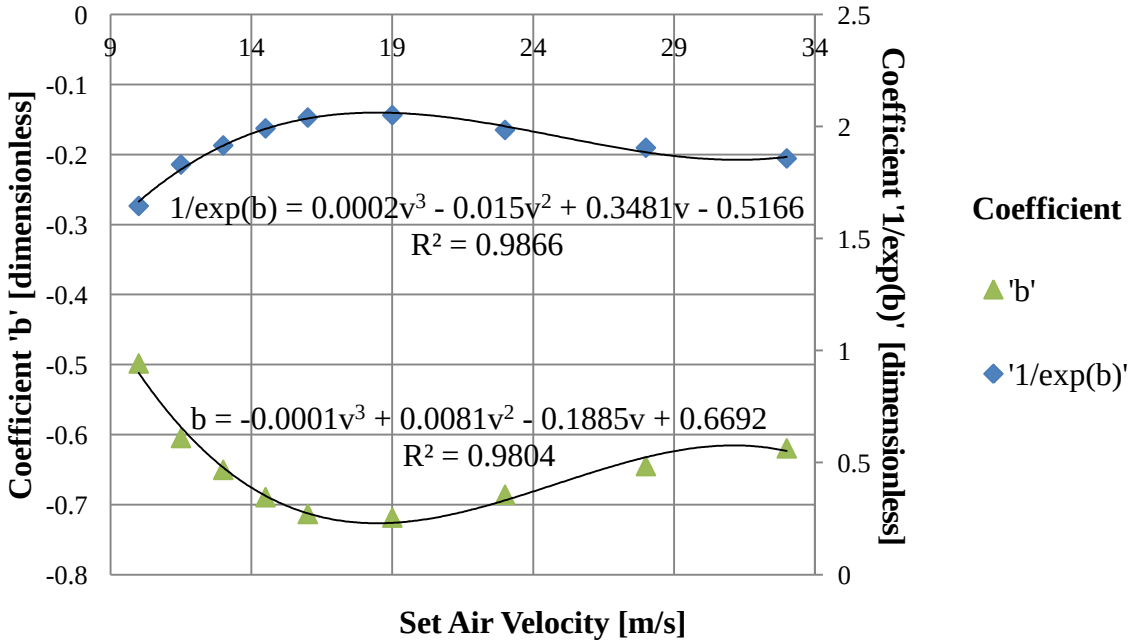

Figure 7-10: The relationship between coefficient ‘b’ and its transformation versus set air velocity with their trends.

7.3.3 Model Establishment

The general model representing the training data set is shown in Equation 7-1.

$$\frac{m_p}{m_a} = a \times \Delta p + b, \qquad 7\text{-}1$$

where m_p is material mass flow rate [kg/s],

m_a is air mass flow rate [kg/s],

Δp is pressure drop or pressure loss [kPa],

a is the coefficient 'a' $\left[\frac{1}{kPa}\right]$, and

b is the coefficient 'b' [dimensionless].

Coefficient 'a' may be expanded and represented by Equation 7-2.

$$a = a_1 \cdot e^{a_2 \cdot v}, \qquad 7\text{-}2$$

where v is set air velocity [m/s].

Finally, the model that represents the transformed coefficient 'b' is shown in Equation 7-3.

$$\frac{1}{e^b} = b_1 \times v^3 \times b_2 \times v^2 + b_3 \times v + b_4, \qquad 7\text{-}3$$

The following equations show steps of solving Equation 7-3 for the coefficient 'b'.

$$\frac{1}{e^b} = b_1 \times v^3 + b_2 \times v^2 + b_3 \times v + b_4$$

$$\ln\left(\frac{1}{e^b}\right) = \ln\left(b_1 \times v^3 + b_2 \times v^2 + b_3 \times v + b_4\right)$$

$$\ln\left(e^{-b}\right) = \ln\left(b_1 \times v^3 + b_2 \times v^2 + b_3 \times v + b_4\right)$$

$$-b = \ln\left(b_1 \times v^3 + b_2 \times v^2 + b_3 \times v + b_4\right)$$

$$b = -\ln\left(b_1 \times v^3 + b_2 \times v^2 + b_3 \times v + b_4\right) \qquad 7\text{-}4$$

Results from the previous Equations 7-2 and 7-4 were substituted to Equation 7-1. Isolating m_p, the result gives Equation 7-5.

$$m_p = m_a \times [(a_1 \times e^{a_2 \cdot v}) \times \Delta p - \ln(b_1 \times v^3 + b_2 \times v^2 + b_3 \times v + b_4)], \qquad 7\text{-}5$$

7.3.4 Model Optimization

According to the model which was developed from Microsoft Excel 2007, the values of the parameters (a_1, a_2, b_1, b_2, b_3, and b_4) were generated based on assumption that the set air velocities were constant. This was not the case, as there were variations in these values. To improve the model Equation 7-5, optimization was required. This optimization was completed using SAS 9.2 (SAS, Cary NC). Parameters in the model were solved using nonlinear regression (procedure NLIN) with the Marquardt option (a combination of the Gauss-Newton and steepest descent methods). The parameter analysis summary is presented below in Table 7-3, as well as the results from Excel. The code and full results from the analysis are shown in the APPENDIX H and APPENDIX I.

From Table 7-3, it shows the estimated values and their 95% confidence limits. The maximum approximate standard error of those parameters was only 0.08, which was from a_1. The estimations obtained by Excel 2007 were slightly different from the estimations using SAS 9.2. Nonetheless, those slight differences could significantly improve the sufficiency of the material mass flow rate estimation model. This will be illustrated in the next section.

When the estimated parameters obtained from SAS 9.2 were substituted into Equation 7-5, the model became as shown in Equation 7-6.

$$m_p = m_a \times [(25.4796 \cdot e^{-0.0882 \cdot v}) \times \Delta p - \ln(9.7 \times e^{-5} \times v^3 - 0.0093 \times v^2 + 0.2585 \times v - 0.1093)], \quad 7\text{-}6$$

Table 7-3: The statistical summary of the model's parameter estimation from Microsoft Excel 2007 and SAS9.2 (SAS, Cary NC)

Parameter	Excel	SAS			
	Estimate	Estimate	Approximate Std. Error	Approximate 95% Confidence Limits	
a_1	25.03	25.4796	0.081	25.3207	25.6384
a_2	-0.087	-0.0882	0.00016	-0.0885	-0.0879
b_1	2.00E-04	9.70E-05	1.41E-06	9.40E-05	9.90E-05
b_2	-0.015	-0.0093	9.50E-05	-0.0095	-0.0091
b_3	0.3481	0.2585	0.00193	0.2547	0.2623
b_4	-0.5166	-0.1093	0.0119	-0.1325	-0.086

7.3.5 Model Verification

The optimized model was validated using the test data reserved and then compared to the pre-optimized model results. To accomplish this, the pre-optimized model and the optimized model were tested with the validation data set. Figure 7-11 and Figure 7-12 illustrate the sufficiency of the model that had been developed and optimized for estimating the material mass flow rate of canola. Note that the box plot presents the minimum, first quartile, median or second quartile, third quartile, and the maximum, respectively. Figure 7-11 shows the relationship between the estimated material mass flow rate obtained from the models for canola before (Excel 2007) and after (SAS 9.2) the optimizations versus the set material mass flow rate. As seen in Figure 7-11, the sufficiency of the material mass flow rate estimation for canola improved noticeably after the model was optimized. This was noticed by the increasing of R^2 value from 93% to almost 99%. It could be also noticed by the decreasing in the variation. After the material mass flow rate estimation model for canola was optimized, the variation of the estimation reduced more than 50%.

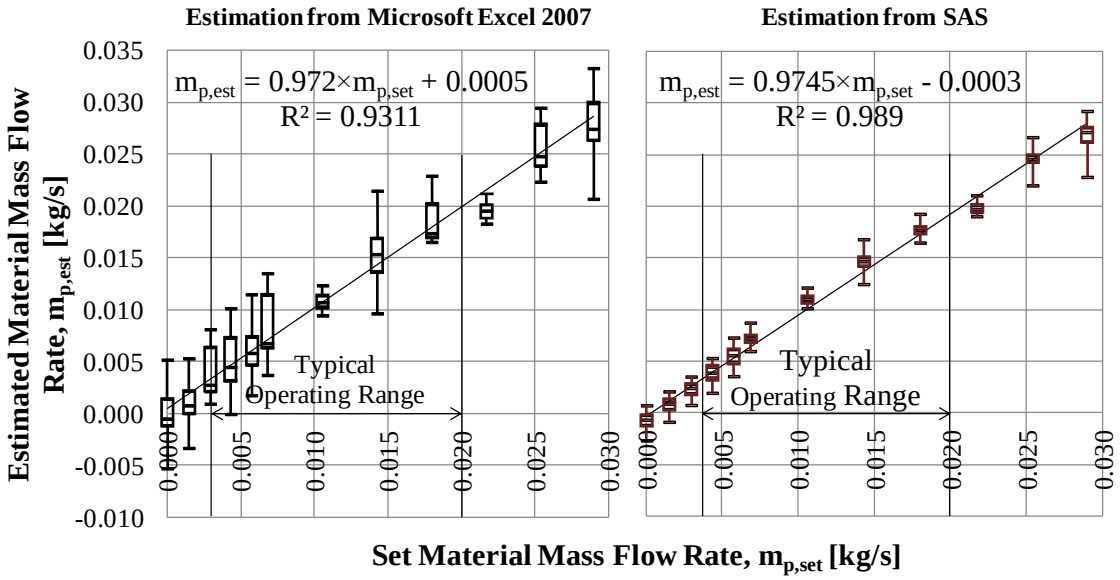

Figure 7-11: The relationship between the estimated and the set material mass flow rate for canola which were results from the model development using Microsoft Excel 2007 (left) and SAS 9.2 (right).

The improvement of the material mass flow rate estimation model for canola could be also seen from Figure 7-12. This diagram shows the relationship between

percent error of the estimations before and after the model optimization versus the material mass flow rate. Note that the percent error in this case was the percent error of the full range of the material mass flow rate which was 0.0290 kg/s. From the diagram (Figure 7-12), it illustrates that the percent error of the model decreased about half at almost every single material mass flow rate, except at the highest rate of 0.0290 kg/s after the model was optimized. The percent error not only decreased, but averaged overall to less than 10%. Moreover, Figure 7-12 also shows that the variation in estimation of the model for canola decreased dramatically after the model was optimized.

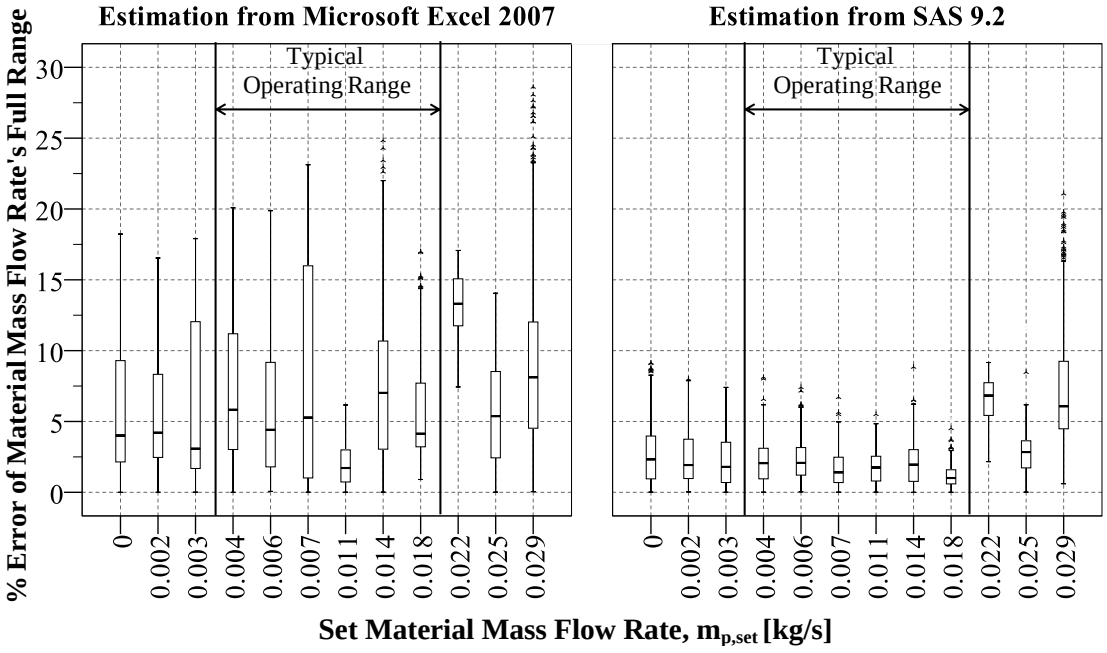

Figure 7-12: The relationship between percent error of the material mass flow rate estimations and the set material mass flow rate from the model development using Microsoft Excel 2007 (left) and SAS 9.2 (right) for canola data set 2.

According to those descriptions, it could be said that the optimized model, Equation 7-6, had a potential for estimating the material mass flow rate of canola satisfactorily. The optimized model was good as seen in the middle of the diagram. Nevertheless, the accuracy appeared to degrade at the end. This was likely due to the models of the coefficient ‘a’ and ‘b’, which could not represent all data points.

7.4 Applying the General Model to Data Set 1

The data in collection set 1 were collected in three repeated groups. Once those data were combined and statistically summarized for checking their variations, they were separated into two groups. The first group was the data from the first and second collection. These data were used for the model training set by applying to the general model in Equation 7-5. The testing data were from the third group. These data were used for the model verification. These processes were the same as the ones used with data set 2 which was used to develop the generalized model of the material mass flow rate estimation for canola.

7.4.1 Applying the General Model to Canola

The optimized results from SAS for canola data set 1 are shown in Table 7-4. It was observed that the parameters generated from the canola data set 1 were slightly different from the parameters generated from the canola data set 2, which were used to develop the general model. The approximate standard errors of the canola data set 1 were slightly higher than the canola data set 2's. This might be due to data set 2 being collected more carefully than data set 1 and the environment was more controlled.

Table 7-4: The statistical summary of the parameter estimation for canola modeling, data set 1

Parameter	Estimate	Approximate Std. Error	Approximate 95% Confidence Limits	
a_1	26.878	0.2449	26.3979	27.358
a_2	-0.0918	0.000673	-0.0931	-0.0904
b_1	-0.0005	0.000043	-0.00058	-0.00041
b_2	0.0138	0.00172	0.0104	0.0172
b_3	-0.0447	0.0225	-0.0887	-0.00062
b_4	1.2916	0.0955	1.1045	1.4787

The estimated parameters from Table 7-4 were substituted to the general model Equation 7-5 and tested with the validation data set. The results are illustrated in the relationship between the estimated and actual material mass flow rate shown in Figure 7-13. It was seen that the estimation of the material mass flow rate from the established

model was very close to the set material mass flow rate with its variation less than 1.5%. This was observed from the slope of trend line, which was about 1, and an R^2 value of 98.77%. The qualities of those estimations are illustrated in Figure 7-14. From the diagram, it could be said that the percent error of the material mass flow rate's full range from the estimation was less than 10%, with more than 50% of the estimation being less than 5% in error. The overall percent error from this data set was slightly higher than the percent error from the data set 2.

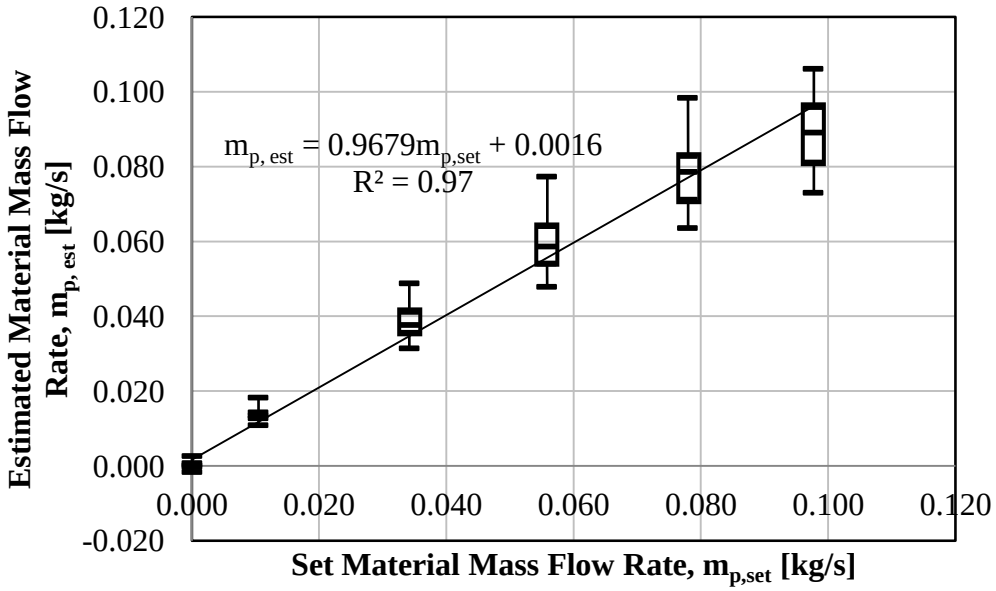

Figure 7-13: The relationship between the estimated material mass flow rate and the set material mass flow rate for canola, data set 1

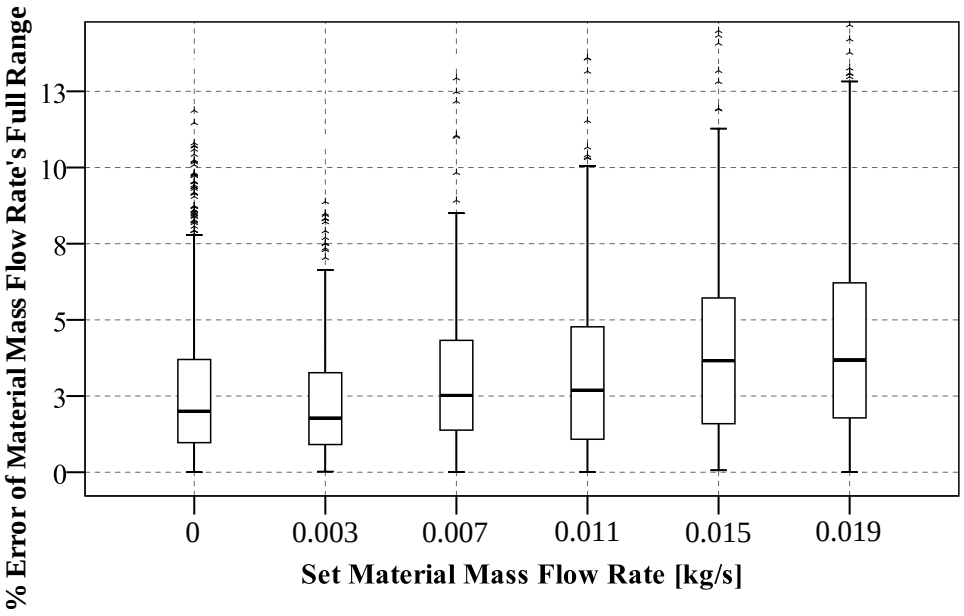

Figure 7-14: The relationship between percent error of the material mass flow rate and the material mass flow rate for canola, data set 1

7.4.2 Applying the General Model to Wheat

The optimized results from SAS for wheat are shown in Table 7-5. Their maximum standard error was around 0.13 from a_1. The estimated parameters were substituted to the general model. The results from the validation test are illustrated in Figure 7-15. The graph shows that the estimation of the material mass flow rate from the established model was close to the set material mass flow rate. This was indicated by their slope, which was 0.97 with a variation of 3% (R^2 = 97%). The qualities of those estimations are displayed in Figure 7-16. From the diagram, it shows that the percent error of the material mass flow rate's full range from the estimation increased as the material mass flow rate increased.

Table 7-5: The statistical summary of the parameter estimation for wheat modeling, data set 1

Parameter	Estimate	Approximate Std. Error	Approximate 95% Confidence Limits	
a_1	8.6501	0.1315	8.3924	8.9079
a_2	-0.0608	0.000579	-0.0619	-0.0597
b_1	3.48E-06	8.29E-06	-0.00001	0.00002
b_2	-0.0011	0.000625	-0.00234	0.000115
b_3	0.0559	0.0152	0.0262	0.0856
b_4	0.8309	0.1179	0.5997	1.062

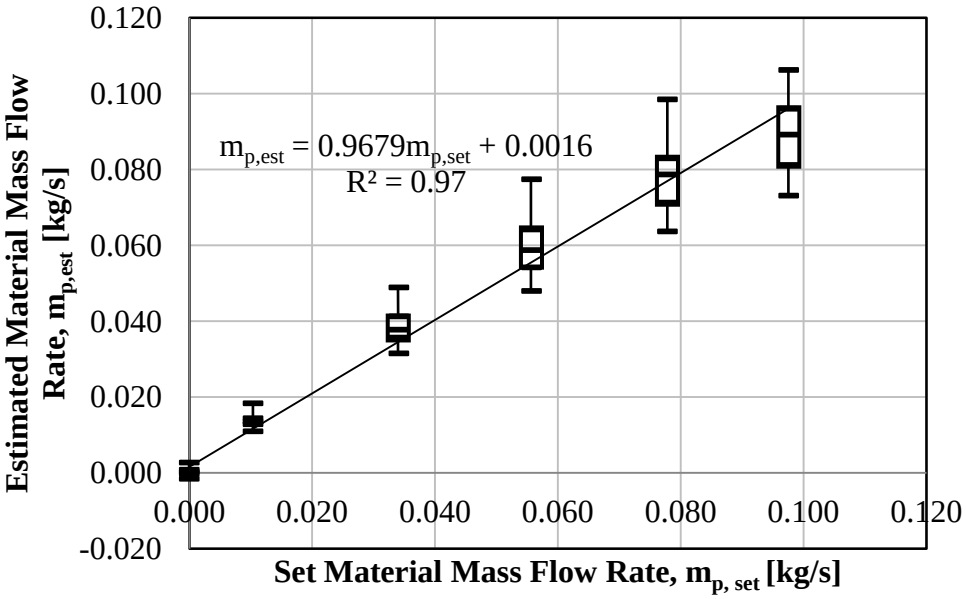

Figure 7-15: The relationship between the estimated material mass flow rate and the set material mass flow rate for wheat, data set 1

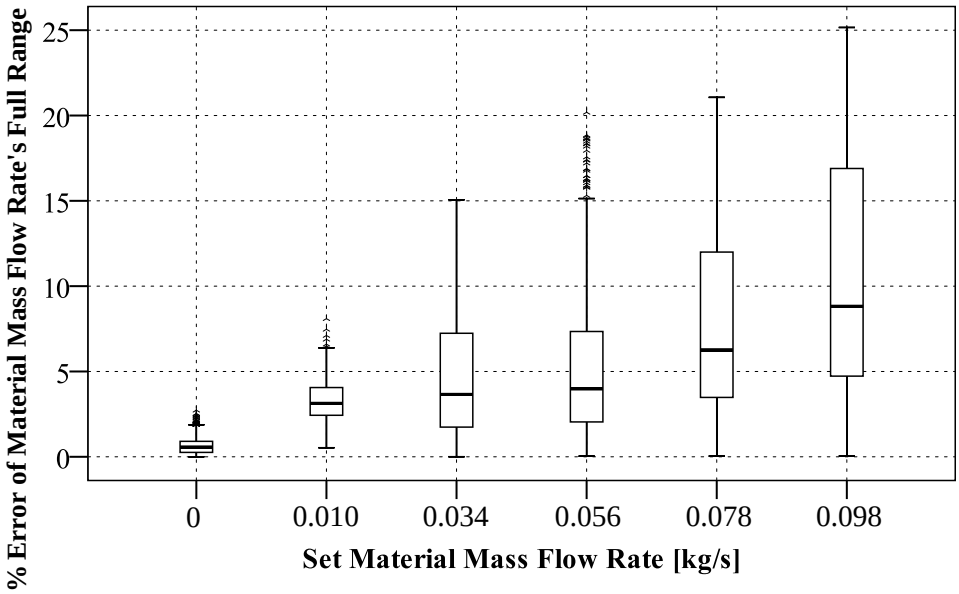

Figure 7-16: The relationship between percent error of the material mass flow rate and material mass flow rate for wheat, data set 1

7.4.3 Applying the General Model to Chickpea

The estimated values of parameters generated from chickpea can be seen from Table 7-6. The test results of the model are shown in Figure 7-17. The trend line shows that the slope of the relationship between the estimated and actual mass flow rate estimation was about 0.95 with R^2 of 0.99. The variation of the estimation was higher at the highest material mass flow rate. The quality of the estimation is shown in Figure 7-18. Other than the highest material mass flow rate, almost 75% of the estimations had a percent error that was less than 5%.

Table 7-6: The statistical summary of the parameter estimation for chickpea modeling, data set 1

Parameter	Estimate	Approximate Std. Error	Approximate 95% Confidence Limits	
a_1	8.0339	0.1521	7.7358	8.332
a_2	-0.0364	0.000622	-0.0376	-0.0352
b_1	0.00035	0.000093	0.000172	0.000537
b_2	-0.0344	0.0084	-0.0508	-0.0179
b_3	1.1371	0.2513	0.6444	1.6298
b_4	-10.64	2.487	-15.5158	-5.7635

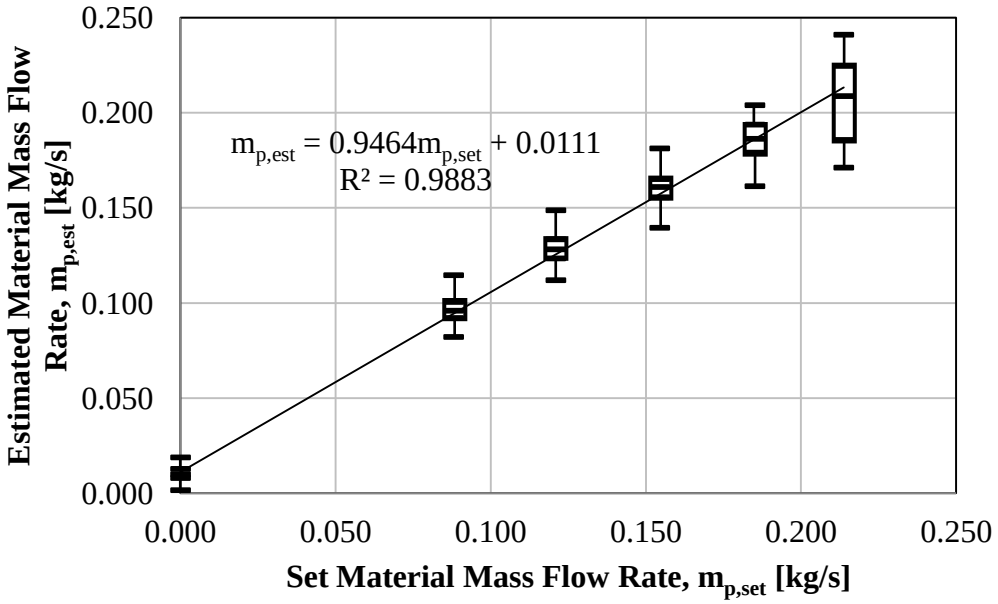

Figure 7-17: The relationship between the estimated material mass flow rate and the set material mass flow rate for chickpea, data set 1

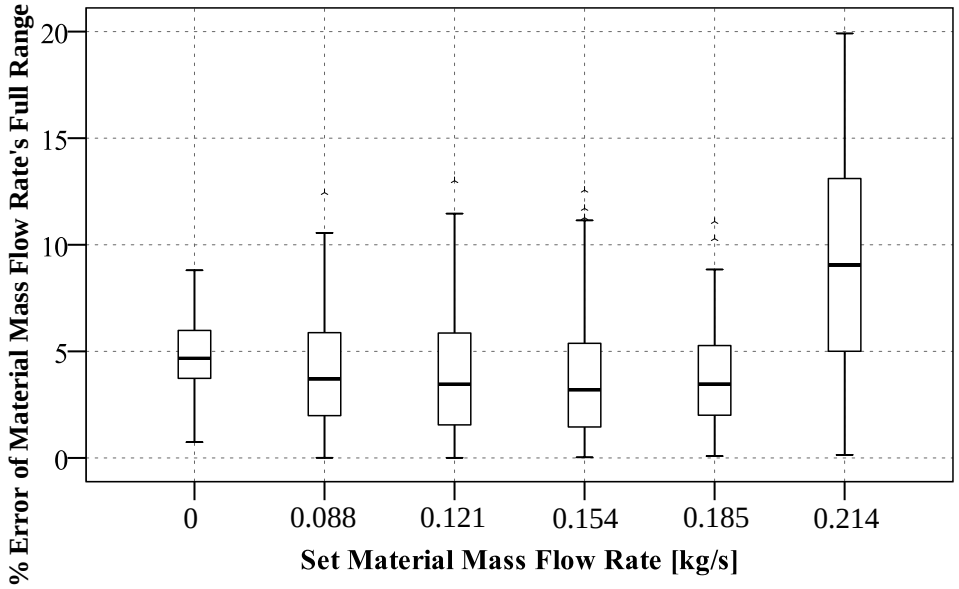

Figure 7-18: The relationship between percent error of the material mass flow rate and material mass flow rate for chickpea, data set 1

7.4.4 Applying the General Model to Fertilizer

The parameter estimation for fertilizer is shown in Table 7-7. The estimation results are shown in Figure 7-19. The slope of the relationship between the estimated and actual material mass flow rate was about 0.95, with the value of R^2 being 99%. Figure 7-20 shows that the quality of the model's estimation fluctuated. However, about 75% of the estimations had percent errors less than 5%, except at the highest material mass flow rate which had error more than 50% of the estimation. This was similar to the result from chickpea.

Table 7-7: The statistical summary of the parameter estimation for fertilizer modeling, data set 1

Parameter	Estimate	Approximate Std Error	Approximate 95% Confidence Limits	
a_1	15.1984	0.1872	14.8313	15.5654
a_2	-0.0509	0.000433	-0.0517	-0.05
b_1	8.81E-06	0.000015	-0.00002	0.000039
b_2	-0.00308	0.00118	-0.00539	-0.00077
b_3	0.1809	0.0291	0.1238	0.2379
b_4	-0.238	0.2276	-0.6842	0.2081

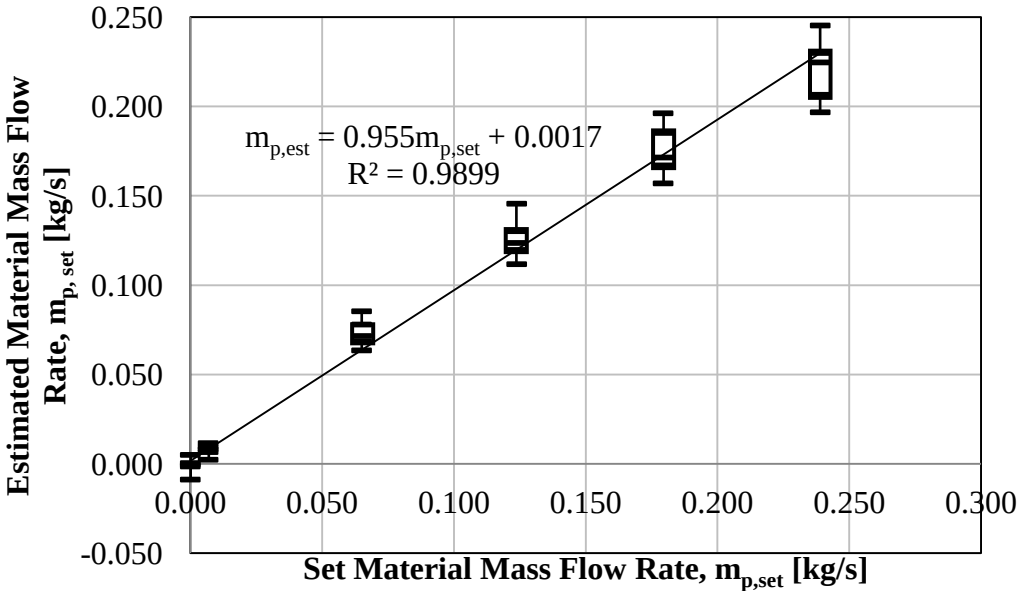

Figure 7-19: The relationship between the estimated material mass flow rate and the actual material mass flow rate for fertilizer, data set 1

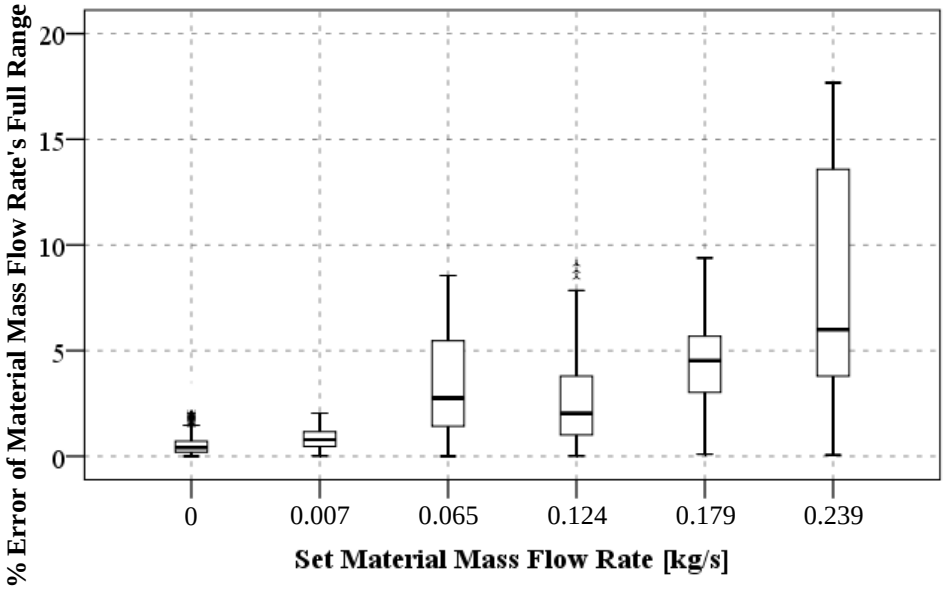

Figure 7-20: The relationship between percent error of the material mass flow rate and material mass flow rate for fertilizer, data set 1

7.4.5 Applying the General Model to Combined Materials

All data from the first set (all four tested materials) were combined together and the general model was filled to the combined data. The estimation of the model parameters is shown in Table 7-8. The relationship between the estimated material mass flow rate and the actual material mass flow rate is shown in Figure 7-21. The slope of this plot was 0.9 and the value of R^2 was 87%.

Figure 7-22 shows the relationship between percent error in the material mass flow rate and material mass flow rate for the combination of all tested material from data set 1. In this case, the percent error was almost about 40%. But, for canola, the percent error from the combined model was less than 5%. This may be due to the fact that the model was established from canola with the material mass flow rate being low compared with the other materials. Nevertheless, this is magnificent because canola seed is one of the most difficult to detect due to the size. Based on these results, this was a good indication that there was a chance to obtain a single model with the same parameter values that could represent all seeding materials.

Table 7-8: The statistical summary of the model's parameter estimation for combination of data set 1 (all tested materials)

Parameter	Estimate	Approximate Std. Error	Approximate 95% Confidence Limits	
a_1	1.9182	0.0606	1.7995	2.0369
a_2	0.0114	0.00108	0.00934	0.0136
b_1	0.00011	0.000013	0.000086	0.000139
b_2	-0.0045	0.000845	-0.00615	-0.00283
b_3	0.0956	0.0172	0.0619	0.1293
b_4	0.3702	0.1126	0.1495	0.5909

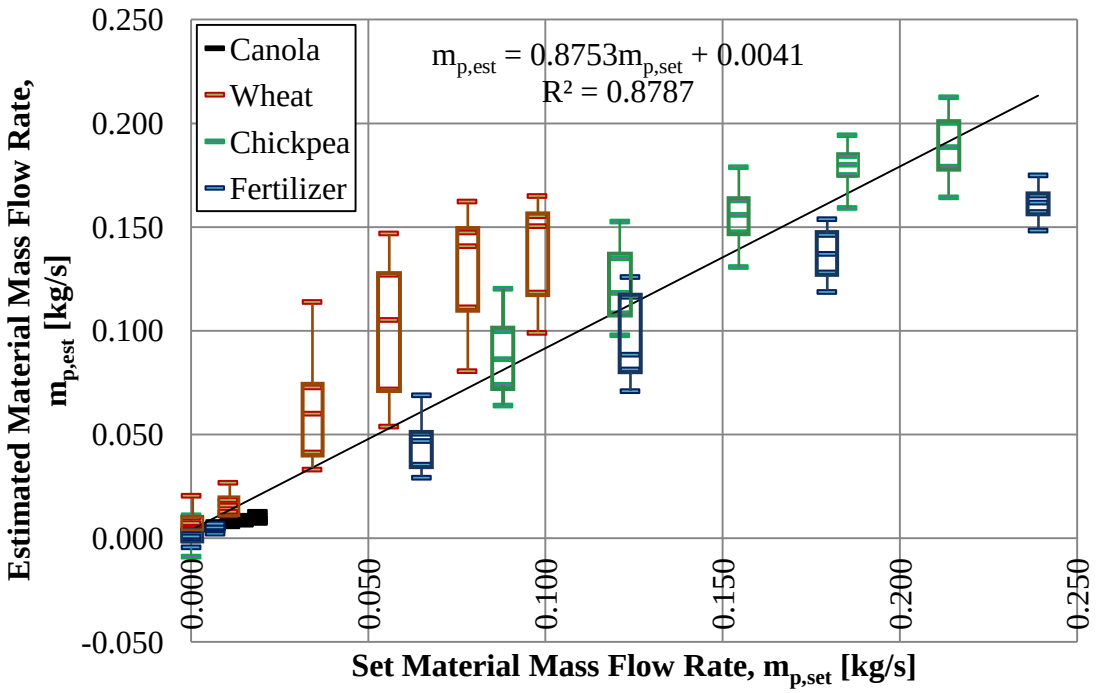

Figure 7-21: The relationship between the estimated material mass flow rate and the set material mass flow rate for combination of all tested materials, data set 1

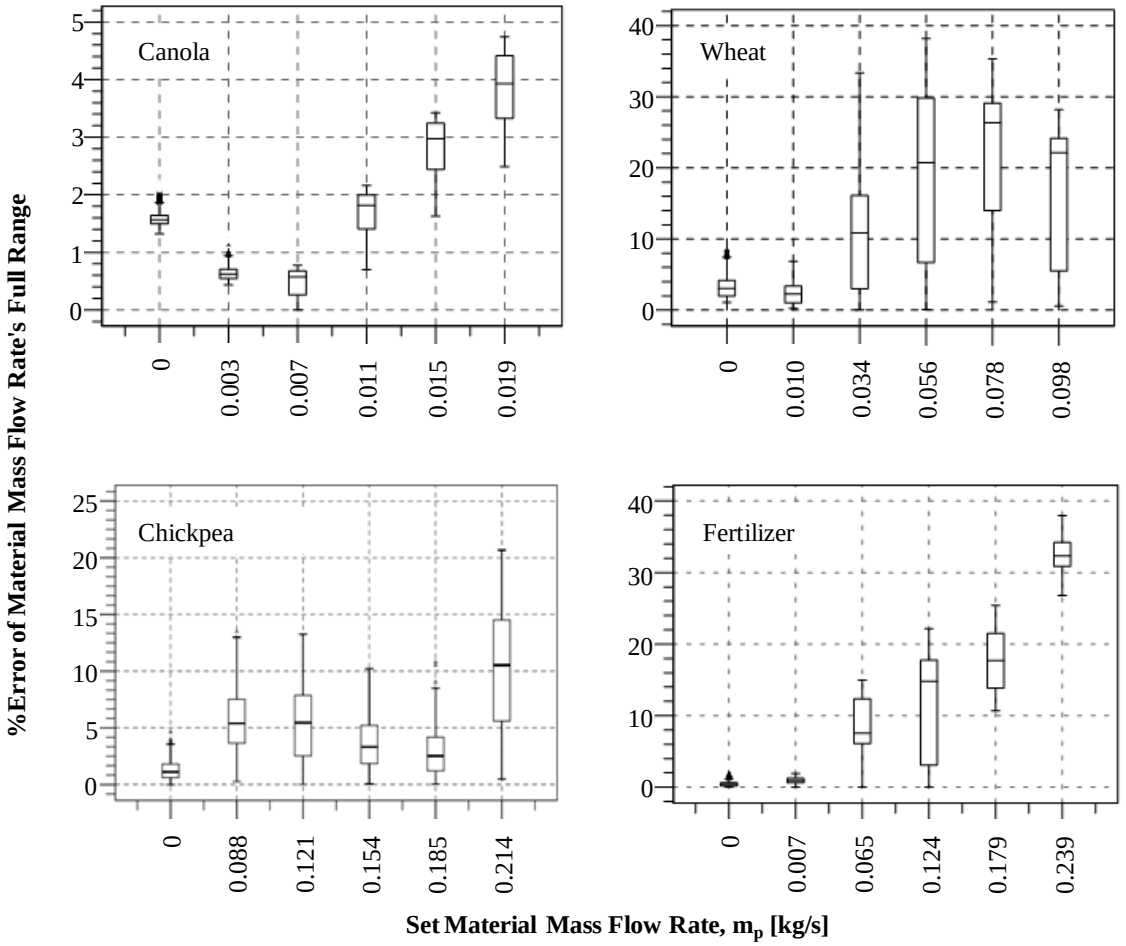

Figure 7-22: The relationship between percent error of the material mass flow rate and material mass flow rate for combination of all tested materials, data set 1

7.4.6 Summary of Applying the General Model to Data Set 1

According to the results from applying the general model to data set 1, the slope values on the individual plots show that the estimated material mass flow rates for those tested materials were quite close to the actual values (slopes $\simeq$ 1), with their variations (R^2) being 3% or less. Canola had the lowest average median percent error among the tested materials. Wheat had the most variation in percent error of the median from as low as 3% to as high as 25%. This might be due to the shape of wheat. In contrast, it seemed like chickpea had the most stable percent error and was consistent at about 10% for all tested material mass flow rates except at the highest rate. Even though the percent errors shown on the plots for those individual materials were up to 20% (maximum percent

error), when these results were inspected, the averages of the estimation were different from the set values in grams or less.

When the data from all tested materials were combined and examined, the results from the estimation were not as good as the individual material modeling. Nevertheless, it demonstrated that there were consistencies between the behaviour of the four tested materials.

7.5 Uncertainty Analysis of the Air Velocity Calculations

According to the assigning expansion factor of air (ε) and the discharge coefficient of the orifice plate (C) as constants for the air velocity calculation, it was imperative to know the uncertainty of the air velocity (v) due to those two parameters. This was to double check whether the values of the expansion factor of the air (ε) and the discharge coefficient of the orifice plate (C), which were assigned to be constant, were reasonable or needed to be adjusted.

The uncertainty of the air velocity, which was calculated from the data test 2 (canola) covering the operation ranges in the experiment, was from about 10 m/s to 33.5 m/s. The information and values of the parameters used in the uncertainty calculations are shown in Table 7-9.

Table 7-9: Values of the parameters used in the air velocity uncertainty calculations

Parameter	Value	Units
ε	0.995	-
C	0.65	-
d_o	0.0445	m
A	0.00278	m^2
β, d_o/D	0.75	-
v_{max}	33.7	m/s
v_{min}	9.8	m/s
ρ at v_{max}	1.08	kg/m^3
ρ at v_{min}	1.10	kg/m^3
Δp at v_{max}	3071	Pa
Δp at v_{min}	272	Pa
Absolute p_1 at v_{max}	101776	Pa
Absolute p_1 at v_{min}	94578	Pa

To obtain the uncertainty of the air velocity it was required to know the percent uncertainty of ε ($\%u_\varepsilon$) and C ($\%u_C$). Equation 7-7 and 7-8 were used to calculated $\%u_\varepsilon$ and $\%u_C$, which were given by the International standard ISO 5167-2 2003 (E). In order to obtain the uncertainty of those two parameters, International standard ISO 5167-2 2003 (E) explained that it was assumed that there was no error in β, $\Delta p/p_1$, or the air isentropic (which was 1.4) for the uncertainty of ε, and for no error in β, D, or the Re_D for the uncertainty of C.

$$\%\,u_\varepsilon = 3.5 \times \left(\frac{\Delta p}{1.4 \times p_1} \right), \qquad 7\text{-}7$$

where p_1 is the upstream pressure of the orifice plate [Pa].

$$\%\,u_C = (1.667 \times \beta - 0.5) + 0.9 \times (0.75 - \beta) \times \left(2.8 - \frac{D}{25.4} \right), \qquad 7\text{-}8$$

Based on Equations 7-7 and 7-8, the calculated results for $\%u_\varepsilon$ was between 0.007% and 0.076%, and $\%u_C$ was 0.753%. The uncertainty of ε was a range because it varied due to pressure drop. The uncertainty of C was a single value because it was only dependent on the orifice design.

The uncertainty of v, due to ε (u_{v_ε}) and C (u_{v_C}), was then calculated by Equation 7-9 and Equation 7-10 (Figliola and Beasley 2006). The pressure drop across the orifice plate (Δp_o) used in these calculations were from the minimum and maximum air velocity.

$$\begin{aligned} u_{v_\varepsilon} &= \frac{\partial v}{\partial \varepsilon} \times \Delta\varepsilon, \\ &= \frac{\frac{C}{\sqrt{1-\beta^4}} \times \frac{\pi}{4} \times d_o^2 \times \sqrt{2 \times \Delta p_o \times \rho}}{A \times \rho} \times (\varepsilon \times \text{Uncertainty of } \varepsilon) \end{aligned} \quad \text{7-9}$$

$$\begin{aligned} u_{v_C} &= \frac{\partial v}{\partial C} \times \Delta C, \\ &= \frac{\frac{1}{\sqrt{1-\beta^4}} \times \varepsilon \times \frac{\pi}{4} \times d_o^2 \times \sqrt{2 \times \Delta p_o \times \rho}}{A \times \rho} \times (C \times \text{Uncertainty of } C) \end{aligned} \quad \text{7-10}$$

The air velocity (v) was computed by Equation 7-11, which was from substituting Equation 4-1 to Equation 4-2.

$$v = \frac{m_a}{A \times \rho} = \frac{\frac{C}{\sqrt{1-\beta^4}} \times \varepsilon \times \frac{\pi}{4} \times d_o^2 \times \sqrt{2 \times \Delta p_o \times \rho}}{A \times \rho} \quad \text{7-11}$$

Based on Equations 7-9 and 7-10, the calculated results for u_{v_ε} were between 0.00-0.03 m/s, and u_{v_C} was between 0.07-0.25 m/s.

According to the uncertainty calculation results, it would be said that the values of ε and C, which were assigned to be constant, were suitable for use in this study with an uncertainty of less than 1 m/s. However, those values could be changed to decrease the uncertainty levels. The uncertainty of ε, C, and v due to ε and C are shown in Table 7-10.

Table 7-10: The uncertainty of ε, C, and v due to ε and C

Air Velocity (LabVIEW)	**ΔP**	**Abs P1**	**$\%u_{\varepsilon}$**	**$\%u_{C}$**	$u_{v_{\varepsilon}}$	u_{v_C}	$\sqrt{u_{v_{\varepsilon}}^2 + u_{v_C}^2}$
[m/s]	[Pa]	[Pa]	[%]	[%]	[m/s]	[m/s]	[m/s]
33.7	3071	101776	0.08	0.75	0.03	0.25	0.25
9.8	272	94578	0.01	0.75	0.00	0.07	0.07

8. SUMMARY AND CONCLUSION

The air seeding cart is a main piece of farming equipment which is used for operation in the seeding process. Current systems on the air seeding cart can monitor and report blockages, but these are not automated closed loop systems. Therefore, a laboratory prototype for mass flow measurement in the primary runs was developed and tested to facilitate automation. In order to do this, an empirical model for material mass flow estimation based on pressure drop in the conveying line was developed. Canola, wheat, chickpea, and fertilizer were chosen and tested in this study. They represented the fine seed, elongated seed, coarse seeds, and granular fertilizer respectively.

Using data collected for canola, Equation 7-5 was the general model developed for the material mass flow rate estimation:

$$m_p = m_a \times [(a_1 \times e^{a_2 \cdot v}) \times \Delta p - \ln(b_1 \times v^3 + b_2 \times v^2 + b_3 \times v + b_4)] \quad 7\text{-}5$$

To estimate the material mass flow rate, the model required information of the pressure loss or pressure drop across the elevation, air flow, and environment measurements. Coefficients were determined using SAS 9.2 (SAS, Cary, NC). From the model validation (data set 2), the average percent error of the material mass flow rate's full range was under 10%, except for the highest rate which tested up to 20%. Overall, more than 75% of the estimations had percent errors less than 5%.

The general model was also applied to data sets representing each product type. It was discovered that the general model was also applicable to the other three products (wheat, chickpea, and fertilizer). Those tested materials seemed to provide good responses from this model. The results showed that the estimations of material mass flow rates from their model were relatively similar to the set values. The results also showed that the variations of those predictions were less than 3%. The overall percent errors of the material mass flow rate's full range based on their medians varied between 3% and 5%. Among the tested material, canola had the lowest average median percent error. Wheat had the highest variation in percent error of material mass flow rate's full range, being as low as 3% to as high as 25%. Even though the maximum percent errors for those individual materials shown on the plots were up to 20% to 25%, when these results were examined, the averages of the estimations were only different from the set values in

grams or less. When the data from all tested materials were combined and observed, the results showed that the ability to estimate of the material mass flow rate was not as accurate as when the model was applied to the individual tested material (slope = 0.875 and R^2 = 87.87%). The median of the percent error (of material mass flow rate's full range) from the combined model was varied from as low as 1% to as high as 30%, which depended on the tested materials. Even though the ability of the estimation of the model was not as high as individual modeling, it at least demonstrated that there were consistencies between the behaviour of the four tested materials

According to the objectives of the study, the air seeding test station was constructed. An orifice plate was designed and made for measuring the air flow in the system. A data acquisition system, including the user interface program, was developed. The connection between the sensing elements and the data acquisition modules were made in the system control panel. The data for the four tested materials were then collected. Lastly, the general model for mass flow rate estimation of seeding materials was fully developed from the data collected for canola. Based on the test results, it could be concluded that the developed model gave pretty accurate estimations for material mass flow rate. The general model was applicable and had good responses with other tested materials.

It was assumed that the metering system would dispense the materials at the constant rate that it was set. However, while the experiment was running, it was observed that the dispensing of tested materials was pulsing as the rollers rotated. This was due to the structure of rollers which had edges (or ridges) between the roller flutes. This was noticeable when the rollers turned at low speed or at the high conveying air velocity. Based on these observations, it is likely that the actual amount of tested materials being dispensed from the metering system was not the same as they were set and certainly not constant. Because of the estimation relying on the information sensed from the conveying system (pressure loss across the elevation, conveying air velocity, air mass flow rate), it was believed that the sensing system could sense the actual material mass flow rate. As a result, the model might have the ability to estimate closer to the actual rate than the set material mass flow rate. This possibility could be analyzed after a study of the metering system conducted by another student is completed.

According to the test system, the fan was supposed to be able to generate an air flow higher than 40 km/s (air only) in accordance with the fan specification. Based on the present system, there were two major things that reduced the fan performance (generated losses). Those were the pipe reducer (reducer coupling) between the fan and the pipe, and the flow measurement equipment (orifice plate). The original pipe reducer installed on the system had the shape of square to circle bottle neck which dramatically changed in diameter and shape (from square to circular shape). A longer pipe reducer with a gradually decreasing diameter and shape would reduce the head pressure loss substantially compared to the original fitting. A venturi meter would have a lower permanent pressure loss than the orifice plate. As a result, the system (fan) would be able to generate higher air flow rate.

Once the data set for all tested materials were combined and tested for modeling, it was noticed that there was a correlation between those tested materials. This showed that there was a potential for having a single model of the material mass flow rate estimation with the same set of the parameter values. If this study continued, the relationship between seeding materials and their properties need to be determined and developed. Dimension analysis could be a solution for this.

Lastly, the air humidity may have a significant effect to the pneumatic conveying. However, this factor was not included in this study. In order to improve the model developed from this study, the air humidity and other air properties ought to be considered.

8.1 Future Works

This study is the first phase of developing a mass flow sensor for an air seeding cart. To have this innovation fully developed, further important research is required. The recommended future studies would involve (1) improvement of the air flow measurement apparatus to increase the air flow in the system, (2) improvement of the metering system to reduce the discontinuity of material dispensing, (3) studying the effect of humidity and the environment on the material mass flow rate estimation, (4) dimensional analysis to achieve a single model, (5) blockage prevention, and (6) cost analysis.

REFERENCES

Abdul Rahim, R., Leong, L.C., Chan, K.S., Rahiman, M.H., and Pang, J.F. 2008. Real time mass flow rate measurement using multiple fan beam optical tomography. In *International Society of Automation Transactions* 47(1): 3-14.

ANSI/AMCA 210-07. 2007. Laboratory Methods of Testing Fan for Certified Aerodynamic Performance Rating: 22.

Arakaki, C., Ratnayake, C., and Halstensen, M. 2009. Online prediction of mass flow rate of solid in dilute phase pneumatic conveying system using multivariate calibration. In *Powder Technology* 195(2): 113-118.

ASHRAE. 2005. ASHRAE Handbook: Fundamentals. SI Edition: 14.17-14.19. ASHRAE Atlanta, Ga.

Barbosa, P.R. and Seleghim Jr.,P. 2003. Improving the power consumption in pneumatic conveying systems by adaptive control of the flow regime. In *Journal of the Brazilian Society of Mechanical Sciences* 25(4): 373-377.

Binsirawanich, P. and Noble, S.D. 2009. Characterizing the flow behaviors of sample materials in an air seeder simulator system. Presented at *ASABE North-Central Intersectional Conference*, South Dakota State University, Brookings, SD. September 18-19, 2009.

Binsirawanich, P., Noble, S.D., Gervais, J. 2010. Velocity of Conveyed Seeds in an Inclined Transition Tube. In *Proc. XVIIth World Congress of the International Commission of Agricultural and Biosystems Engineering (CIGR)*, Paper # 101428. Québec City, QC., Canada.

Figliola, R.S. and Beasley, D.E. 2006. Chapter 5: Uncertainty analysis. In *Theory and Design for Mechanical Measurements*: 148-181. NJ: John Wiley & Sons, Inc. 4th ed.

Flexi-coil Air Cart Operator's manual. 1997. In *20 Series Air Cart Operator's Manual GH-001V9.* Section 2: 2-6.

Gerhart, P. M. and Gross, R. J. 1985. Chapter 1: Introduction and Chapter 7: Steady Incompressible Flow in Pipes and Ducts. In *Fundamentals of Fluid Mechanics*: 5-10 and 484-494. Massachusetts: Addison-Wesley Publishing Company.

Gervais, J. 2011. Unpublished data. Saskatoon, SK: University of Saskatchewan, Department of Chemical and Biological Engineering.

Henry, J. 2009. Personal communication.

Hinkle, B. L. 1953. Acceleration of particles and pressure drops encountered in horizontal pneumatic conveying. PhD Thesis. Atlanta, GA: Georgia Institute of Technology, Department of Chemical Engineering.

Institute of Gas Technology. 1978. Preparation of a coal conversion system technical data book. Project 8979, ERDA Contract No. EX 76-C-01-2286. October.

International Standards Organization. 2003. Measurement of fluid flow by means of pressure differential devices inserted in circular cross-section conduits running full - Part 1: General principles and requirement. ISO 5167-1 (E). 2nd ed.

International Standards Organization. 2003. Measurement of fluid flow by means of pressure differential devices inserted in circular cross-section conduits running full- Part 2: Orifice plate. ISO 5167-2 (E). 1st ed.

Kenno, H. and Saito, S. 1969. Pneumatic conveying of solids through straight pipes. In *Journal of the Chemical Engineering of Japan* 2(2): 211-217

Klinzing, G.E. 2001. Pneumatic conveying: transport solutions, pitfalls, measurements. In *Handbook of Conveying and Handling of Particulate Solids*, edited by Levy, A. and Kalman, H. Amsterdam: Elsevier Science B.V.

Klinzing, G.E., Rizk, F., Marcus, R., and Leung, L.S. 2010. Chapter 4: Fundamentals. In *Pneumatic Conveying of Solids: A Theoretical and Practical Approach*: 95-98. New York: Springer. 3rd ed.

Marcus, R., Leung, L.S., Klinzing, G.E., and Rizk, F. 1990. Chapter 4: Fundamentals. In *Pneumatic Conveying of Solids: A Theoretical and Practical Approach*. London: Chapman and Hall. 1rd ed.

Memory, R. and Atkins, R. 2005. Air seeding-the North American Situation. Available at: http://www1.agric.gov.ab.ca/$department/deptdocs.nsf/all/eng9937. Accessed 11 August 2009.

Mills, D., Jones, M. G., and Agarwal, V. K. 2004. Chapter 1: Types of Pneumatic Conveying Systems and Chapter 2: Feeding Devices. In *Handbook of Pneumatic Conveying Engineering:* 1-26 & 65-66. New York: M. Dekker.

New Holland. 2006. In *New Holland Air Cart Operator's Manual* SC380 SC430. 1st printing. Section 2: 2-4.

NIST. 2011. Thermodynamic Quantities: The National Institute of Standards and Technology. Available at: http://www.nist.gov/calibrations/thermocouples.cfm. Last updated 27 June 2011. Accessed 15 August 2011.

Princo Instruments, Inc. 2000. *Instruction Booklet of use with PRINCO Fortin type mercurial Barometers.* English Language Ed. Revised 1/07. Southampton, PA.

Raheman, H. and Jindal, V.K. 1993. Estimation of pressure drop in pneumatic conveying of agricultural grains. In *Powder Handling & Processing* 5(3): 15-20 & 245-252.

Shamlou, P.A. 1988. Chapter 5: Pneumatic conveying of bulk solids. In *Handling of Bulk Solids, Theory and Practice:* 104-122. Boston: Butterworths.

Smits, A.J. and Dussauge, J.P. 2006. Chapter 2: Equation of Motion. In *Turbulent Shear Layers in Supersonic Flow:* 46. New York: Springger.

Srivastava, A. K., Goering, C. E., Rohrbach, P. R., and Buckmaster, D. R. 2007. Section 12.1: Pneumatic Conveyors. In *Engineering Principles of Agricultural Machines*. 2nd ed.: 516-526. St. Joseph, Michigan: ASABE.

Stoess, H. A., Jr. 1983. What is a pneumatic conveyor?. In *Pneumatic Conveying*. 2nd ed.: 1-36. New York: John Wiley and Sons.

Sun, M., Liu, S., Lei, J., and Li, Z. 2008. Mass flow measurement of pneumatically conveyed solids using electrical capacitance tomography. In *Measurement Science & Technology*. 19(4)-045503: 1-6.

APPENDIX A ITERATIVE CALCULATIONS FOR THE AIR FLOW RATE

Two pieces of information about the air flow were required for processing the experiment. The first one was the air mass flow rate and the second was the air velocity. Equation A-1 and Equation A-2 were given by International Standard ISO 5167-2 2003 (E) and used to calculate the air mass flow rate and the air velocity. From Equation A-2, it can be seen that the calculation for air velocity is dependent on the air mass flow rate. If the mass flow rate of the air was known, the air velocity was also known from dividing the air mass flow rate by the multiplication of the cross section area of the pipe and the air density.

$$m_a = \frac{C}{\sqrt{1-\beta^4}} \times \varepsilon \times \frac{\pi}{4} \times d_o^2 \times \sqrt{2 \times \Delta p_o \times \rho} \qquad \text{A-1}$$

where m_a is the mass flow rate of the air [kg/s]

C is the discharge coefficient from the orifice plate

ε is the expansion factor of the air

d_o is the diameter of the orifice plate [m]

Δp_o is the pressure difference across the orifice plate [Pa]

ρ is the air density [kg/m^3]

β is the diameter ratio of the orifice to the pipe

$$v = \frac{m_a}{A \times \rho} = \frac{m_a}{0.00278 \times \rho} \qquad \text{A-2}$$

where v is the air velocity [m/s]

A is the cross section of the pipe [m^2]

If all of the variables in Equation A-1 were known, it would be easy to calculate the air mass flow rate. However, the discharge coefficient (C) was an unknown and was required for the air mass flow rate calculation. The discharge coefficient is a function of Reynolds number (Re_D) which itself is dependent on the air mass flow rate. In consequence, the direct calculation of the mass flow rate was not possible and the iterative calculation was required instead. The iterative calculation of the air flow was

computed using the suggestion of International Standard ISO 5167-1 2003 (E). The following are details of the iterative calculation for the air mass flow rate.

Step 1: Defining the input parameters

The iterative calculation for the air mass flow rate required the following parameters as inputs: density (ρ), air viscosity (μ), upstream (p_1) and downstream (p_2) pressures of the orifice plate, diameters of the orifice plate (d_o) and the pipe (D).

The viscosity of the air was calculated by Sutherland's formula which is shown in Equation A-3 (Smiths and Dussauge 2006).

$$\frac{\mu}{\mu_0} = \frac{T_0 + 110.3}{T = 110.3}\left(\frac{T}{T_0}\right)^{\frac{3}{2}}, \qquad \text{A-3}$$

Where μ is the absolute viscosity at input temperature T [Pa·s],

μ_0 is the reference viscosity at reference temperature T_0 [18.27 $\times 10^{-6}$ Pa·s],

T is the input temperature [^{o}K],

T_0 is the reference temperature [291.15 ^{o}K].

Step 2: Calculating the expansion factor

Based on the parameters from Step 1, the expansion factor (ε) could initially be determined using Equation A-4 (ISO 5167-2 2003 (E)).

$$\varepsilon = 1 - (0.351 + 0.256 \times \beta^4 + 0.93 \times \beta^8) \times \left[1 - \left(\frac{p_2}{p_1}\right)^{1/1.4}\right] \qquad \text{A-4}$$

where p_1 is the absolute upstream pressure of the orifice plate [Pa]

p_2 is the absolute downstream pressure of the orifice plate [Pa]

Step 3: Calculating an invariant, A_n

The known variables from Equation A-1 were rearranged and used as an invariant in the iterative calculation. This invariant was denoted as 'A_n' and is shown in Equation A-5 which is given by International Standard ISO 5167-1 2003 (E).

$$A_n = \frac{\varepsilon \times d_o^2 \times \sqrt{2 \times \Delta p \times \rho}}{\mu \times D \times \sqrt{1-\beta^4}} \qquad \text{A-5}$$

where n is the number of the iteration

Step 4: Calculating Reynolds number, Re_D

After that, the Reynolds number was determined using A_1 which was the result obtained from the previous step. Equation A-6 shown below was used to calculate the Reynolds number (ISO 5167-1 2003 (E)).

$$Re_D = C_n \times A_1 \qquad \text{A-6}$$

For the first iteration, the initial guess of the discharge coefficient (C_1) used in Equation A-6 was 0.5916. This initial guess was from the assumption that all the terms in the equation used for calculating the discharge coefficient (Equation A-7) were equal to zero ($\beta = 0$), except the first one. This assumption was not true; however, the value of C was corrected in later iterations.

Step 5: Calculating the discharge coefficient, C

After Reynolds number was determined, the value of C was re-calculated by using Equation A-7 (ISO 5167-1 2003 (E)).

$$\begin{aligned} C = {} & 0.5961 + 0.0261 \times \beta^2 - 0.261 \times \beta^8 + 0.000521 \times \left(\frac{10^6 \times \beta}{Re_D} \right)^{0.7} \\ & + \beta^{3.5} \times \left(\frac{10^6}{Re_D} \right)^{0.3} \times \left(0.0188 + 0.0063 \times \left(\frac{19{,}000 \times \beta}{Re_D} \right)^{0.8} \right) \\ & + (0.043 + 0.080 \times e^{-10} - 0.123 \times e^{-7}) \times \left(\frac{\beta^4}{1-\beta^4} \right) \times \left(1 - 0.11 \times \left(\frac{19{,}000 \times \beta}{Re_D} \right)^{0.8} \right) \\ & - 0.031 \times \beta^{1.3} \times \left(\left(\frac{0.94}{1-\beta} \right) - 0.8 \times \left(\frac{0.94}{1-\beta} \right)^{1.1} \right) + 0.011 \times (0.75 - \beta) \times \left(2.8 - \frac{D}{25.4} \right) \end{aligned} \qquad \text{A-7}$$

Step 6: Verifying the precision of the discharge coefficient

Then the value of C obtained from Equation A-7 was checked for its precision by Equation A-8 (ISO 5167-1 2003 (E)).

$$\left| \frac{A_1 - \frac{Re_D}{C}}{A_1} \right| < 1 \times 10^{-n} \qquad \text{A-8}$$

If this inequality was true, the values of Re_D and C were used for calculating the air mass flow rate (m_a) through Equation A-9 (ISO 5167-1 2003 (E)).

$$m_a = \frac{\pi}{4} \times \mu \times D \times Re_D \qquad \text{A-9}$$

If the inequality in Equation A-8 was false, Re_D was re-calculated by Equation A-6 in Step 4, using the value of C from the last iteration. Steps 4 to Step 6 were repeated until the inequality in Equation A-8 was true.

The details of the iterative calculation for the air mass flow rate are summarized in Figure A-1.

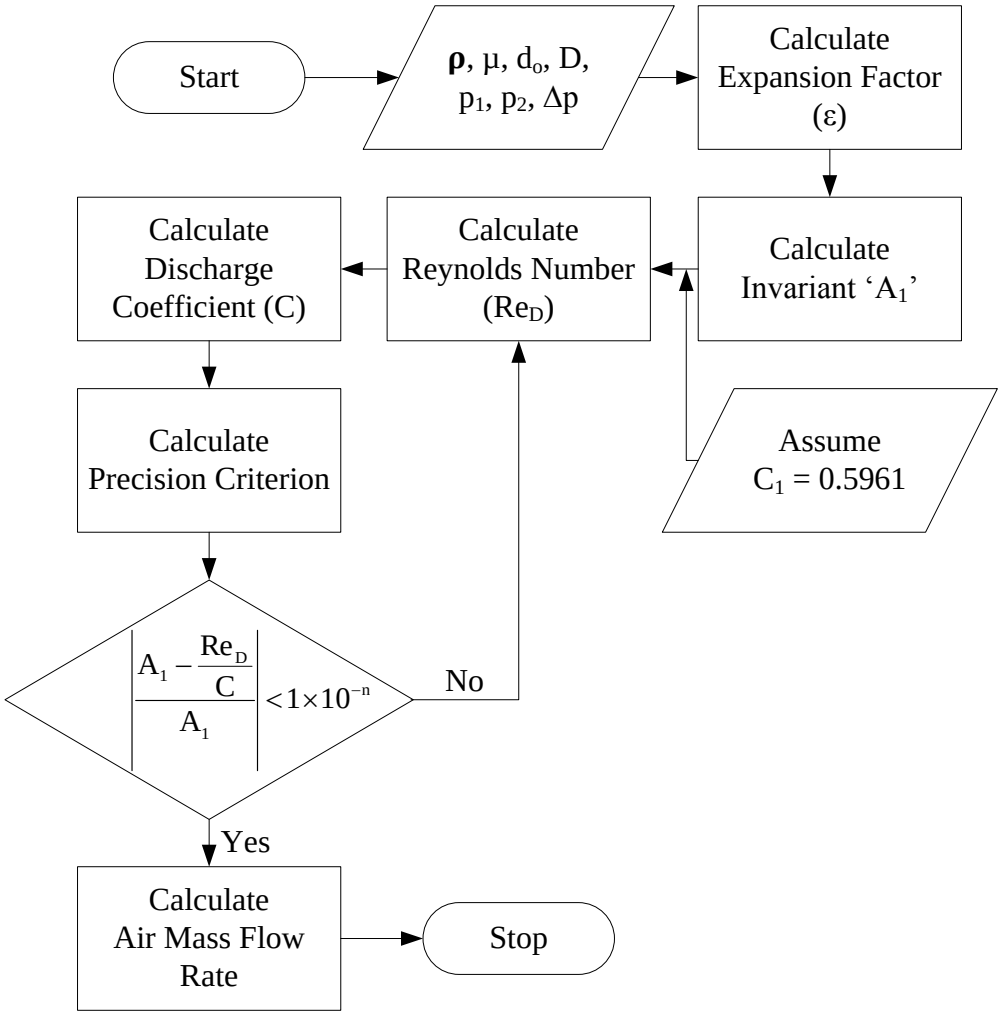

Figure A-1: The flow chart of the iterative calculation for the air mass flow rate

APPENDIX B EXPERIMENTAL SCHEMATICS

Schematics below show the connections between sensing elements and modules, and the wire connection for the air handling control panel.

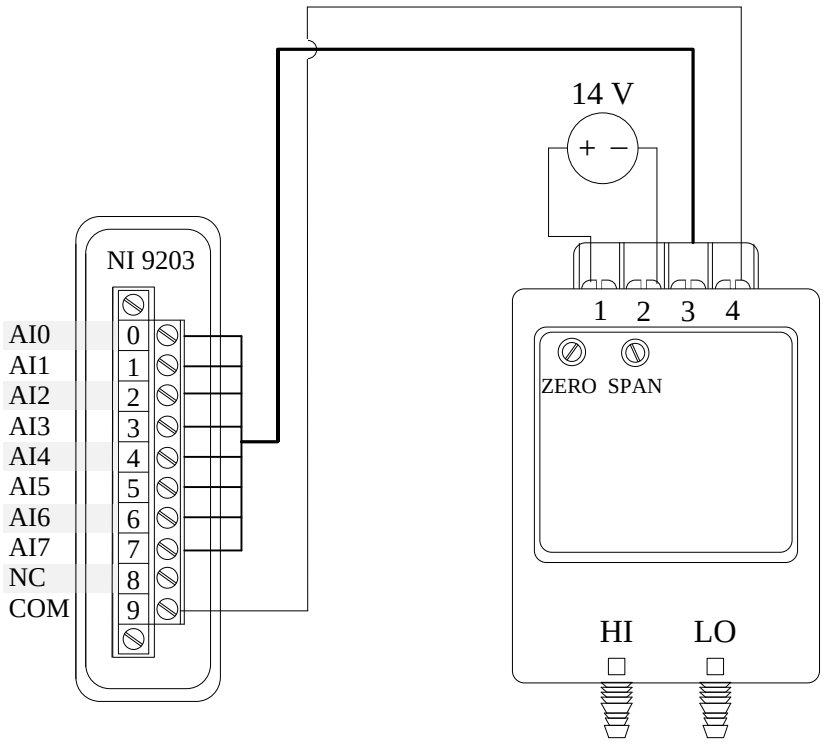

Figure B-1: The schematic of wire connections between analog current input model and pressure transducers

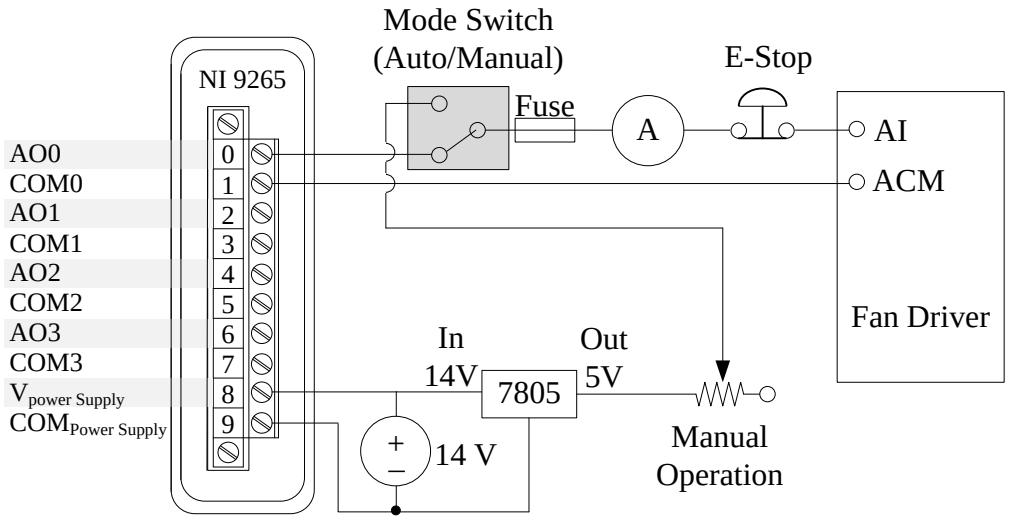

Figure B-2: The schematic of wire connections between analog current output model and fan driver

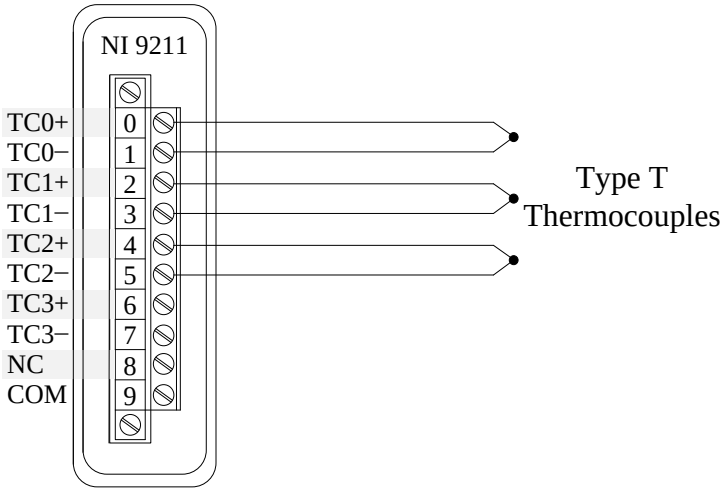

Figure B-3: The schematic of wire connections between thermocouple input module and thermocouples

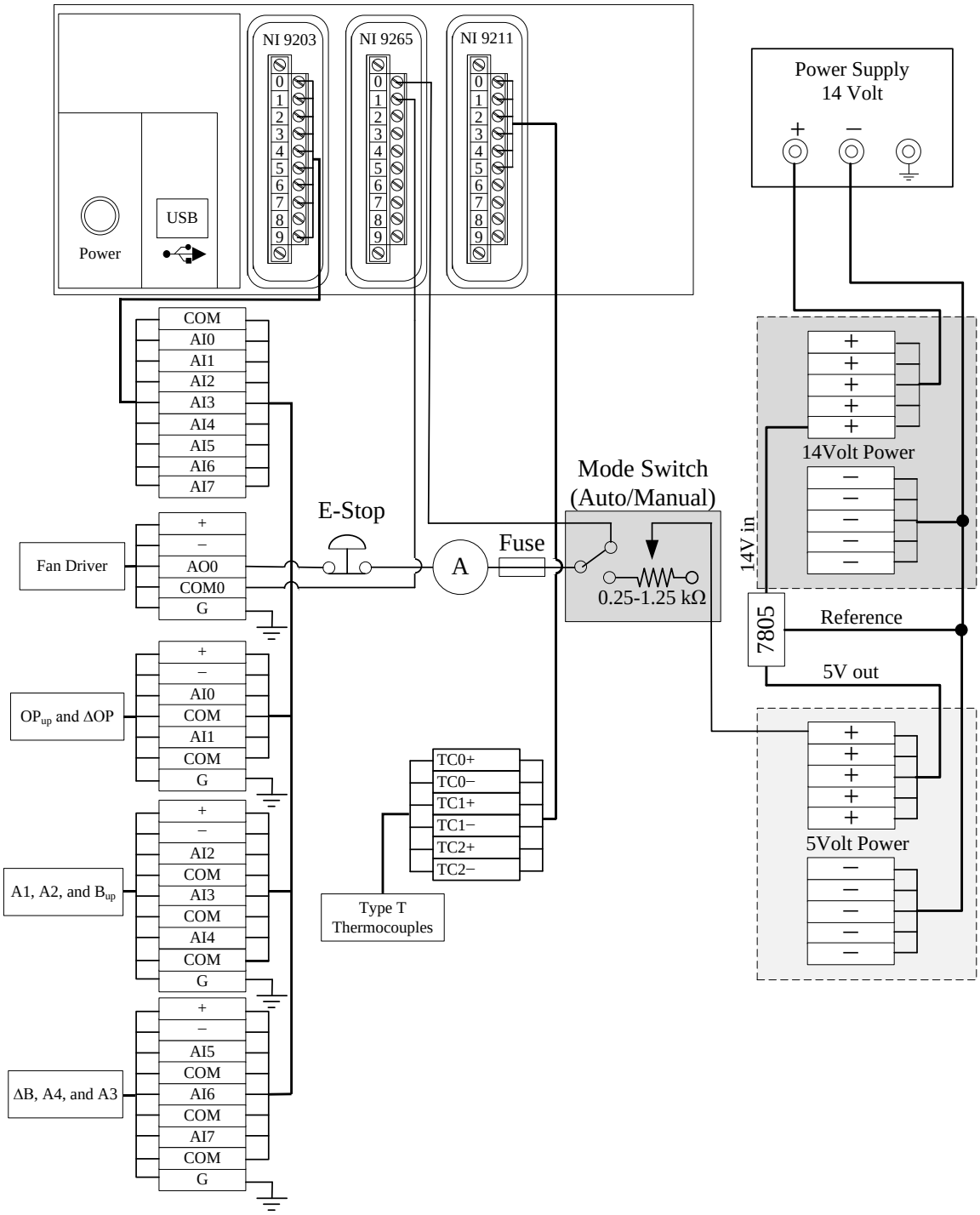

Figure B-4: The schematic of wire connection for the air handling control panel

APPENDIX C SYSTEM OPERATING PROCEDURES

Lab safety and system operating procedures for this study are described below.

C.1 Lab Safety

For safety reasons, before performing any procedures in the air handling lab, the following must be observed.

1) **Safety glasses are mandatory** while operating the fan, filling or emptying the seed tank, or working with tools.
2) **A respirator is not mandatory**, but is recommended when using fertilizer in particular, or if you have dust sensitivities.
3) **Ear plugs** are required when operating the fan at conveying-test speed due to the noise level.
4) **Fan and fan drive** plugs must be locked out after the test is done, or if left unattended for extended periods of time. Only authorized key holders may unlock and operate the fan.
5) **Spills of materials** must be cleaned up promptly as they present a slipping hazard and a potential food source for mice.
6) **Cords and cables** must be managed appropriately to avoid tripping hazards.

C.2 Fan Operation Procedure

There were two methods to operate the fan. The first one was the manual operation and the other one was operating via the LabVIEW program.

C.2.1 Manual Operation

1. The fan mode control switch (three way switch) was turned to the manual operation mode. This switch was located around the central area inside the control panel.
2. The potentiometer was turned all the way counter-clockwise. This protected the fan from operating right away when it was energized. The potentiometer was mounted on the top of the control panel.

3. The power bar which was mounted on the left wall inside the control panel was energized.
4. The power supply was energized. This was located on the top of the control panel.
5. The fan and VFD (Variable-Frequency Drive) were energized. These plugs were on the air cart.
6. The fan switch was switched to the 'ON' position. This switch was on the fan drive box door, underneath the fan.
7. The 'Run' button was pressed. This was the green button on the VFD controller which was beside the fan switch.
8. The fan was ready to be operated.
9. The fan speed was varied by turning the potentiometer.

C.2.2 Auto Operation

1. The fan mode control switch (three way switch) was turned to the auto operation mode.
2. Step 2 to step 7 as described in **Manual Operation** were performed**.** Then the fan was ready to be operated.

The flow chart in Figure C-1 shows the summary of fan operation.

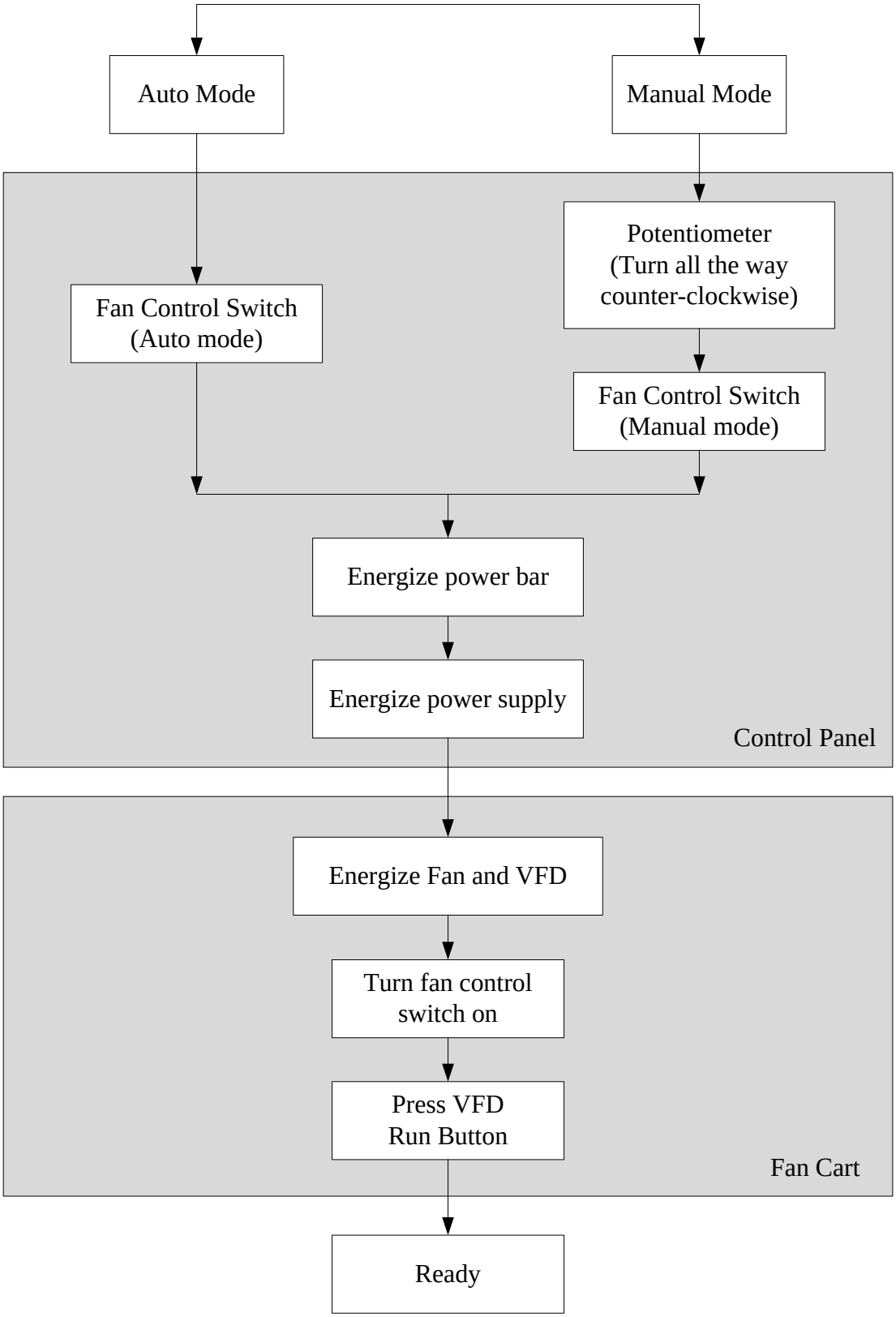

Figure C-1: The procedure of fan operation

C.3 Procedure of Operating Front Panel on LabVIEW Program

The LabVIEW program was used to control the experiment's parameters and monitor the system.The following steps describe the procedure of operating the Front Panel of the LabVIEW program.

C.3.1 To run the program:

1. The LabVIEW program was opened.
2. The atmospheric pressure reading in mmHg was entered into the 'Barometer Reading' block. This block was in the Air Information section.
3. The run button (arrow sign) was pressed to run the program. This button was on the top left of the screen.

At this point, the fan was ready to operate. It was important to ensure that the fan was operating before dispensing the material to the conveying line. Otherwise, blockage may have occurred in the conveying line.

C.3.2 To operate the fan:

4. The fan operating mode switch needed to be on the 'Auto Mode'.
5. The desired air velocity was entered into the 'Target Airspeed' block.
6. The green button beside the 'Target Airspeed' block was pressed to operate the fan.
7. To stop the fan, the same green button needed to be pressed again.
8. The fan control current could be locked or unlocked by pressing 'HOLD DRIVE CURRENT' button which was located below the fan run button.

C.3.3 To operate the stepper motor:

9. Inputting the desired roller speed into the 'Stepper Motor Set RPM' block.
10. Pressing the green button beside the roller speed input block to operate the step motor. To stop the motor, pressing the green button again.

The rest of the sections on the screen displayed the gauge or different pressure reading along the system, velocity and temperature of the conveying air, and lab temperature.

The flow chart in Figure C-2 shows the summary of the procedure of operating the Front Panel on the LabVIEW Program.

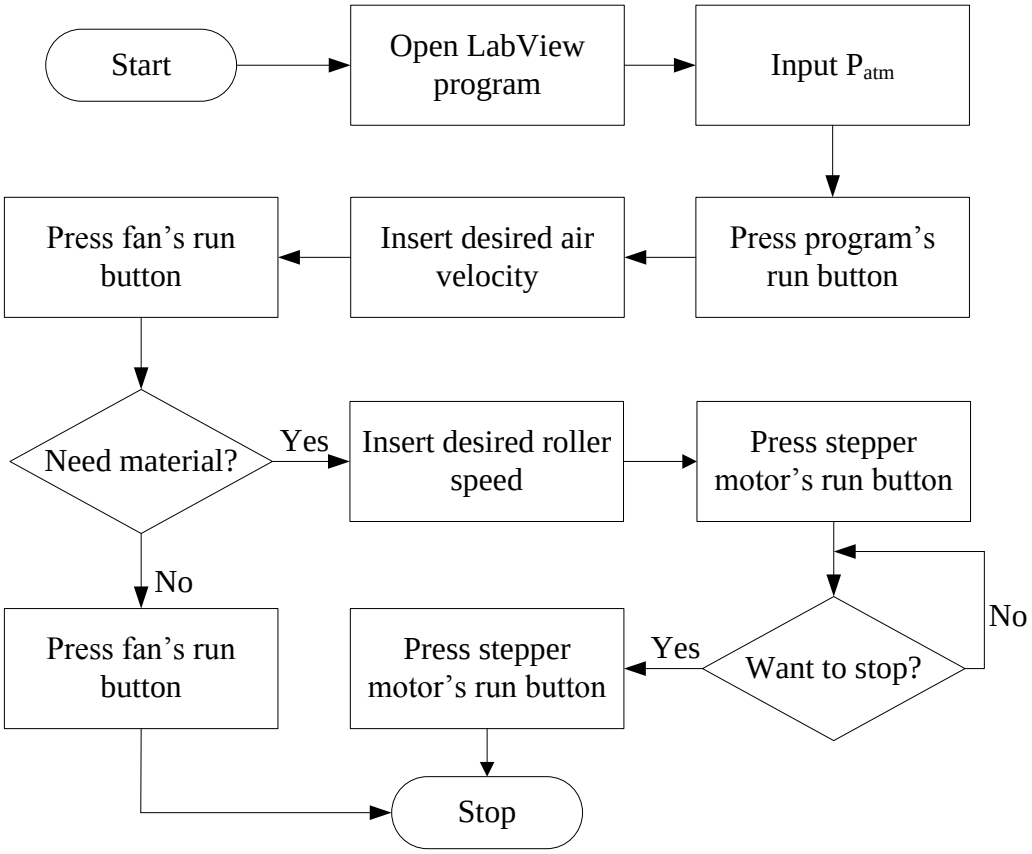

Figure C-2: Procedure of Operating the Front Panel on the LabVIEW Program

C.4 Procedure of Emptying the Tank

The tank needed to be emptied before having the tested materials or rollers changed. The following details explain the procedure of emptying the tank. A summary flow chart is provided in Figure C-3.

1. The fan was operated. The fan speed was dependent on the type of material and material mass flow rate. It was important to have the fan speed high enough to protect blockages from occurring in the conveying line. When the tank was almost empty, the fan speed was decreased. If the speed was too high, the air would blow the materials back to the tank.
2. The stepper motor was operated. The motor speed could be up to 80 rpm.
3. The stepper motor was stopped if the tank was empty.
4. The fan was stopped if the conveying line had no materials left.

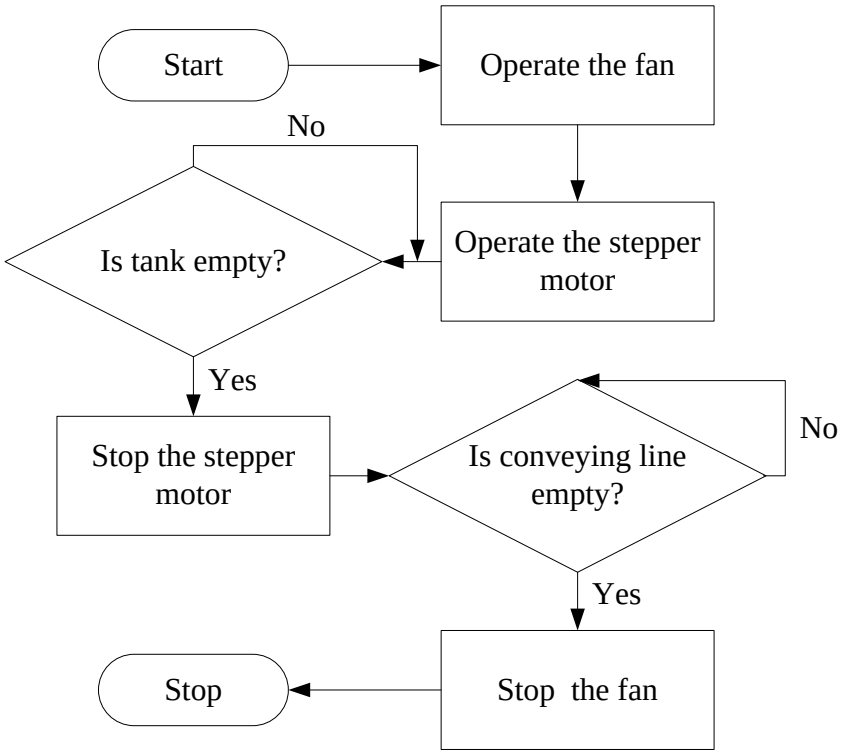

Figure C-3: Procedure of emptying the tank

C.5 Procedure of Changing the Roller

There were three different rollers used for the experiment. The extra fine roller was used for testing canola, the fine roller was used with wheat, and the extra coarse roller was used for testing chickpea and fertilizer. When the testing materials were changed, the roller was changed to match the next testing material. The following explanation describes the procedure of changing roller.

1. The tank was emptied.
2. If changing from chickpea to fertilizer or fertilizer to chickpea, the roller was not changed. Otherwise, the roller was changed based on the testing materials.
3. The metering box was opened. This was at the bottom of the air cart simulator.
4. The roller shaft was removed.
5. The roller was replaced with the one being used for the next testing material.
6. The roller shaft was reinstalled back to its place. Some of the time, this required pulling the stepper motor back a little bit by loosening the bolts used

for holding stepper motor. This way, the roller shaft could be aligned and reinstalled easily.

7. The metering box was closed.
8. At this point, the air cart simulator was ready to be loaded with the testing materials.

The flow chart of the procedure for changing the roller is shown below.

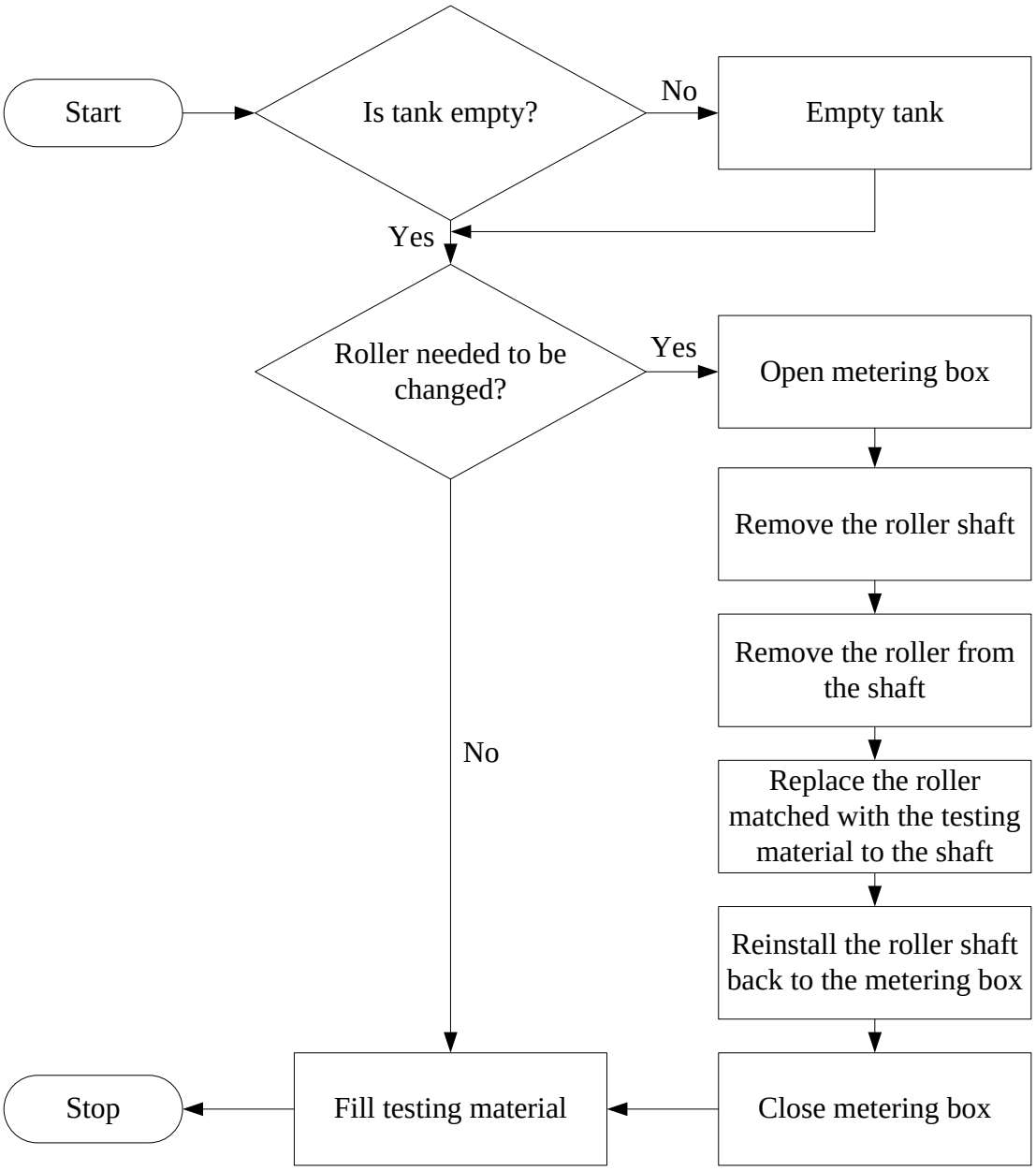

Figure C-4: The procedure of changing the roller

C.6 Procedure of Refilling the Products

The system required at least half pail of the testing material left in the tank. If the amount of the materials was less than that, the materials needed to be refilled. This protected from back pressure blowing the material away from the metering box. The following procedures describe the steps of refilling the testing materials.

1. The stepper motor was stopped.
2. The fan was stopped after the conveying line had no materials left.
3. The tank was opened.
4. The testing material was refilled.
5. The tank was closed.

The flow chart below shows the procedure of refilling the material.

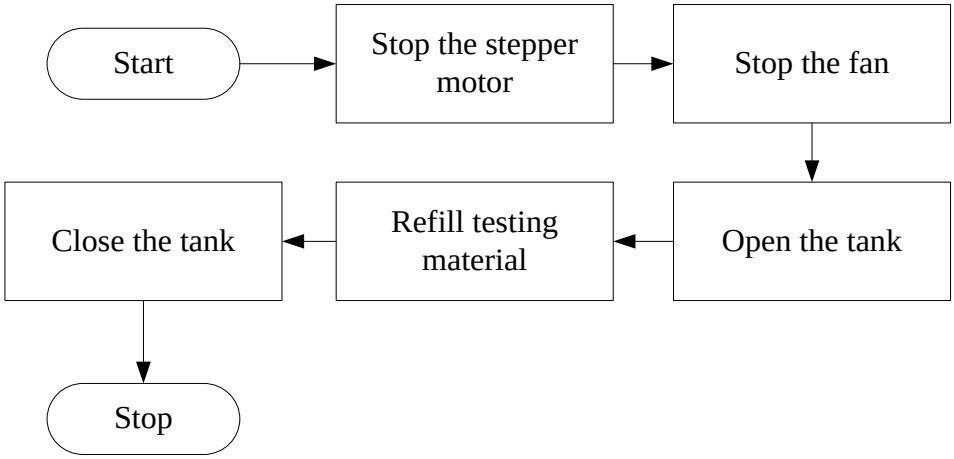

Figure C-5: The procedure of refilling the material

C.7 Procedure of Shutting Down the Air Handling System

The following are the recommended steps of shutting down the air handling system.

1. The stepper motor was stopped.
2. The fan was stopped, if the conveying line was clear.
3. The LabVIEW program was stopped.
4. The LabVIEW program was closed.
5. The power supply was shut down.

6. The power bar was shut down.
7. The fan drive's switch was turned to the 'OFF' position.
8. The fan and fan drive cords were de-energized.
9. The power cords were locked out.
10. The digital multimeter was turned off.
11. The potentiometer was turned all the way counter clockwise.
12. The control panel door was closed.

The flow chart of the shutting down procedures is shown in Figure C-6.

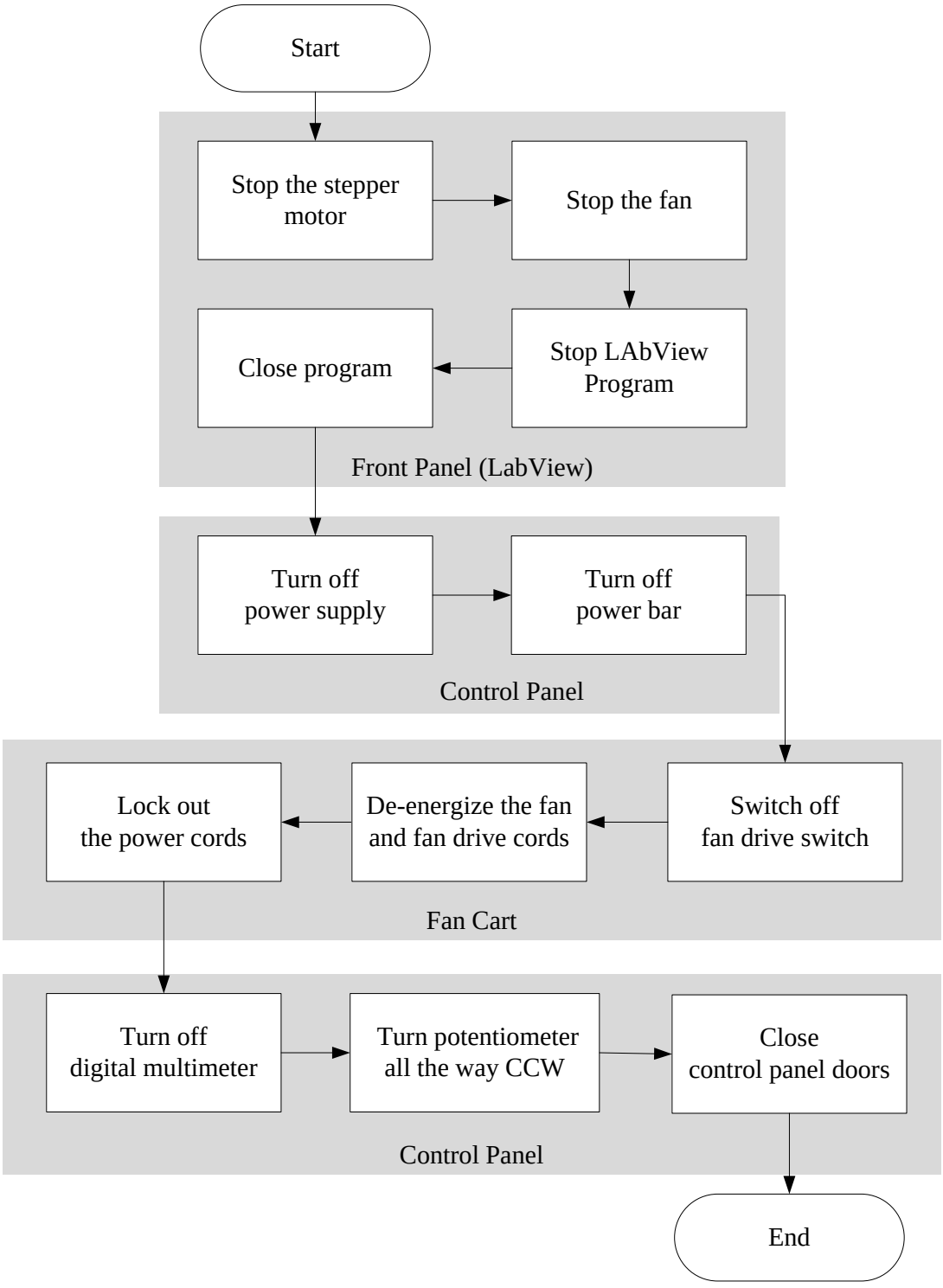

Figure C-6: The procedure of shutting down the air handling system

APPENDIX D METERING SYSTEM CALIBRATION PROCEDURE

The metering system (roller) calibration of tested material was done by the following steps.

Step 1 was choosing the material that would be tested. There were four materials used in the experiment. The first one was canola, the second was wheat, the third was chickpea and the last one was fertilizer.

Step 2 was choosing the roller speed for the material chosen in Step 1, then replacing or installing the chosen roller into the metering system.

There were three different types of rollers used in the experiment. The first one was the extra fine roller which was used for testing canola. The second was the fine roller which was used for testing wheat. The last one was the extra coarse roller which was used for testing both chickpea and fertilizer.

Step 3 was operating the fan. The fan was turned on after the roller was installed and material was loaded into the tank. The fan speed was dependent on the type of materials and material dispense rate. The bigger size of the tested material or higher material dispense rate required the higher fan speed.

Step 4 was operating the roller. This was operated by using the LabVIEW program. On the user interface page there is a roller operating section called “Stepper Motor”.

Step 5 was calibrating the roller. The calibration was initiated by inputting the desired roller speed to the “Stepper Motor Set RPM” block and pressing run button (a green rectangular block beside Stepper Motor Set RPM block). The material was collected for 3 minutes and the weight was averaged to get the material flow represented for 1 minute. After the roller had operated for 3 minutes, the run button was pressed again to stop the roller. At this point, the conveying line was checked. If there was no material left, the fan was stopped and dispensed material was weighed. In the opposite, if there were still some materials left in the line, the operator had to wait until the line was empty. Then the fan was stopped and the dispensed material was weighed. The weighed materials would be measured in grams per 3 minutes. It was important that the operator made sure that the fan was operating before dispensing the material to the conveying line. Otherwise, blockage may have occurred in the conveying line.

Step 6 was the unit conversion. The units of the result from Step were in grams per 3 minutes but it needed to be converted to kilograms per second. This was done by dividing the weight (g/3min) by 180,000. The detail of the conversion is shown in Equation D-1.

$$\frac{\text{weight}\,[\text{g}]}{3\,[\text{min}]} \times \frac{1\,[\text{kg}]}{1000\,[\text{g}]} \times \frac{1\,[\text{min}]}{60\,[\text{s}]} = \frac{\text{weight}}{180{,}000}\left[\frac{\text{kg}}{\text{s}}\right] \qquad \text{D-1}$$

Step 3 to 6 were repeated for calibrating the next desired roller speed. The summary of the roller calibration is depicted in the flow chart below, Figure D-1.

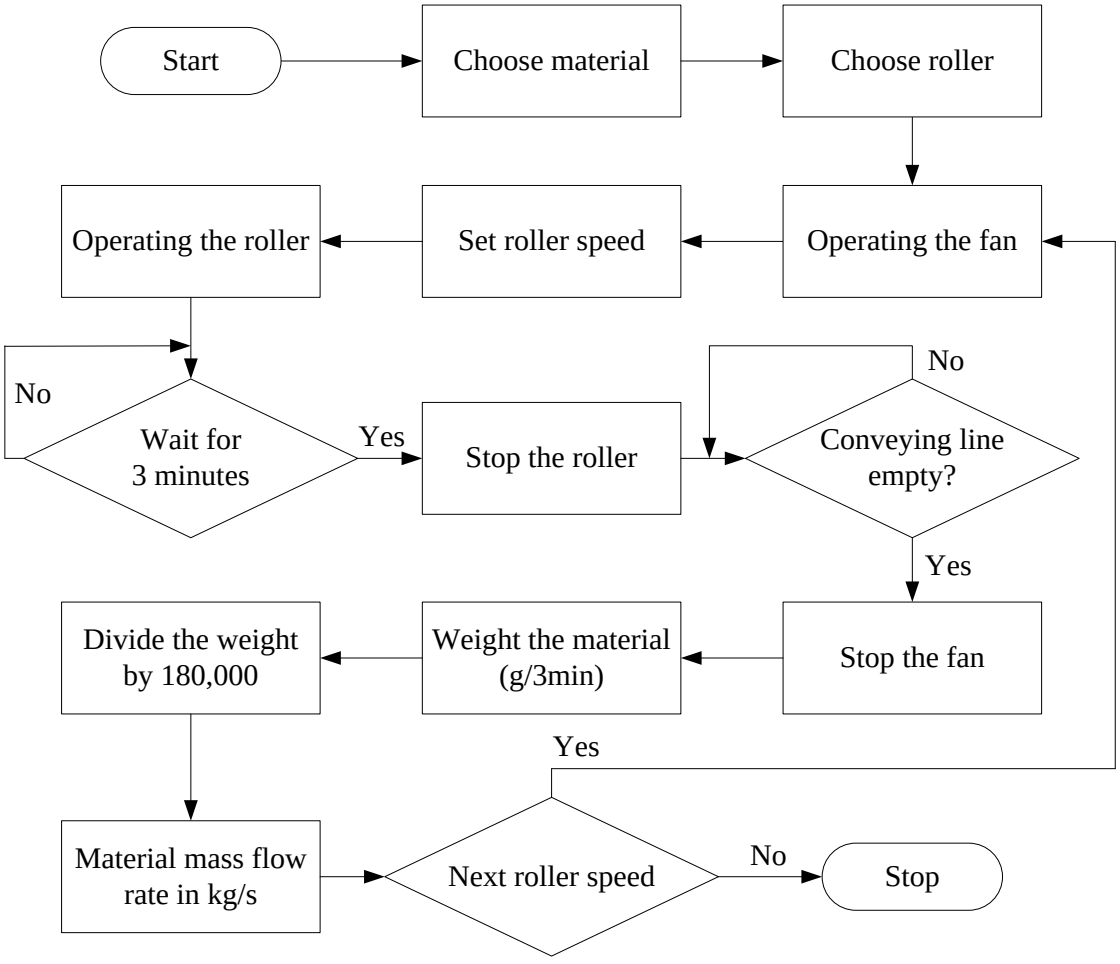

Figure D-1: The flow chart of roller calibration

APPENDIX E ROLLER SPEED TO MASS FLOW RATE CONVERSION

There were four input parameters required for this calculation. The first was a tractor's ground speed which ranged from 7 km/h to16 km/h (4.5-10 mph), varied by the soil condition. The second parameter was the width of the tilling implement (air hoe drill) per run, which was 3 m. The third was the seeding rate. The last parameter was the calibration equations for each tested material. The flow chart below shows the overall steps of the roller speed calculations and conversions.

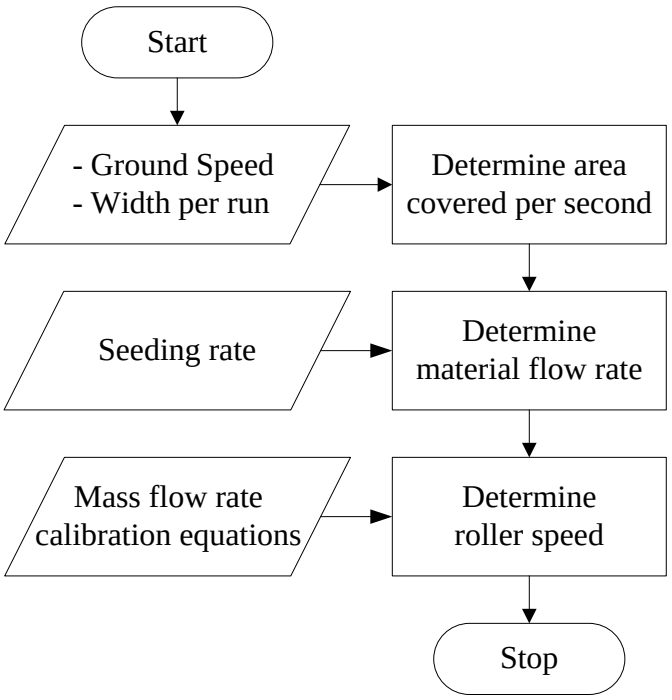

Figure E-1: The flow chart of roller speed calculation

The following details show the calculation of the roller speed.

Step 1: Determining the area covered per second

The first step was determining the area in hectare covered by one single width per second. This was determined by multiplying the tractor's ground speed by the width of tilling implement. Then the units were converted to hectare per second. The calculation details are shown in E-1 and E-2.

$$7\left[\frac{\text{km}}{\text{h}}\right]\times\frac{1[\text{h}]}{3600[\text{s}]}\times 3[\text{m}]\times\frac{1[\text{km}]}{1000[\text{m}]}\times\frac{100[\text{ha}]}{1[\text{km}^2]}=0.0006\left[\frac{\text{ha}}{\text{s}}\right] \quad \text{E-1}$$

And

$$16\left[\frac{\text{km}}{\text{h}}\right]\times\frac{1[\text{h}]}{3600[\text{s}]}\times 3\text{m}\times\frac{1[\text{km}]}{1000[\text{m}]}\times\frac{100[\text{ha}]}{1[\text{km}^2]}=0.0013\left[\frac{\text{ha}}{\text{s}}\right] \quad \text{E-2}$$

As a result, the area covered by a single width of roller per second was between 0.0006-0.0013 ha/s.

Step 2: Determining the material mass flow rate

Before determining the material mass flow rate, the seeding range of the tested materials needed to be identified. The seeding ranges were initially obtained from the air cart operator's manual (New Holland, 2006) which were 6-13, 45-135, 168-280, and 34-392 kg/ha for canola, wheat, chickpea, and fertilizer respectively (Table E-1). Then, this knowledge was combined with the information of the seeding rates gathered by Gervais (2011) which were 3.4-6.7, 100-151, 135-210, 11-100 kg/ha for canola, wheat, chickpea, and fertilizer, respectively (Table E-2). As a result, the ranges of seeding were expanded and became 3.4-13, 45-151, 135-280, 11-392 kg/ha for canola, wheat, chickpea, and fertilizer, respectively. This is shown in Table E-3.

Table E-1: The seeding ranges recommended from the manufacturer (New Holland, 2006).

Product	**Seeding Rate Range** [kg/ha] per roller
Canola	6-13
Wheat	45-135
Chickpea	168-280
Fertilizer	34-392

Table E-2: The seeding rates being gathered by Gervais (2011).

Product	**Seeding Rate Range** [kg/ha] per roller
Canola	3.4-6.7
Wheat	100-151
Chickpea	135-210
Fertilizer	11-100

Table E-3: The adjusted seeding ranges for the experiment.

Product	**Seeding Rate Range** [kg/ha] per roller
Canola	3.4-13
Wheat	45-151
Chickpea	135-280
Fertilizer	11-392

The material mass flow rate could then be calculated by multiplying the result from the previous calculation (Step 1) with the seeding rate (Table E-3). The calculation of the materials mass flow rate of the canola is illustrated as an example. The calculation in E-3 is the maximum seeding rate and E-4 is the minimum one. The results of the calculations for all tested materials are shown in Table E-4.

$$13\left[\frac{\text{kg}}{\text{ha}}\right]\times 0.0013\left[\frac{\text{ha}}{\text{s}}\right]=0.0173\left[\frac{\text{kg}}{\text{s}}\right] \qquad \text{E-3}$$

and

$$3.4\left[\frac{\text{kg}}{\text{ha}}\right]\times 0.0013\left[\frac{\text{ha}}{\text{s}}\right]=0.0020\left[\frac{\text{kg}}{\text{s}}\right] \qquad \text{E-4}$$

Table E-4: The materials mass flow rate from the calculation in Step 2.

Product	**Seeding Rates** [kg/ha]		**Materials Flow Rates,** m_p [kg/s]	
	Max	Min	Max	Min
Canola	13	3.4	0.017	0.002
Wheat	151	45	0.201	0.026
Chickpeas	280	135	0.373	0.079
Fertilizer	392	11	0.523	0.006

Step 3: Determining the roller speed

The last step was to calculate the roller speed. This was determined by substituting the mass flow rates from the Step 2 to the rollers calibration equations achieved from Figure E-2. Then the roller speeds were solved. The calculation of canola was chosen again to show as an example. However, it was found that the upper ranges of chickpea and fertilizer could not be determined based on the calibration data. This was due to the materials mass flow rates of those two materials exceeding the ranges that the calibration equations could predict. Figure E-3 shows that the maximum mass flow rate of chickpea and fertilizer that the system could dispense was about 0.34 and 0.35 kg/s, respectively. In contrast, the upper ranges of the materials mass flow rates calculated from Step 2 were higher (0.373 kg/s for chickpea and 0.523 kg/s for fertilizer). Therefore, the upper ranges of chickpea and fertilizer were chosen from the maximum speed the system could achieve which were about 200 and 220 rpm, respectively. The results of all roller speed calculations are shown in Table E-5.

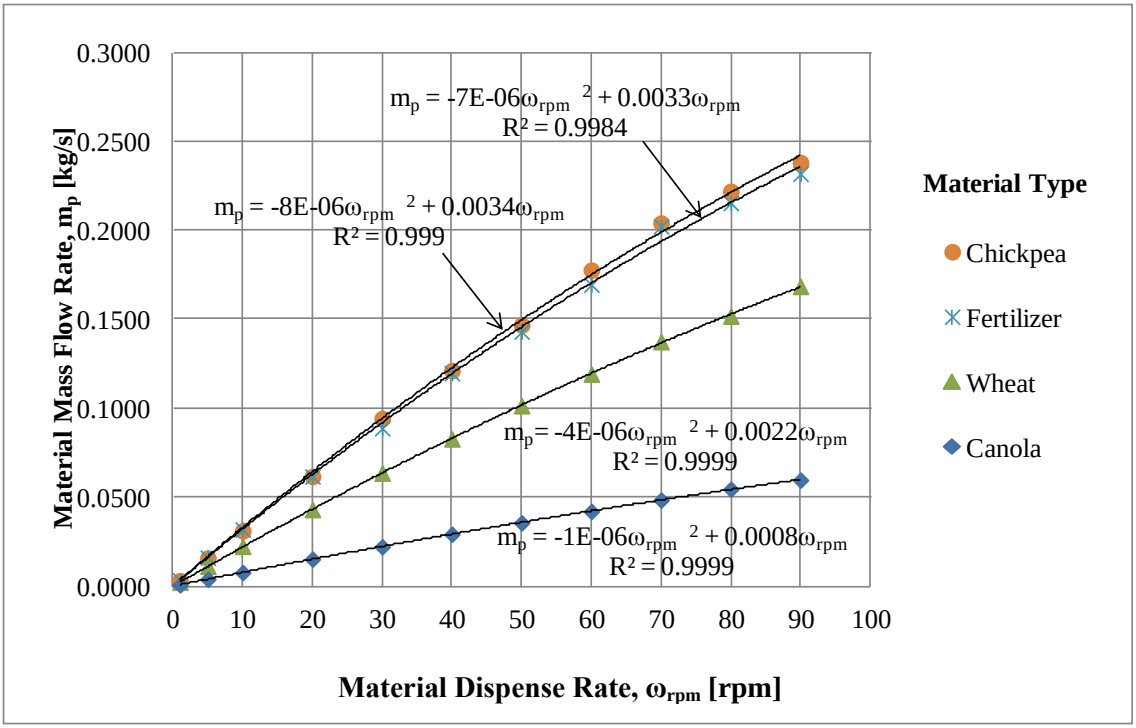

Figure E-2: The roller calibration chart for tested materials

$$m_p = -10^{-6} \times \omega_{rpm}^{\ 2} + 0.0008 \times \omega_{rpm}$$

$$0.01733 = -10^{-6} \times \omega_{rpm}^{\ 2} + 0.0008 \times \omega_{rpm}$$

$$\omega_{rpm} = 23.22, 777.72 [rpm]$$

$$0.00198 = -10^{-6} \times \omega_{rpm}^{\ 2} + 0.0008 \times \omega_{rpm}$$

$$\omega_{rpm} = 4.67, 795.60 [rpm]$$ E-5

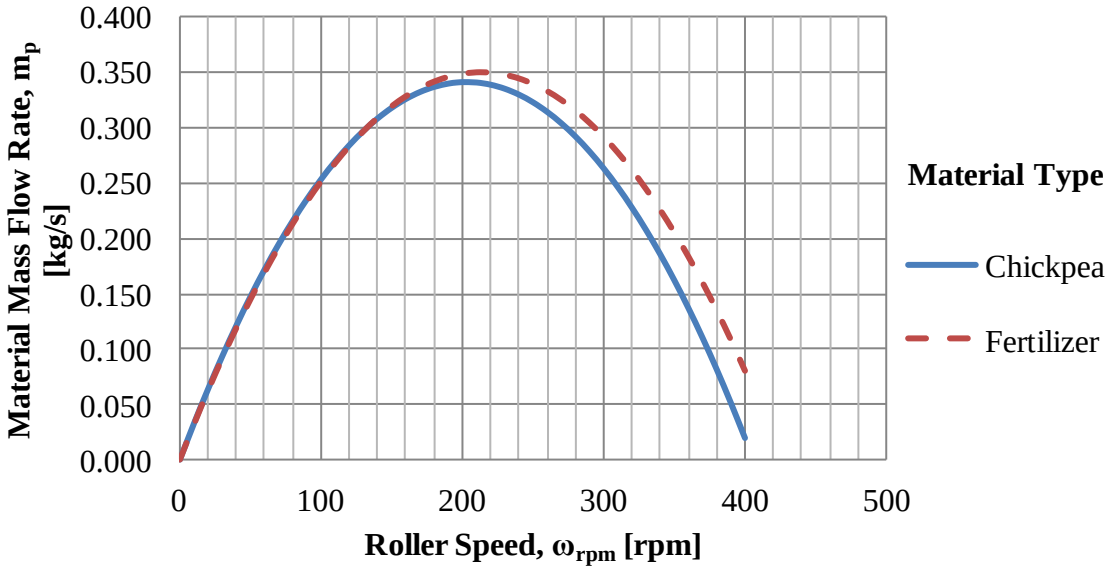

Figure E-3: Estimation of the mass flow rate of chickpea and fertilizer from the calibration models

Table E-5: The roller speed from the calculations

Product	**Material Mass Flow Rate** [kg/s]		**Roller Calibration Equation**	**Roller Speed** [rpm]	
	Max	Min		Max	Min
Canola	0.017	0.002	m_p = -1E-06$\omega_{rpm}^{\ 2}$ + 0.0008 ω_{rpm}	23	5
Wheat	0.201	0.026	m_p = -4E-06 $\omega_{rpm}^{\ 2}$ + 0.0022 ω_{rpm}	98	12
Chickpea	0.373	0.079	m_p = -8E-06 $\omega_{rpm}^{\ 2}$ + 0.0034 ω_{rpm}	200	26
Fertilizer	0.523	0.006	m_p = -7E-06 $\omega_{rpm}^{\ 2}$ + 0.0033 ω_{rpm}	220	2

APPENDIX F AIR FLOW VERIFICATION DATA

The table below shows data collected from the air flow test by using a Pitot-static tube to verify the air flow measusmtnet from an orifice plate.

Table F-1: Verification data for the air flow test (traverse test)

Radius [mm]	T [ºC]	Barometer Reading [mmHg]	Air Density [kg/m^3]	p_{total} [Pa] (Pitot)	p_1 [Pa] (Orifice)	Δp [Pa] (Orifice)	Air Velocity [m/s]
0	19	715.9	1.14	361	911	1356	21.3
0	19	715.9	1.14	360	912	1356	21.3
0	19	715.9	1.14	361	912	1355	21.3
0	19	715.9	1.14	361	912	1356	21.3
0	19	715.9	1.14	360	912	1355	21.3
0	19	715.9	1.14	361	911	1354	21.3
3	19	715.9	1.14	358	911	1356	21.2
3	19	715.9	1.14	359	912	1356	21.3
3	19	715.9	1.14	359	912	1356	21.3
3	19	715.9	1.14	359	912	1356	21.3
3	19	715.9	1.14	359	912	1355	21.3
3	19	715.9	1.14	359	912	1357	21.3
6	19	715.9	1.14	352	912	1357	21.3
6	19	715.9	1.14	352	911	1355	21.3
6	19	715.9	1.14	352	911	1356	21.3
6	19	715.9	1.14	352	913	1357	21.3
6	19	715.9	1.14	352	912	1357	21.3
6	19	715.9	1.14	352	913	1357	21.3
9	19	715.9	1.14	340	912	1357	21.3
9	19	715.9	1.14	340	912	1356	21.3
9	19	715.9	1.14	341	912	1357	21.3
9	19	715.9	1.14	340	911	1355	21.3
9	19	715.9	1.14	340	912	1356	21.3
9	19	715.9	1.14	340	912	1358	21.3
12	19	715.9	1.14	327	912	1357	21.1
12	19	715.9	1.14	327	911	1356	21.3
12	19	715.9	1.14	326	912	1356	21.3
12	19	715.9	1.14	327	912	1357	21.3
12	19	715.9	1.14	327	913	1358	21.3
12	19	715.9	1.14	327	912	1358	21.3
15	19	715.9	1.14	306	911	1357	21.3

Table F-1: Verification data for the air flow test (traverse test)

Radius [mm]	T [ºC]	Barometer Reading [mmHg]	Air Density [kg/m^3]	p_{total} [Pa] (Pitot)	p_1 [Pa] (Orifice)	Δp [Pa] (Orifice)	Air Velocity [m/s]
15	19	715.9	1.14	306	911	1355	21.3
15	19	715.9	1.14	306	911	1355	21.3
15	19	715.9	1.14	306	910	1354	21.3
15	19	715.9	1.14	306	909	1352	21.3
15	19	715.9	1.14	306	909	1353	21.2
18	19	715.9	1.14	287	911	1355	21.1
18	19	715.9	1.14	287	909	1354	21.3
18	19	715.9	1.14	288	909	1353	21.3
18	19	715.9	1.14	287	909	1352	21.3
18	19	715.9	1.14	287	910	1354	21.2
18	19	715.9	1.14	287	909	1354	21.3
21	19	715.9	1.14	267	907	1350	21.2
21	19	715.9	1.14	267	908	1351	21.2
21	19	715.9	1.14	268	908	1351	21.2
21	19	715.9	1.14	268	908	1351	21.2
21	19	715.9	1.14	267	907	1350	21.2
21	19	715.9	1.14	268	908	1351	21.2
21	19	715.9	1.14	267	908	1351	21.2
24	19	715.9	1.14	247	908	1352	21.3
24	19	715.9	1.14	246	907	1351	21.2
24	19	715.9	1.14	246	909	1352	21.2
24	19	715.9	1.14	246	909	1352	21.2
24	19	715.9	1.14	246	909	1354	21.2
24	19	715.9	1.14	246	915	1336	21.2
25.93	19	715.9	1.14	232	910	1353	21.1
25.93	19	715.9	1.14	231	909	1352	21.3
25.93	19	715.9	1.14	230	908	1351	21.2
25.93	19	715.9	1.14	232	908	1350	21.2
25.93	19	715.9	1.14	231	908	1351	21.2
25.93	19	715.9	1.14	231	909	1353	21.2
Average			1.14		910	1354	21.3

APPENDIX G PRESSURE DROP TEST SUMMARIZED DATA

Data collected from the experiment for both data set 1 and 2 were statistically summarized in this section.

G.1 Data Set 1 Statistical Summary

Please note that the category column uses a two digit indicating the air velocity (first digit) and the material mass flow rate (second digit).

Table G-1: The statistical summary of the actual air velocity and the pressure drop across the elevation due to the air only for canola in data set 1.

Test Category	Obs #	Actual Air Velocity [m/s]				Pressure Loss [kPa]			
		Mean	Std Dev	Min	Max	Mean	Std Dev	Min	Max
11	187	9	0	9	9.1	0.043	0.001	0.041	0.045
12	188	10	0.1	9.9	10.2	0.052	0.001	0.049	0.055
13	193	10.1	0.1	9.9	10.2	0.052	0.001	0.050	0.055
14	189	10	0.1	9.8	10.1	0.051	0.001	0.049	0.054
15	188	11	0.1	10.9	11.1	0.061	0.001	0.058	0.064
21	252	10.5	0.1	10.4	10.6	0.056	0.001	0.053	0.060
22	185	11.5	0.1	11.4	11.6	0.066	0.001	0.063	0.070
23	188	11.5	0.1	11.4	11.6	0.066	0.001	0.063	0.069
24	190	11.5	0	11.4	11.6	0.066	0.001	0.063	0.070
25	187	12.5	0.1	12.4	12.7	0.078	0.001	0.075	0.082
31	189	12	0.1	11.9	12.2	0.072	0.002	0.068	0.077
32	190	13	0.1	12.9	13.1	0.082	0.002	0.079	0.088
33	201	13	0.1	12.9	13.2	0.083	0.002	0.079	0.089
34	187	13.1	0.1	12.9	13.2	0.083	0.001	0.080	0.088
35	251	14	0.1	13.8	14.2	0.094	0.002	0.089	0.100
41	196	13.5	0.1	13.3	13.6	0.088	0.001	0.085	0.092
42	191	14.5	0.1	14.3	14.7	0.100	0.002	0.096	0.107
43	188	14.5	0.1	14.3	14.7	0.100	0.002	0.095	0.105
44	189	14.5	0.1	14.3	14.7	0.100	0.002	0.094	0.106
45	184	15.4	0.3	14.8	15.7	0.111	0.005	0.101	0.122
51	190	15	0.1	14.8	15.2	0.106	0.002	0.101	0.113
52	193	16	0.1	15.7	16.2	0.119	0.003	0.112	0.127
53	187	16	0.1	15.8	16.2	0.119	0.003	0.112	0.127
54	192	16.1	0.1	15.9	16.4	0.121	0.003	0.114	0.127
55	195	17.1	0.2	16.6	17.5	0.133	0.003	0.127	0.140

Table G-2: The statistical summary of the actual air velocity and the pressure drop across the elevation due to the tested material for canola in data set 1.

Test Category	Obs #	Actual Air Velocity [m/s]				Pressure Loss [kPa]			
		Mean	Std Dev	Min	Max	Mean	Std Dev	Min	Max
11	190	9	0.1	8.9	9.1	0.052	0.001	0.048	0.054
12	187	10	0	9.9	10.2	0.072	0.001	0.069	0.076
13	193	10	0	9.9	10.1	0.083	0.002	0.080	0.089
14	194	9.9	0	9.9	10	0.094	0.002	0.088	0.099
15	186	11	0.1	10.8	11.1	0.114	0.002	0.109	0.119
21	251	10.6	0.1	10.4	11.1	0.066	0.002	0.062	0.071
22	185	11.5	0.1	11.3	11.6	0.087	0.002	0.083	0.091
23	186	11.5	0.1	11.3	11.6	0.098	0.002	0.094	0.104
24	192	11.5	0.1	11.4	11.7	0.109	0.002	0.104	0.117
25	185	12.5	0.1	12.4	12.7	0.130	0.003	0.124	0.137
31	187	12	0.1	11.9	12.2	0.081	0.002	0.078	0.087
32	194	13	0.1	12.9	13.3	0.104	0.002	0.098	0.109
33	188	13	0.1	12.9	13.1	0.115	0.002	0.110	0.120
34	191	13	0.1	12.8	13.2	0.127	0.002	0.121	0.134
35	191	14	0.1	13.8	14.2	0.150	0.003	0.142	0.158
41	195	13.5	0.1	13.4	13.7	0.099	0.002	0.093	0.107
42	190	14.5	0.1	14.3	14.7	0.123	0.003	0.116	0.130
43	189	14.5	0.1	14.4	14.8	0.135	0.002	0.129	0.141
44	191	14.6	0.1	14.4	14.7	0.147	0.003	0.140	0.153
45	191	15.4	0.1	15.2	15.7	0.169	0.003	0.162	0.177
51	196	15	0.1	14.8	15.3	0.118	0.003	0.111	0.126
52	190	16.1	0.1	15.9	16.4	0.145	0.003	0.137	0.150
53	187	16.1	0.1	15.8	16.4	0.156	0.003	0.148	0.163
54	187	16	0.1	15.8	16.2	0.168	0.003	0.160	0.177
55	191	17.1	0.1	16.8	17.4	0.192	0.003	0.183	0.202

Table G-3: The statistical summary of the actual air velocity and the pressure drop across the elevation due to the air only for wheat in data set 1.

Test Category	Obs #	Actual Air Velocity [m/s]				Pressure Loss [kPa]			
		Mean	Std Dev	Min	Max	Mean	Std Dev	Min	Max
11	203	15.1	0.2	14.8	15.4	0.098	0.002	0.092	0.106
12	186	19.0	0.1	18.8	19.4	0.15	0.003	0.143	0.158
13	186	21.1	0.1	20.7	21.4	0.179	0.003	0.17	0.187
14	188	22.9	0.2	22.7	23.2	0.209	0.003	0.2	0.217
15	182	24.9	0.2	24.5	25.2	0.247	0.004	0.238	0.256
21	187	17.0	0.1	16.7	17.3	0.124	0.003	0.118	0.133
22	187	22.1	0.1	21.8	22.3	0.197	0.004	0.186	0.208
23	184	24.1	0.2	23.7	24.3	0.23	0.005	0.22	0.243
24	188	26.2	0.2	25.9	26.6	0.267	0.005	0.252	0.28
25	186	28.0	0.1	27.6	28.3	0.299	0.007	0.286	0.316
31	192	19.1	0.1	18.9	19.6	0.15	0.003	0.142	0.158
32	189	24.9	0.1	24.6	25.3	0.246	0.006	0.233	0.259
33	185	27.1	0.2	26.7	27.4	0.28	0.005	0.268	0.291
34	187	29.0	0.2	28.7	29.4	0.317	0.006	0.303	0.331
35	187	31.0	0.3	30.5	31.7	0.354	0.009	0.335	0.374
41	183	21.0	0.2	20.7	21.4	0.179	0.005	0.169	0.194
42	189	28.1	0.2	27.7	28.4	0.302	0.005	0.288	0.316
43	202	30.1	0.1	29.7	30.4	0.34	0.005	0.324	0.35
44	185	32.0	0.2	31.6	32.6	0.374	0.005	0.36	0.387
45	124	34.2	0.3	33.6	34.7	0.424	0.005	0.411	0.437
51	191	22.9	0.1	22.7	23.2	0.209	0.003	0.2	0.219
52	187	31.0	0.2	30.5	31.4	0.356	0.009	0.338	0.38
53	185	32.9	0.2	32.4	33.4	0.399	0.007	0.383	0.416
54	122	34.7	0.2	34.2	35.2	0.439	0.009	0.421	0.458

Table G-4: The statistical summary of the actual air velocity and the pressure drop across the elevation due to the tested material for wheat in data set 1.

Test Category	Obs #	Actual Air Velocity [m/s]				Pressure Loss [kPa]			
		Mean	Std Dev	Min	Max	Mean	Std Dev	Min	Max
11	188	14.9	0.1	14.6	15.1	0.177	0.01	0.154	0.194
12	182	19.1	0.2	18.9	19.5	0.380	0.022	0.334	0.428
13	185	21.0	0.2	20.6	21.4	0.551	0.024	0.50	0.605
14	186	23.1	0.2	22.6	23.6	0.707	0.035	0.650	0.774
15	186	25.0	0.5	24.0	25.7	0.865	0.072	0.740	0.959
21	189	17.1	0.1	16.9	17.4	0.201	0.009	0.180	0.220
22	194	22.1	0.3	21.5	22.7	0.433	0.028	0.381	0.491
23	185	24.0	0.2	23.5	24.4	0.623	0.030	0.577	0.696
24	186	26.1	0.2	25.7	26.6	0.797	0.022	0.754	0.847
25	235	27.1	0.4	26.3	28.0	0.956	0.019	0.905	1.000
31	187	18.9	0.2	18.5	19.2	0.228	0.011	0.200	0.251
32	184	24.9	0.2	24.4	25.2	0.509	0.030	0.446	0.555
33	184	27.2	0.2	26.8	27.7	0.725	0.031	0.656	0.781
34	189	28.3	0.4	27.6	29.0	0.892	0.022	0.838	0.934
35	187	27.0	0.3	26.3	27.5	0.959	0.020	0.908	1.001
41	184	21.1	0.2	20.8	21.4	0.26	0.009	0.24	0.281
42	185	28.1	0.2	27.7	28.4	0.58	0.027	0.529	0.631
43	191	29.8	0.4	29.1	30.7	0.805	0.024	0.744	0.856
44	199	28.2	0.7	26.9	31.0	0.892	0.060	0.576	0.975
45	122	26.4	0.3	25.8	26.9	1.001	0.016	0.959	1.040
51	191	23.0	0.2	22.6	23.5	0.299	0.018	0.271	0.336
52	185	31.1	0.2	30.7	31.6	0.686	0.038	0.621	0.766
53	188	29.5	0.5	28.6	30.5	0.830	0.039	0.758	0.915
54	126	27.4	0.4	26.8	28.1	0.950	0.033	0.883	1.011

Table G-5: The statistical summary of the actual air velocity and the pressure drop across the elevation due to the air only and the tested material for chickpea in data set 1.

Test Category		Obs #	Actual Air Velocity [m/s]				Pressure Loss [kPa]			
			Mean	Std Dev	Min	Max	Mean	Std Dev	Min	Max
Air Only	11	186	25.1	0.1	24.9	25.4	0.207	0.013	0.185	0.227
	12	198	26.9	0.2	26.5	27.2	0.237	0.010	0.222	0.257
	13	216	29.1	0.2	28.7	29.4	0.269	0.012	0.249	0.294
	14	188	31.0	0.2	30.6	31.5	0.304	0.012	0.285	0.33
	15	187	32.2	0.2	31.8	32.8	0.316	0.006	0.298	0.328
	21	189	27.9	0.2	27.6	28.3	0.255	0.011	0.237	0.274
	22	188	30.1	0.1	29.8	30.4	0.293	0.015	0.274	0.321
	23	261	32.7	1.4	31.3	35.6	0.336	0.021	0.311	0.378
	24	189	34.1	0.2	33.8	34.5	0.362	0.018	0.336	0.394
	25	194	34.0	0.2	33.4	34.5	0.354	0.029	0.312	0.400
	31	189	31.0	0.2	30.5	31.4	0.311	0.017	0.291	0.338
	32	191	33.1	0.2	32.5	33.5	0.342	0.018	0.319	0.376
	33	130	35.0	0.3	34.4	35.5	0.388	0.019	0.360	0.417
	41	190	34.1	0.2	33.5	34.5	0.363	0.020	0.339	0.397
With Tested Material	11	191	25.1	0.1	24.8	25.4	0.556	0.026	0.496	0.629
	12	190	27.0	0.3	26.6	27.6	0.732	0.022	0.675	0.787
	13	193	28.9	0.2	28.6	29.4	0.898	0.023	0.841	0.955
	14	193	30.8	0.3	30.3	31.5	1.042	0.032	0.946	1.119
	15	186	29.8	0.3	29.3	30.5	1.113	0.062	0.974	1.226
	21	209	28.1	0.2	27.3	28.4	0.605	0.024	0.535	0.676
	22	190	30.1	0.2	29.7	30.5	0.773	0.024	0.704	0.843
	23	252	31.7	0.6	30.8	32.7	0.947	0.029	0.864	1.039
	24	188	30.4	0.6	29.2	31.2	1.059	0.025	0.986	1.147
	25	188	29.3	0.9	27.7	30.7	1.149	0.035	1.062	1.232
	31	187	31.1	0.3	30.6	31.8	0.665	0.032	0.582	0.732
	32	192	32.7	0.5	31.5	33.4	0.840	0.028	0.774	0.908
	33	126	31.3	0.7	30.3	32.5	0.961	0.026	0.894	1.033
	41	189	33.9	0.4	32.7	34.5	0.720	0.029	0.657	0.788

Table G-6: The statistical summary of the actual air velocity and the pressure drop across the elevation due to the air only for fertilizer in data set 1.

Test Category	Obs #	Actual Air Velocity [m/s]				Pressure Loss [kPa]			
		Mean	Std Dev	Min	Max	Mean	Std Dev	Min	Max
11	189	15.0	0.1	14.9	15.2	0.083	0.003	0.076	0.088
12	189	20.1	0.1	19.8	20.3	0.142	0.004	0.133	0.15
13	193	25.1	0.1	24.8	25.3	0.212	0.003	0.204	0.222
14	186	27.9	0.1	27.6	28.1	0.255	0.003	0.246	0.265
15	186	31.1	0.2	30.7	31.5	0.307	0.011	0.285	0.323
21	195	17.1	0.2	16.8	17.6	0.107	0.003	0.101	0.116
22	185	22.6	0.1	22.3	22.8	0.174	0.004	0.164	0.183
23	189	28.1	0.1	27.8	28.3	0.257	0.006	0.244	0.268
24	196	30.9	0.2	30.6	31.3	0.310	0.004	0.300	0.320
25	190	33.1	0.2	32.8	33.6	0.342	0.011	0.319	0.363
31	191	19.1	0.1	18.8	19.3	0.13	0.003	0.123	0.137
32	183	25.1	0.1	24.8	25.4	0.213	0.005	0.202	0.225
33	206	31.2	0.1	30.8	31.4	0.314	0.006	0.296	0.327
34	188	34.0	0.2	33.6	34.4	0.364	0.006	0.346	0.375
35	125	35.0	0.2	34.7	35.5	0.387	0.004	0.376	0.395
41	186	21.1	0.1	20.8	21.3	0.156	0.003	0.148	0.164
42	188	27.5	0.2	27.1	27.8	0.250	0.007	0.232	0.264
43	192	34.1	0.3	33.7	34.7	0.368	0.009	0.349	0.385
51	186	23.1	0.1	22.9	23.3	0.183	0.004	0.172	0.194
52	187	30.0	0.2	29.5	30.3	0.295	0.007	0.281	0.311

Table G-7: The statistical summary of the actual air velocity and the pressure drop across the elevation due to the tested material for fertilizer in data set 1.

Test Category	Obs #	Actual Air Velocity [m/s]				Pressure Loss [kPa]			
		Mean	Std Dev	Min	Max	Mean	Std Dev	Min	Max
11	187	15.0	0.1	14.9	15.3	0.107	0.005	0.097	0.117
12	181	20.4	0.4	20.0	21.1	0.350	0.008	0.329	0.378
13	190	24.9	0.2	24.4	25.4	0.595	0.011	0.572	0.623
14	186	28.2	0.2	27.8	28.6	0.834	0.018	0.789	0.879
15	195	28.5	0.4	27.7	29.5	1.001	0.042	0.917	1.073
21	189	17.0	0.2	16.6	17.3	0.129	0.006	0.112	0.142
22	187	22.6	0.2	22.3	23.1	0.385	0.006	0.370	0.401
23	199	27.9	0.3	27.4	28.4	0.654	0.012	0.626	0.695
24	189	30.2	0.2	29.6	30.8	0.884	0.025	0.827	0.933
25	186	28.2	0.3	27.6	28.7	1.014	0.028	0.930	1.076
31	183	19.0	0.2	18.6	19.5	0.153	0.006	0.135	0.168
32	188	25.0	0.1	24.8	25.3	0.437	0.016	0.406	0.469
33	186	31.0	0.3	30.3	31.8	0.758	0.022	0.722	0.807
34	188	29.9	0.4	29.1	30.4	0.906	0.012	0.876	0.935
35	122	27.8	0.3	27.3	28.4	1.026	0.029	0.971	1.096
41	186	21.1	0.2	20.7	21.5	0.181	0.006	0.168	0.192
42	188	27.5	0.2	27.1	27.8	0.483	0.008	0.464	0.505
43	184	32.1	0.3	31.5	32.9	0.775	0.015	0.737	0.828
51	185	23.0	0.2	22.6	23.3	0.207	0.008	0.185	0.224
52	186	30.1	0.2	29.7	30.5	0.541	0.019	0.513	0.580

G.2 Statistical Summary For Data Set 2

Please note that the category column uses two or three digits indicating the air velocity (first digit) and the material mass flow rate (second digit or second and third digits).

Table G-8: The statistical summary of the actual air velocity and the pressure drop across the elevation due to the air only for canola set 2.

Test Category	Obs #	Actual Air Velocity [m/s]				Pressure Loss [kPa]			
		Mean	Std Dev	Min	Max	Mean	Std Dev	Min	Max
10	294	10.1	0	10	10.2	0.049	0.001	0.046	0.051
20	299	11.5	0	11.4	11.6	0.063	0.001	0.06	0.065
30	292	13	0	13	13.1	0.078	0.002	0.075	0.082
40	295	14.5	0	14.4	14.6	0.095	0.002	0.091	0.098
50	292	16	0.1	15.9	16.1	0.113	0.002	0.11	0.117
60	325	19	0.1	18.7	19.3	0.155	0.002	0.15	0.160
70	306	23	0.1	22.7	23.2	0.214	0.004	0.206	0.221
80	330	28	0.1	27.7	28.4	0.306	0.004	0.295	0.313
90	299	33.1	0.1	32.7	33.4	0.404	0.007	0.39	0.416

Table G-9: The statistical summary of the actual air velocity and the pressure drop across the elevation due to the tested material for canola in data set 2.

Test Category	Obs #	Actual Air Velocity [m/s]				Pressure Loss [kPa]			
		Mean	Std Dev	Min	Max	Mean	Std Dev	Min	Max
11	147	10.0	0.0	10.0	10.1	0.052	0.001	0.051	0.054
12	98	10.0	0.0	9.9	10.1	0.057	0.001	0.055	0.059
13	144	10.1	0.0	10.0	10.2	0.061	0.002	0.058	0.064
14	147	10.1	0.0	10.0	10.1	0.066	0.002	0.062	0.068
15	145	10.0	0.0	9.9	10.1	0.07	0.001	0.068	0.071
16	99	10.1	0.1	10.0	10.2	0.081	0.001	0.079	0.084
17	147	10.0	0.1	9.8	10.3	0.092	0.001	0.089	0.094
21	98	11.5	0.0	11.4	11.6	0.066	0.001	0.065	0.068
22	147	11.5	0.0	11.4	11.6	0.071	0.002	0.068	0.074
23	107	11.5	0.0	11.5	11.6	0.076	0.002	0.073	0.079
24	154	11.5	0.0	11.4	11.6	0.08	0.002	0.076	0.083
25	99	11.5	0.0	11.4	11.6	0.085	0.001	0.083	0.087
26	145	11.5	0.0	11.4	11.6	0.096	0.001	0.093	0.098
27	98	11.5	0.0	11.5	11.6	0.106	0.001	0.104	0.109
28	148	11.5	0.0	11.4	11.6	0.117	0.001	0.114	0.119
29	116	11.5	0.1	11.4	11.7	0.127	0.001	0.125	0.13
31	147	13.0	0.1	12.9	13.2	0.082	0.001	0.079	0.084
32	104	13.0	0.0	12.9	13.1	0.087	0.002	0.084	0.09
33	162	13.0	0.1	12.9	13.1	0.091	0.002	0.088	0.094
34	98	13.0	0.0	13.0	13.1	0.096	0.002	0.092	0.098
35	154	13.0	0.1	12.9	13.2	0.101	0.001	0.098	0.104
36	96	13.0	0.0	12.9	13.1	0.113	0.001	0.11	0.115
37	98	13.0	0.1	12.9	13.2	0.125	0.001	0.123	0.128
38	147	13.1	0.0	13.0	13.2	0.134	0.001	0.132	0.136
39	101	13.1	0.0	13.0	13.1	0.145	0.001	0.143	0.147
41	147	14.5	0.0	14.4	14.7	0.099	0.001	0.097	0.102
42	97	14.5	0.1	14.4	14.6	0.104	0.002	0.101	0.108
43	162	14.5	0.1	14.4	14.7	0.109	0.002	0.105	0.112
44	102	14.5	0.0	14.4	14.6	0.113	0.002	0.11	0.117
45	96	14.6	0.0	14.5	14.7	0.12	0.001	0.118	0.122
46	144	14.5	0.0	14.4	14.6	0.131	0.001	0.128	0.134
47	96	14.5	0.0	14.4	14.6	0.143	0.001	0.139	0.146
48	119	14.5	0.0	14.4	14.6	0.153	0.001	0.151	0.155
49	98	14.5	0.1	14.4	14.7	0.164	0.001	0.162	0.167
51	96	16.0	0.1	15.9	16.2	0.118	0.002	0.115	0.121

Table G-9: The statistical summary of the actual air velocity and the pressure drop across the elevation due to the tested material for canola in data set 2.

Test Category	Obs #	Actual Air Velocity [m/s]				Pressure Loss [kPa]			
		Mean	Std Dev	Min	Max	Mean	Std Dev	Min	Max
52	160	16.0	0.1	15.8	16.2	0.123	0.002	0.12	0.127
53	106	16.0	0.1	15.9	16.1	0.128	0.001	0.126	0.13
54	145	16.0	0.1	15.9	16.2	0.134	0.002	0.129	0.138
55	98	16.0	0.1	15.9	16.2	0.141	0.001	0.138	0.144
56	145	16.0	0.1	15.9	16.2	0.152	0.001	0.149	0.156
57	146	16.0	0.1	15.9	16.2	0.165	0.001	0.161	0.168
58	104	16.1	0.1	15.8	16.4	0.176	0.002	0.171	0.181
59	97	16.0	0.2	15.5	16.6	0.186	0.003	0.178	0.199
61	148	19.0	0.1	18.8	19.3	0.159	0.002	0.155	0.164
62	111	19.1	0.1	18.8	19.3	0.165	0.002	0.161	0.169
63	151	19.0	0.1	18.8	19.2	0.170	0.003	0.163	0.174
64	154	19.0	0.1	18.8	19.3	0.176	0.003	0.168	0.183
65	97	19.1	0.1	18.8	19.3	0.187	0.001	0.184	0.19
66	96	19.0	0.1	18.7	19.1	0.200	0.002	0.194	0.204
67	146	19.0	0.1	18.8	19.2	0.211	0.003	0.205	0.217
68	146	19.0	0.1	18.8	19.3	0.223	0.003	0.216	0.228
69	96	19.0	0.1	18.8	19.1	0.238	0.002	0.234	0.241
71	151	23.0	0.1	22.8	23.2	0.220	0.002	0.216	0.226
72	98	23.0	0.1	22.8	23.3	0.228	0.003	0.223	0.233
73	182	23.0	0.1	22.8	23.2	0.235	0.003	0.229	0.242
74	102	23.0	0.1	22.8	23.1	0.241	0.003	0.236	0.248
75	147	23.1	0.1	22.9	23.3	0.252	0.003	0.248	0.258
76	96	22.9	0.1	22.7	23.1	0.268	0.004	0.261	0.274
77	97	23.0	0.1	22.7	23.2	0.284	0.003	0.279	0.29
78	144	23.0	0.1	22.8	23.2	0.297	0.003	0.292	0.303
79	97	23.0	0.1	22.7	23.2	0.315	0.001	0.311	0.318
81	105	28.0	0.1	27.8	28.2	0.311	0.002	0.306	0.317
82	173	28.0	0.1	27.7	28.3	0.321	0.003	0.313	0.327
83	146	28.0	0.1	27.7	28.4	0.330	0.004	0.322	0.339
84	148	28.0	0.1	27.7	28.2	0.338	0.004	0.329	0.348
85	147	28.0	0.1	27.6	28.2	0.353	0.002	0.347	0.359
86	98	28.0	0.1	27.7	28.2	0.375	0.003	0.366	0.381
87	176	27.9	0.1	27.6	28.2	0.394	0.005	0.386	0.404
88	97	28.0	0.2	27.7	28.4	0.414	0.003	0.406	0.421
89	99	28.0	0.1	27.7	28.3	0.428	0.006	0.416	0.437

Table G-9: The statistical summary of the actual air velocity and the pressure drop across the elevation due to the tested material for canola in data set 2.

Test Category	Obs #	Actual Air Velocity [m/s]				Pressure Loss [kPa]			
		Mean	Std Dev	Min	Max	Mean	Std Dev	Min	Max
91	153	33.1	0.1	32.8	33.3	0.415	0.003	0.408	0.422
92	97	33.1	0.1	32.8	33.3	0.427	0.005	0.416	0.439
93	146	33.0	0.1	32.7	33.2	0.438	0.007	0.425	0.454
94	170	33.0	0.1	32.8	33.3	0.447	0.005	0.437	0.457
95	145	33.1	0.1	32.8	33.3	0.467	0.005	0.456	0.476
96	98	32.9	0.1	32.7	33.3	0.491	0.003	0.482	0.499
97	146	33.0	0.1	32.6	33.2	0.513	0.004	0.504	0.52
98	97	33.0	0.1	32.7	33.2	0.535	0.003	0.529	0.543
99	158	33.0	0.1	32.6	33.2	0.553	0.003	0.546	0.561
210	147	11.5	0.1	11.4	11.7	0.137	0.001	0.135	0.138
211	96	11.5	0.0	11.5	11.6	0.146	0.001	0.144	0.148
310	96	13.0	0.0	13.0	13.1	0.154	0.001	0.152	0.156
311	144	13.0	0.0	12.8	13.1	0.162	0.001	0.159	0.165
410	146	14.5	0.1	14.4	14.6	0.174	0.001	0.172	0.176
411	150	14.5	0.1	14.4	14.7	0.183	0.001	0.180	0.186
510	197	15.9	0.2	15.5	16.3	0.194	0.002	0.188	0.201
511	147	16.0	0.1	15.8	16.5	0.207	0.004	0.176	0.214
610	101	19.0	0.1	18.8	19.2	0.248	0.002	0.243	0.252
611	146	19.0	0.1	18.8	19.2	0.258	0.002	0.253	0.263
710	147	23.1	0.1	22.9	23.4	0.327	0.004	0.318	0.334
711	97	23.0	0.1	22.6	23.3	0.341	0.004	0.333	0.349
810	102	28.0	0.1	27.7	28.2	0.443	0.007	0.434	0.453
811	145	28.1	0.1	27.8	28.3	0.460	0.005	0.452	0.472
910	99	33.0	0.2	32.5	33.3	0.575	0.002	0.570	0.580
911	147	33.1	0.2	32.8	33.7	0.591	0.007	0.576	0.609

APPENDIX H PROGRAM CODE FOR SAS

SAS Program Code

PROC NLIN Data=WORK.Canolamodelling Outest=CanolaParameters SAVE METHOD=MARQUARDT;
PARAMETERS a1=**30** a2=**-1** b1=**0.0001** b2=**-0.01** b3=**0.3** b4=**-0.5**;
MODEL mp=ma*(a1*(exp(a2*v))*Ploss-log(b1*v**3+b2*v**2+b3*v+b4));
run;

APPENDIX I DETAIS AND RESULTS FOR MODELLING

The following are details of the compiled results from SAS which were applied to both data set 1 and 2 to obtain their coefficients for the models.

I.1 Compiled Results for Data Set 1

There were four different materials tested for data set 1 which were canola, wheat, chickpea, and fertilizer. The individual compiled results for each tested material are shown below.

I.1.1 Complied Results for Canola

The NLIN Procedure
NOTE: An intercept was not specified for this model.

Estimation Summary

Method:	Marquardt
Iterations:	17
Subiterations:	17
Average Subiterations:	1
R:	1.897E-6
PPC(b3) :	0.000051
RPC(b3) :	0.00044
Object:	2.578E-7
Objective:	0.003833
Observations Read:	6506
Observations Used:	6506
Observations Missing:	0

Table I-1: Summary of the model estimation

Source	DF	Sum of Squares	Mean Square	F Value	Approx Pr > F
Model	6	0.4722	0.0787	133454	<.0001
Error	6500	0.00383	5.90E-07	-	-
Uncorrected Total	6506	0.476	-	-	-

Table I-2: Model parameter estimation results

Parameter	Estimate	Approximate Std Error	Approximate 95% Confidence Limits	
a1	26.878	0.2449	26.3979	27.358
a2	-0.0918	0.000673	-0.0931	-0.0904
b1	-0.0005	0.000043	-0.00058	-0.00041
b2	0.0138	0.00172	0.0104	0.0172
b3	-0.0447	0.0225	-0.0887	-0.00062
b4	1.2916	0.0955	1.1045	1.4787

Table I-3: Approximate Correlation Matrix

	a1	a2	b1	b2	b3	b4
a1	1	-0.9872	0.16911	-0.21	0.20924	-0.1599
a2	-0.9872	1	-0.1625	0.20285	-0.1999	0.1504
b1	0.16911	-0.1625	1	-0.9976	0.99271	-0.9849
b2	-0.21	0.20285	-0.9976	1	-0.9982	0.99162
b3	0.20924	-0.1999	0.99271	-0.9982	1	-0.9969
b4	-0.1599	0.1504	-0.9849	0.99162	-0.9969	1

I.1.2 Complied Results for Wheat

The NLIN Procedure
NOTE: An intercept was not specified for this model.

Estimation Summary

Method:	Marquardt
Iterations:	36
Subiterations:	38
Average Subiterations:	1.055556
R:	8.473E-6
PPC(b1) :	0.000695
RPC(b1) :	0.013185
Object:	2.707E-8
Objective:	0.076144
Observations Read:	5806
Observations Used:	5806
Observations Missing:	0

Table I-4: Summary of the model estimation

Source	DF	Sum of Squares	Mean Square	F Value	Approx Pr > F
Model	6	10.7285	1.7881	136200	<.0001
Error	5800	0.0761	0.000013	-	-
Uncorrected Total	5806	10.8046	-	-	-

Table I-5: Model parameter estimation results

Parameter	Estimate	Approximate Std Error	Approximate 95% Confidence Limits	
a1	8.6501	0.1315	8.3924	8.9079
a2	-0.0608	0.000579	-0.0619	-0.0597
b1	3.48E-06	8.29E-06	-0.00001	0.00002
b2	-0.0011	0.000625	-0.00234	0.000115
b3	0.0559	0.0152	0.0262	0.0856
b4	0.8309	0.1179	0.5997	1.062

Table I-6: Approximate Correlation Matrix

	a1	a2	b1	b2	b3	b4
a1	1	-0.9947	0.44693	-0.4492	0.42144	-0.3492
a2	-0.9947	1	-0.4637	0.46285	-0.4315	0.35687
b1	0.44693	-0.4637	1	-0.9974	0.9879	-0.9655
b2	-0.4492	0.46285	-0.9974	1	-0.9962	0.97973
b3	0.42144	-0.4315	0.9879	-0.9962	1	-0.993
b4	-0.3492	0.35687	-0.9655	0.97973	-0.993	1

I.1.3 Complied Results for Chickpea

The NLIN Procedure
NOTE: An intercept was not specified for this model.

Estimation Summary

Method:	Marquardt
Iterations:	42
Subiterations:	53
Average Subiterations:	1.261905
R:	1.615E-6
PPC(b1) :	0.000024
RPC(b1) :	0.003452
Object:	0.000026
Objective:	0.085833
Observations Read:	3604
Observations Used	3604
Observations Missing:	0

Table I-7: Summary of the model estimation

Source	DF	Sum of Squares	Mean Square	F Value	Approx Pr > F
Model	6	38.8852	6.4809	271669	<.0001
Error	3598	0.0858	0.000024	-	-
Uncorrected Total	3604	38.9711	-	-	-

Table I-8: Model parameter estimation results

Parameter	Estimate	Approximate Std Error	Approximate 95% Confidence Limits	
a1	8.0339	0.1521	7.7358	8.332
a2	-0.0364	0.000622	-0.0376	-0.0352
b1	0.00035	0.000093	0.000172	0.000537
b2	-0.0344	0.0084	-0.0508	-0.0179
b3	1.1371	0.2513	0.6444	1.6298
b4	-10.64	2.487	-15.5158	-5.7635

Table I-9: Approximate Correlation Matrix

	a1	a2	b1	b2	b3	b4
a1	1	-0.9981	0.32599	-0.3245	0.31708	-0.3033
a2	-0.9981	1	-0.3285	0.32627	-0.3182	0.30376
b1	0.32599	-0.3285	1	-0.9995	0.99808	-0.9954
b2	-0.3245	0.32627	-0.9995	1	-0.9995	0.99779
b3	0.31708	-0.3182	0.99808	-0.9995	1	-0.9994
b4	-0.3033	0.30376	-0.9954	0.99779	-0.9994	1

I.1.4 Complied Results for Fertilizer

The NLIN Procedure
NOTE: An intercept was not specified for this model.

Estimation Summary

Method:	Marquardt
Iterations:	38
Subiterations:	41
Average Subiterations:	1.078947
R:	5.261E-6
PPC(b1) :	0.000308
RPC(b1) :	0.075932
Object:	8.003E-7
Objective:	0.248829
Observations Read:	7415
Observations Used:	7415
Observations Missing:	0

Table I-10: Summary of the model estimation

Source	DF	Sum of Squares	Mean Square	F Value	Approx Pr > F
Model	6	62.2225	10.3704	308785	<.0001
Error	7409	0.2488	0.000034	-	-
Uncorrected Total	7415	62.4714	-	-	-

Table I-11: Model parameter estimation results

Parameter	Estimate	Approximate Std Error	Approximate 95% Confidence Limits	
a1	15.1984	0.1872	14.8313	15.5654
a2	-0.0509	0.000433	-0.0517	-0.05
b1	8.81E-06	0.000015	-0.00002	0.000039
b2	-0.00308	0.00118	-0.00539	-0.00077
b3	0.1809	0.0291	0.1238	0.2379
b4	-0.238	0.2276	-0.6842	0.2081

Table I-12: Approximate Correlation Matrix

	a1	a2	b1	b2	b3	b4
a1	1	-0.9964	0.38536	-0.4251	0.438	-0.4064
a2	-0.9964	1	-0.4128	0.44982	-0.4595	0.42551
b1	0.38536	-0.4128	1	-0.9967	0.98758	-0.9728
b2	-0.4251	0.44982	-0.9967	1	-0.9968	0.9863
b3	0.438	-0.4595	0.98758	-0.9968	1	-0.9957
b4	-0.4064	0.42551	-0.9728	0.9863	-0.9957	1

I.1.5 Complied Results for Combined Tested Materials

The NLIN Procedure
NOTE: An intercept was not specified for this model.

Estimation Summary

Method:	Marquardt
Iterations:	29
Subiterations:	32
Average Subiterations:	1.103448
R:	3.249E-6
PPC(b4) :	0.00003
RPC(b4) :	0.021306
Object:	1.201E-6
Objective:	10.14625
Observations Read:	23331
Observations Used:	23331
Observations Missing:	0

Table I-13: Summary of the model estimation

Source	DF	Sum of Squares	Mean Square	F Value	Approx Pr > F
Model	6	102.6	17.0961	39302	<.0001
Error	23325	10.1462	0.000435	-	-
Uncorrected Total	23331	112.7	-	-	-

Table I-14: Model parameter estimation results

Parameter	Estimate	Approximate Std Error	Approximate 95% Confidence Limits	
a1	1.9182	0.0606	1.7995	2.0369
a2	0.0114	0.00108	0.00934	0.0136
b1	0.00011	0.000013	0.000086	0.000139
b2	-0.0045	0.000845	-0.00615	-0.00283
b3	0.0956	0.0172	0.0619	0.1293
b4	0.3702	0.1126	0.1495	0.5909

Table I-15: Approximate Correlation Matrix

	a1	a2	b1	b2	b3	b4
a1	1	-0.9959	-0.5253	0.41454	-0.2975	0.23426
a2	-0.9959	1	0.50749	-0.3936	0.27665	-0.2147
b1	-0.5253	0.50749	1	-0.9878	0.95011	-0.9044
b2	0.41454	-0.3936	-0.9878	1	-0.9866	0.95625
b3	-0.2975	0.27665	0.95011	-0.9866	1	-0.9897
b4	0.23426	-0.2147	-0.9044	0.95625	-0.9897	1

I.2 Compiled Results for Data Set 2

The NLIN Procedure
NOTE: An intercept was not specified for this model.

Estimation Summary

Method:	Marquardt
Iterations:	20
Subiterations:	21
Average Subiterations:	1.05
R:	7.018E-6
PPC(b4) :	0.000015
RPC(b4) :	0.000155
Object:	2.647E-8
Objective :	0.013538
Observations Read:	11358
Observations Used:	11358
Observations Missing:	0

Table I-16: Summary of the model estimation

Source	DF	Sum of Squares	Mean Square	F Value	Approx Pr > F
Model	6	2.2137	0.369	309391	<.0001
Error	11352	0.0135	1.19E-06	-	-
Uncorrected Total	11358	2.2273	-	-	-

Table I-17: Model parameter estimation results

Parameter	Estimate	Approximate Std Error	Approximate 95% Confidence Limits	
a1	25.4796	0.081	25.3207	25.6384
a2	-0.0882	0.00016	-0.0885	-0.0879
b1	9.70E-05	1.41E-06	9.4E-05	9.9E-05
b2	-0.0093	9.50E-05	-0.0095	-0.0091
b3	0.2585	0.00193	0.2547	0.2623
b4	-0.1093	0.0119	-0.1325	-0.086

Table I-18: Approximate Correlation Matrix

	a1	a2	b1	b2	b3	b4
a1	1	-0.9391	0.56101	-0.5393	0.4258	-0.1435
a2	-0.9391	1	-0.5248	0.48168	-0.3388	0.07235
b1	0.56101	-0.5248	1	-0.9949	0.96115	-0.8501
b2	-0.5393	0.48168	-0.9949	1	-0.9828	0.88667
b3	0.4258	-0.3388	0.96115	-0.9828	1	-0.95
b4	-0.1435	0.07235	-0.8501	0.88667	-0.95	1